THE UNIVERSITY OF CHICAGO

# THE KINEMATICS AND NEUROFEEDBACK OF MASTICATION IN *DIDELPHIS VIRGINIANA*

A DISSERTATION SUBMITTED TO

THE FACULTY OF THE DIVISION OF THE BIOLOGICAL SCIENCES

AND THE PRITZKER SCHOOL OF MEDICINE

IN CANDIDACY FOR THE DEGREE OF

DOCTOR OF PHILOSOPHY

GRADUATE PROGRAM IN INTEGRATIVE BIOLOGY

BY

KELSEY TULL STILSON

CHICAGO, ILLINOIS

AUGUST 2021

TABLE OF CONTENTS

# Acknowledgments

It is impossible to thank all the people that have contributed to my growth as a scientist and human being in the order they deserve. As Chapter 1 shows, the importance is dependent upon the dimensions you measure, and life is so much more than six dimensions.

So, in a rather traditional order, I would first like to thank my committee. Dr. Callum F. Ross for all the biomechanical knowledge, wisdom, and exuberance you have imparted to me. You were there from the good times to the bad, and that means everything. You are a great colleague and friend, as well as mentor, and are always willing to listen. I look forward to many more adventures and papers! Dr. Zhe-Xi Luo, you have been my paleontological mentor since I arrived at UC. You are always incredibly supportive and genuine. I have learned not only about what questions to ask, but how to ask them. I cannot wait to work on osteological correlates with you. Dr. David Reed, thank you for being my early career mentor. You bridged the gap for me between the world of students and professors. You also were the first person to really encourage me to work at the bench. Our immunohistochemistry work did not make it into this thesis, but that is more a reflection of the time it takes to do histology in a pandemic and my fundamental misunderstanding of the physics of decalcified bone and glass than a reflection of your teaching. Results forthcoming! Dr. Nicholas Hatsopoulos, although you haven't seen me around lately, those early years working with macaques and hanging around the lab were fundamental to my understanding of neurophysiology, motor learning, and cortical plasticity. I will take these with me wherever I go. Dr. Sliman Bensmaia, I always learn a great deal from you, although it may not seem like it. Thank you to the entire committee for supporting me as my project has changed and grown over these six years.

I'd also like to thank the OBA department and IB program. They say it takes a village to raise a child and I feel that has never been more true than with me. Thank you to Dr. Mike Coates for taking me in for my first rotation. We always have such wonderful discussions about teeth and I will never forget about petalodonts! Thank you Dr. Stephanie Palmer I learned math could be fun, was inspired to start learning to code again (and now I am a Matlab wizard!) and thank you for the borrowed soldering equipment. Dr. Palmer also ran 'Intro to OBA' and 'Topics in OBA', along with Dr. Urs Schmidt-Ott, two courses that literally changed my career. Thank you also to Urs for letting me into various rooms I have locked myself out of over the years. Thank you to Dr. Mark Westneat for letting me help TA biomechanics and all my pre and post quals discussions. Thank you Dr. Dan Margoliash for reminding me about the limitations of nerve transections and for letting the Ross lab borrow the vacuum oven. Thank you Dr. Zeray Alemseged for allowing me into Anthropology Journal Club. Your lab is always so welcoming. Thank you Dr. Neil Shubin for giving me access to your amazing lab and the people in it. Thank you Dr. Vicky Prince for working with me on Dean's Council. Thank you Dr. Robert Ho for supporting my paleopathology in osteopathologis in Rhinocerotidae paper. Thank you Dr. Jim Hopson for our wonderful conversations about early synapsids and OBA department history. Thank you to Carrie Anne, thank you for teaching me animal husbandry and being there for the early messy days. You kept me grounded when everything was in flux. You are right, we are probably never going to write that paper. Thank you April Neander for teaching all of us about microCT scanning and of course our wonderful conversations about art. Thank you to Rebecca Junod. Thank you Audrey Aronowsky for absolutely everything. Thank you Garnett Kirk, Marcy Hochberg, Cindy King, Mike Guerra, Annetha Bartley, Max Zmija, Dale Janeczko, and America Barrera for keeping the lights on and things running. Scientists would be lost without you.

Thank you to my past advisors Dr. Samantha S. B. Hopkins, Dr. Edward Byrd Davis, and Dr. Chris Bell. Your advice, support, and the communities you built were the foundation for where I am now.

Thank you past, present, and future IB students! This program is amazing and magical (in a scientific way) and you are all so fantastic. Thank you to my cohort Dr. Stephanie Baumgart and Dr. Erick Bayala. We made it!!! Thank you to my wonderful friends: Katie Whitlow, Peishu Li, Rossy Natale, Sam Gartner, Dr. J.D. Laurence-Chasen, Stephanie Sang, Dr. Courtney Orsbon, Alec Wilken, Vishrush Venkataraman, Weldeyard Reda, Dr. Tom Stewart, Laura Hunter, Alexa Lamprecht, Daniel Sanchez, Dr. Jackie Lungmus, Gayani Senevirathne, Hannah Farrell, Dr. Adam Hardy, Dr. Katie Henderson, and Dr. Brett Aiello.

Thank you to the amazing Ross Lab postdoc that have semi raised me over the years: Dr. Amanda Smith, Dr. Kara Feilich, Dr. Ellen Schulz-Kornas, Dr. Julia A. Schultz, Dr. Michael "Granny" Granatosky, Dr. Myra Laird, Dr. Nick Gidmark, and Dr. Jose "Pepe" Iriarte-Diaz.

Thank you to the UC Animal Resource Center veterinarians, staff, and husbandry. You helped me through some of my darkest, scariest days in animal surgery and helped me gain the confidence to be a researcher with resilience. Thank you to the UC Human Tissue Resource Center.

Thank you Running Crew for meeting at odd hours at Runner's Roost and going on amazing adventures. Everything from brunch runs to 40 miles on the waterfront. We are the living metaphor of a thesis project. We just keep going.

Thank you to the friends that keep me sane (and have not been mentioned yet): Tony (Melvin) M. Bonilla- besties for life! Brianna McHorse, the womance never dies. Sam, na na na na na na na. Jessy Morgan, Travis Bee, Aileen Tartanian, Anna Petrosky, Anna Wisniewski,

Michael Fankiewicz, Dakota Lane, Dr. Nick Famoso, Dr. Win McLaughlin, Dr. Kristen MacKenzie, Dr. John Orcutt, John Jaicisn III, Dr. Robert Burroughs, Catherine Burroughs, Dr. James Proffitt III, Selina Robson, Eileen, Devynn, Zeke, Sarah N., Sarah F., Hillary, Matt, and Emily. And my parasocial thesis companion, Dr. G: Medical Examiner.

Thank you to my family. Always there whether I like it or not. And I love you all for it. Alicia, Matthew, Zach, and Sam. Aunt Steph and Aunt Becca, E and Nicho. Renee, Stephen, and Nathan- loves! Love you, Mom, Love you, Dad. Love you, James.

And, finally, thank you to Opossum Li, Opossum Lu, Opossum W, Opossum A, and Opossum M. They have done more for hemimandibular biomechanics than possibly any animal in the world.

LIST OF FIGURES

LIST OF FIGURES (CONTINUED)

LIST OF FIGURES (CONTINUED)

LIST OF TABLES

# Funding

Integrative Neuromechanics GAANN scholar (2017-2018),

Harold and Annette Dubner Scholar (2019-2020)

Funding for the UChicago XROMM Facility was provided by National Science Foundation

Major Research Instrumentation Grants MRI 1338036 and 1626552.

# Abstract

Quantitative analyses of hemimandibular kinematics during mastication have not yet received much attention during the past two decades as the technology for measuring the kinematics have greatly improved. Chew cycle kinematics and inferred tooth occlusion have been applied to hemimandibles as if they were a fused single mandibular system, or as if they were a half mandible in 2-D lateral view, despite the well-established understanding that hemimandibles are rendered semi-independent by their semi-mobile symphysis. Treating the hemimandibles as relatively independent and mobile can have major implications for interpreting functional morphology of the fossils of early mammals. The research of this thesis measures hemimandibular kinematics during mastication in six *Didelphis virginiana* individuals eating two food types, almonds and cheese (Chapter 1). A traditional coordinate axis is applied to the system to measure the pitch, yaw, and roll of each hemimandible, as well as a novel helical axis analysis. Here, I find that for description and quantification of hemimandibular kinematics the four chew cycle phases previously defined and deployed in chewing studies are more appropriately divided into six chew cycle phases: fast close 1 (FC1), fast close 2 (FC2), slow close 1 (SC1), slow close 2 (SC2), slow open (SO), and fast open (FO). No one dimension of rotation predominates or is "more important" during slow close. Roll and yaw, especially, vary in relative magnitude depending on the side of an individual and between individuals. This variation has important implications for the degree of stereotypy of the hemimandibular system. The novel helical axis method provides valuable understanding the whole mandibular system. Importantly, the rotational data show that the axis of rotation was found to be outside the working side hemimandible for the majority of the chew cycle. Hemimandibular mastication is

fundamentally different from mastication in a fused mandible and this thesis represents a critical first step in precisely measuring and defining kinematics of the hemimandibular system.

In the second half of my thesis, I studied the dentoalveolar neurofeedback system during mastication by transecting the left inferior alveolar nerve, while leaving the right one intact. Overall, the kinematics measured during post-transection mastication were found to be a mix of individual learned responses to nerve transection and a stereotyped change to the entire system. A couple of patterns emerged: (1) Both hemimandibles show changes in kinematics after the transection, even when the healthy right side is the working side. (2) Transected individuals preferentially evert either their right or left hemimandible for the entire cycle. (3) Roll is the rotational dimension with the most change, and mediolateral translation of the M1 talonid basin is the translational dimension with the most change. These results suggest that the phases of the chew cycle where tooth-tooth or tooth-food-tooth contact are likely to occur (end of FC2, SC1, SC2, and start of SO) are controlled bilaterally through dentoalveolar neurofeedback. Transecting the inferior alveolar nerve unilaterally does not entirely inhibit mastication, but limits the ability of the animal to respond to changes in food physical properties in all dimensions, primarily roll. This is relevant for interpreting the early mammalian evolution as the earliest mammaliaforms had at least partially mobile symphyses. The hemimandibular kinematics in *Didelphis virginiana* are particularly important for interpreting the functional evolution of the therian mammals, in which changes in the tribosphenic molar are coupled with changes to the jaw shape, such as the angular region. The opossums of didelphid marsupials have been used as proxies to infer function of the Mesozoic therian mammals. For an early therian mammal that has a tribosphenic molar with complex occlusal surfaces, it is a pre-requisite that it

also has a neurofeedback system, for coordinated and effective function of the mandible and teeth.

# Introduction

*Orienting the Reader*

This thesis examines the functional kinematic relationship between the hemimandibles, and between the hemimandibles and the cranium, during mastication in *Didelphis virginiana* (Virginian Opossums). Once the system is defined I focus on one of the sensory systems active during mastication, the dentoalveolar neurofeedback system. I have organized this work into two major chapters. Chapter 1 describes the function and measures the kinematic movement of the hemimandibles and cranium during mastication of healthy animals. This expands on the quantitative methods proposed by Reed and Ross (2010) to identify and describe the phases of the chew cycle defined by Hiiemae and Crompton (1985). Chapter 2 examines the function of hemimandibular mastication after dentoalveolar neurofeedback is disrupted. I used biplanar videoradiography and the X-Ray Reconstruction of Moving Morphology (XROMM) workflow to record jaw movements in *Didelphis virginiana* during mastication, before and after transection of the left inferior alveolar nerve. The foods used were almonds and cheddar cheese, two types of food with different degrees of hardness, structure, and texture. Performing a nerve transection of the inferior alveolar nerve makes it possible to evaluate how hemimandibular kinematics respond to a complete lack of unilateral input. This allows me to directly relate the movement of the hemimandibles to the influence of neurofeedback in controlling the biomechanical and behavioral system of mastication.

## Scientific Significance

The first intent of this thesis is to establish a lexicon and a framework for quantitative analysis of the kinematics of the hemimandibular system, which consists of two hemimandibles

separated by a semi-mobile syndesmotic mandibular symphysis (Lieberman and Crompton 2000). Early work on hemimandibular kinematics in the 1950's and 1960's (see Chapter 1) was limited by the computational power and physical technology of the time. Few studies in these decades attempted to measure the kinematics at the hemimandibular level, as it was extremely difficult to resolve the relative movements of the hemimandibles. In fact, only in the last five years has it been possible to achieve the resolution necessary to study the relatively small movements of mastication when the teeth are in contact with statistical reliability.

The framework for understanding mastication in mammals with fused mandibles is well-established. This thesis work takes the established concepts and kinematic metrics of mastication (which are primarily based on a fused mandibular system) and augments these masticatory kinematic definitions for hemimandibular systems. The analyses used here such as chew cycle timing, phase identification, analyses of rotations and translations, and helical axis analyses have been established by previous studies (Crompton and Hiiemae 1969, 1970, Hiiemae and Crompton 1971, Hylander et al. 2000, Liberman and Crompton 2000, Reed and Ross 2010, and Iriate-Diaz et al. 2017). However, applying these methods to the hemimandibular system results in a novel characterization of chew cycle phases and the first preliminary helical axis analysis of hemimandibular movement and mastication. In this thesis work I also demonstrate the limitations of using only a single method, such as an analysis of rotations and translations, or a helical axis analysis to characterize the kinematic masticatory movement.

The second intent of this thesis is to evaluate the contribution of the dentoalveolar neurofeedback system to the changes in timing and movement of the different chew cycle phases. Teeth and their periodontal ligaments (as part of the dentoalveolar complex) are an essential part of the feedback system in mastication. Loss of this system in humans can have a

catastrophic and deleterious impacts on the quality of a person's life (see below). However, it is difficult to directly study the changes in masticatory function, with or without the loss of dentoalveolar feedback, because the methods used to measure mastication kinematics are highly invasive. Dentoalveolar feedback through the mammalian periodontal ligament and inferior alveolar nerve is intimately associated with the modern mammal-like tooth roots and root implantation in the mandible that first appear in the Late Triassic mammaliaforms (see Chapter 1 introduction and Luo et al. 2004 for more details). Many clades of these fossil mammaliaforms of the Mesozoic are already fully established in the early Jurassic (Luo 2007; Kielan-Jaworowska et al. 2004). These fossils provide a morphological proxy of the soft tissue structure of the periodontal ligament and inferior alveolar nerve that are modern mammal-like, for inference of neurofeedback associated with masticatory function, as seen in modern mammals. Both the australosphenidan lineage and the therian mammals of the Mesozoic evolve tribosphenic molars. *Didelphis virginiana*, the organism used in previous biomechanical studies of mastication (Crompton and Hiiemae 1969, 1970, Hiiemae and Crompton 1971; Schultz and Martin 2014) as well as in this study, is a common species of marsupial with tribosphenic molars and the marsupials are a descendant lineage of the Mesozoic metatherians (Crompton 1971; Luo et al. 2001a). Therefore, this thesis is also a significant contribution to functional understanding of early mammalian evolution, and to the understanding of neurofeedback in kinematic movement for jaw functions.

General Background in Mammal Mastication

Chewing is a risky business. Food is essential for survival, but food items must be soft and friable enough that it can be broken down before it can be chewed and swallowed. The

ingested “food” items that cannot be broken down or chewed must be expelled out of the mouth in order to protect the soft tissue structures in the mouth, including the oral and dental sensory structures.

The mammalian mouth is a multi-modal sensory system innervated by several cranial nerves providing sensory information on taste, pressure, temperature, texture, hardness, and acidity of food and liquids. The sensory feedback from the mouth is relayed to the central nervous system for further processing. This sensory information is used to protect the relatively soft lips, tongue, and cheeks from the teeth, protect the teeth from each other, and to protect and maintain the integrity of the mouth structure. Food is broken down by the process of chewing to increase the surface area of the particles, which allows for efficient digestion and protects the esophagus during deglutition (swallowing).

What makes mammalian chewing so special? Chewing is defined as cyclic intraoral food breakdown. Chewing occurs in all major lineages of Vertebrata, including actinopterygians, Reptilia, Amphibia, and Aves (Sibbing 1982; Reilly et al. 2001; Ross et al. 2010; Gidmark et al. 2014; Laurence-Chasen et al. 2019). Chewing in mammals is functionally different and evolutionarily derived from non-mammalian vertebrates. In mammals, the breakdown of the food occurs between the matching upper and lower teeth capable of precise occlusion (Lucas 2004), powered by the muscles of mastication (Hiiemae and Crompton 1971, Hylander et al. 2000). In most tooth-bearing mammals, food material is broken down by mastication faster and more efficiently for swallowing than in their non-mammalian counterparts (Ross et al. 2012).

The sensory portion of the peripheral nervous system innervating the muscles of mastication and oral cavity in Mammalia is unique in several respects. Mammalian masticatory muscles have muscle spindles (Morquette et al. 2012) that allow for rapid modulation and reflex

arcs during mastication, as well as a novel temporomandibular joint populated with joint sensory receptors (Morquette et al. 2012). The dentoalveolar complex is defined as the tooth root(s), periodontal ligament, nerves, blood vessels, cells, and the surrounding alveolar bone. The nerves within this complex encode sensations of pain, pressure, temperature, and vibration (Trulsson et al. 2006, Morquette et al. 2012, Grigoriadis et al. 2020). Mammals continuously maintain and regenerate the sensory feedback system of the denotoalveolar complex in the face of disruption of the periondontal ligament during tooth replacement (Miki et al. 2015).

Rhythmicity and the ability to modulate rhythmicity are also key. Mammalian mastication is characterized by rhythmic chewing sequences generated by central pattern generators in the brainstem (Dellow and Lund 1971, Lund and Kolta 2006, Morquette et al. 2012) that are then *modulated* by neural networks. One example of this modulation is the fast open reflex, which activates the jaw-opening muscles when a piece of food debris is encountered during mastication (Sessle 2006, Lund and Kolta 2006, Sessle et al. 2007, Morquette et al. 2012). Another is the anticipatory/feed-forward response, which augments jaw-closing muscle activity during each chew cycle based on feedback from the previous cycle (Liu et al. 1993, Ottenhoff et al. 1993, Komuro et al. 2000, Van der Glas et al. 2007). Both the fast open reflex and feed-forward response require input from tactile sensation of the teeth and other oral structures. Mammals also have a large number of afferent nerves from the oral cavity to the brain and novel connections to distinctly mammalian neocortical brain structures, such as the sensorimotor cortex, with which a mammal can consciously control mastication (Rowe et al. 2011, Sessle 2006, Kaas 2016, Krubitzer and Prescott 2018).

During the origins and the earliest evolution of modern mammals from their cynodont evolutionary predecessors, there is a great deal of morphological change in the dental and

mandibular structure (Crompton and Parker 1978; Kielan-Jaworowska et al. 2004; Luo et al. 2004; Luo 2007; Kemp 2005). Tooth tactile sensitivity is thought to be enhanced in mammals through dental occlusion and the elaboration of the tooth root structure over evolutionary time, creating a feedback loop for the precisely matching upper and lower molars, specialized root structure, and increased dental sensitivity (Lucas 2004; Kielan-Jaworowska et al. 2004; Luo et al. 2004; Luo 2007; Langenbach and van Eijden 2005, Ungar 2010).

In this thesis research, I have applied the established concepts and kinematic metrics to characterize the mobile hemimandibular system of *Didelphis virginiana* (Figure 0.1). I present a novel characterization of chew cycle phases, and the first preliminary helical axis analysis of hemimandibular movement and mastication using biplanar videoradiography and the XROMM (X-Ray Reconstruction of Moving Morphology) workflow.

Humans, Tooth Loss, and Cognitive Decline

Dental health in humans is often seen as a vanity project or a chore, but there are also serious medical implications for tooth infection and loss, both physically and mentally. Tooth loss is associated with a lower quality of life, difficulty in eating, substantial maxillary and mandibular bone loss, and even cognitive impairment (Grigoriadis et al. 2020). Dentures that attach to screws embedded in maxillary or mandibular bone have been shown to be more effective for mastication than dentures that only sit on the gums. There is also a significant correlation between tooth loss and cognitive decline in geriatric individuals (Arce-McShane 2021). Recent research has shown that, in mice selected for genes related to Alzheimer's, extraction of the teeth of lower molar tooth row leads to neurodegeneration of the mesencephalic

nucleus, which then spreads to the neighboring structure, the locus coeruleus (LC) (Goto et al. 2020). The locus coeruleus produces norepinephrine (i.e. noradrenaline) and connects to almost all brain regions except the basal ganglia (Espana and Clotman 2012). Neuronal loss in the LC is associated with a loss of arousal, vigilance, motivation, memory, and attention-related tasks (Ramos and Arnsten 2007) and is related to Alzheimer's disease, Parkinson's disease, and Chronic Traumatic Encephalopathy (Zarow et al. 2003 Arce-McShane 2021). The biggest risk factor for physical and cognitive decline is still aging, but tooth loss while aging appears to be a significant secondary risk factor for humans, which may well be a shared pattern of Mammalia.

Dental infections were the 5$^{th}$ or 6$^{th}$ leading cause of death in 17$^{th}$ century England (Robertson and Smith 2009), and today more than one in five living adults in the United States of America has untreated cavities (health survey from 2005-2008, Dye et al. 2012). Dental pathologies are common in wild animals, especially carnivorans (Van Valkenburgh and White 2021). So why preserve this sensitive system instead of fusing the teeth to the jaw, which would reduce potential sites of pain and infection? The answer may lie in the sensory functions of the teeth: this thesis explores the effects of loss of dental sensory function on jaw kinematics in *Didelphis virginiana*.

**INTRODUCTION**

**FIGURE**

**Figure 0.1.** Depiction of adult *Didelphis virginiana* as drawn by April I. Neander. Digital media.

# CHAPTER 1:

The kinematics of mastication in *Didelphis virginiana*: Uniting roll and yaw with a helical axis analysis

## Background

The majority of species of early mammaliaforms and crown mammals of the Mesozoic have unfused mandibular symphyses, meaning the two hemi-mandibles moved semi-independently of each other, forming a third jaw joint of the mandible (Scapino 1965; Kielan-Jaworowska et al. 2004; Scott et al. 2012; Ravosa and Vinyard, 2020). Mesozoic mammaliaforms also have molars capable of precise occlusion. By comparison, the vast majority of non-mammaliaform cynodonts have fused mandibular symphysis in adults, and lack dental occlusion (Crompton and Jenkins 1968; Hopson and Crompton 1969; Crompton and Parker 1978; Crompton and Luo 1993). Based on such broad phylogenetic comparison, it was generally accepted that the mobile symphyses of hemimandibles are instrumental for early mammals to develop precise dental occlusion that is absent in most (although not all) premammaliaform cynodonts (Hopson and Crompton 1969; Crompton and Luo 1993). Development of an unfused symphyseal joint is one of a wide suite of morphological traits associated with diversification of dental function in all Mesozoic mammals (Luo 2007; Martin 2018) and the majority of extant therian mammals (Lucas 2005; Ungar 2010; Scott et al. 2012).

Despite the ubiquity of unfused symphyses in living mammals, especially in comparison with the much better studied system of the fused mandibles (Hylander 1984, 1985; Reed and Ross, 2010; Iriarte-Diaz et al. 2017, Menegaz et al., 2015, Olson et al., 2019), hemimandibular kinematics have seldom been studied quantitatively, and have mostly been studied in 2D

(Crompton and Hiiemae, 1970; Oron and Crompton, 1985; Lieberman et al, 2000). A ground-breaking 3D study of hemimandibular kinematics in *Monodelphis domestica* is also largely qualitative in nature (Bhullar et al., 2019). Here I present quantification of 3D hemimandibular kinematics of the marsupial *Didelphis virginiana* and use the data to test hypotheses regarding the relative magnitudes of roll and yaw during the chewing cycle, and to evaluate the utility of the vertical kinematic gape cycle phases (sensu Ross and Iriarte-Diaz, 2019) traditionally used to measure jaw kinematics in amniotes (Bramble and Wake, 1985; Hiiemae and Crompton 1985).

*Hemimandibular Kinematics*

I use the term hemimandibular kinematics to refer to kinematics of mandibles in which the mandibular symphysis is not rigidly fused and thus mobile to a varying extent, as has long been recognized by early naturalists. Late 17$^{th}$ century publications on the function of the mobile symphysis focused on specific incisal functions, such as opening nuts by squirrels and cropping using a scissor action by kangaroos (reviewed in Beecher 1979). When researchers began to systematically study fossil mammal taxa, attention turned to the significance of symphyseal mobility for molar function. Ryder (1878), Cope (1889), Osborn (1907), and others attempted to infer mandibular movement from occlusal surfaces of maxillary and mandibular teeth. Anteroposterior movement in rodents and lateral jaw movement were proposed to explain the severe wear to teeth and condylar morphologies (Ryder 1878). However, it was not possible to test these hypotheses using *in vivo* data until cineradiographical studies of live animals began in the late 1950's. Ride (1959) observed that *Wallabia rufogrisea fructica* (Bennet's wallaby) splays the incisors while biting food, but reduces the inter-incisor distance during mastication. Scapino (1965) studied fresh-tissue morphology of symphyses in dogs, and concluded that dogs must rotate their dentaries around their long axes for proper occlusion. Hiiemae and Ardran

(1968) measured bilateral chewing in rats with cineradiography and concluded that the only way a rat could masticate on both sides simultaneously is through a mobile symphysis. Mills (1966, 1967) spurred a renewed interest in *D. virginiana* by a schematic modeling of the mastication with a dried *D. virginiana* skull, concluding that there was a little if any symphyseal movement. Mills hypothesized that mastication and the observed occlusal surface wear could be explained primarily by lateral translation , which would account for the functionally fused symphysis that could rotate slightly, anterior to the incisors, due to condylar movement.

Mills' (1966, 1967) proposal was re-evaluated by Crompton and Hiiemae (1969, 1970, Hiiemae and Crompton 1971) who measured mastication in live opossums using cineradiography. They documented the presence of a highly mobile symphysis, which they described as a third joint allowing semi-independent movement of the two hemimandibles, contrary to the interpretation of little or no symphyseal movement by Mills (1966, 1967). The movements included bilateral lateral condylar translation (i.e., Bennett movement; Bennett 1908) during the power stroke. Inversion and eversion of the molars during the power stroke could not be observed because of technical limitations of 2-D cineradiography available in 1960s, but they inferred it from morphological data of the tooth occlusal surface, and kinematic data. In a light camera cinefilm study of mastication in *Myotis lucifugus* (the little brown bat), Kallen and Gans (1972) reported "rotation about all three axes" and "a translational motion while the molars are near occlusion." In their cineradiographic study of the tenrec, which also has an unfused symphysis, Oron and Crompton (1985) reported inversion of the working side tooth row during fast close (FC) and "during occlusion and the power stroke" (p. 168 and p. 178).

Once the presence and mobility of an unfused symphysis were established, the question became: what are the advantages and disadvantages of an unfused symphysis? Mammals with

unfused symphyses were hypothesized to have more vertically (superoinferiorly) oriented occlusal facets on the cusps of molars relative to fused individuals (Butler 1972). This was invoked to suggest that mammals with unfused symphyses transferred vertically oriented forces more efficiently, while fused symphyses transferred transverse loads more efficiently (Lieberman and Crompton, 2000). However, as Hylander et al. (2000) argued, fused symphyses transmit forces equally well regardless of their orientation; only in an unfused symphysis is there a wide range in the transmission of forces because of variation in ligament orientation. Instead, the data from primates support the hypothesis that symphyseal fusion is an adaptation to strengthen symphyses, not stiffen them.

Other workers focused on the importance of hemimandibular kinematics for occlusal movements, rather than force transfer. Kallen and Gans (1972) reported that in the little brown bat hemimandible "... the tooth will alternately tilt to the left and to the right as the mandibular body rotates about its longitudinal axis". Lieberman and Crompton (2000) reported on rotation of the mandible in opossums and goats, noting that "the *ventral* margin of the working side mandible tends to evert" (emphasis added) during FC and then inverts slightly during SC; the balancing side hemimandible showed the opposite pattern. They also reported a phase lag from the working to the balancing side hemimandibles. Unfortunately, the methods at the time of their research did not allow quantification of rotation and were only derived from a single subject. Crompton et al. (2008) used relative positions of coronoid and ventral border of the mandible to estimate eversion-inversion of the ventral borders of the working and balancing side hemimandibles of tammar wallabies and red kangaroos during chewing. The ventral border of the working hemimandible everts during the first part of the power stroke (the orthal phase), and then it inverts during the second part (transverse phase), with the working side inverting about

100 ms before the balancing side. Crompton et al. (2008) note that the balancing side inverts when the working side everts and conclude that the mandibles are moving independently. It is important to note here that the terms inversion and eversion are often used almost qualitatively. Without precise 3D kinematic data it is sometimes difficult to tell whether inversion of tooth row is associated with eversion of the ventral margin of the mandible. While this is often assumed to be true, the relative magnitudes of eversion and inversion of the toothrow and mandibular base are related to the location of the axis of rotation. Hence, without precise 3D data on jaw kinematics, qualitative descriptions of jaw kinematics are prone to error.

Bhullar et al. (2019) used biplanar videoradiography and the XROMM workflow to characterize the rotations of the hemimandibles during mastication and relate them to movements of the molars during occlusion. They documented inversion, eversion, then inversion of the toothrow "at the deepest part of the bite", hypothesizing that this facilitates food break down using a rotational grinding stroke. Without a quantitative analysis, they argued qualitatively that food type and chew side did not significantly change their results. They also argued that their data on jaw roll and molar movement in *Monodelphis* falsified a prior hypothesis that molar movement was related primarily to jaw yaw driven the pterygoid muscle by Grossnickle (2017). Grossnickle's hypothesis is based on lever mechanics, and quantitative shape data of hemimandibles of Mesozoic therian mammals and their near relatives collectively known as cladotherians (Grossnickle 2017). This hypothesis is based on a lever-system estimate that jaw yaw can generate a greater moment value than jaw roll. Grossnickle argued that evolution of a posterior angular process coincided with the evolution of tribosphenic molars and the loss of middle ear bony attachments to the jaw. Primarily driven by the jaw yaw mechanism by muscles inserting on modern therian like angular process, the hemimandibles and molars experience more

mediolateral excursion (Grossnickle 2017). Grossnickle et al. (2021) further argue that the tribosphenic mammals and their close relatives of cladotherians show a great prevalence in molar wear striations caused by forward (proal) movement of the molar (Grossnickle et al. 2021), consistent with the anterior vector of molar movement by the yaw mechanism. Bhullar et al. (2019) directly contradicted this hypothesis by describing the large degree of roll observed during "the rotational grinding stroke", but little yaw. Debate ensued (Bhullar et al. 2020, Grossnickle 2020; Grossnickle et al. 2021).

***Mastication and Phases of the Gape Cycle***

The overarching goal of this thesis is to report precise quantification of 3D hemimandibular kinematics of the opossum, *Didelphis virginiana,* during chewing, when food is broken down by teeth in the oral cavity, prior to deglutition (swallowing). Mastication occurs as part of a feeding sequence, which begins with ingestion of food through the oral fissure and ends with the final swallow. After ingestion, the animal transports the food item from the oral fissure to the postcanine toothrow in the oral cavity proper (stage 1 transport; Bramble and Wake 1985) for chewing. Many mammals only chew on one side at a time. Hence there is usually a 'working side' tooth row and hemimandible, where the food is being broken down, and a balancing side on which no (or less) food breakdown occurs (Hylander 1984). (There may be food on the 'balancing side' toothrow, but in many mammals it is assumed that the balancing side is involved in food breakdown to far less an extent). After stage 1 transport of food to the postcanine toothrow, the animal employs a series of jaw depression and elevation (gape) cycles to break down the food. During each chew cycle the food is positioned between the upper and lower molars of the working side. The working side may switch between left and right every cycle (as in pigs) or after a number of cycles (macaques, opossums). During chew cycles, the

tongue initiates stage 2 transport of food bolus particles past the palatoglossal arch (pillars of the fauces) into the valleculae in the oropharynx. Stage 2 transport also occurs when the food bolus is large enough and the swallowing reflex is initiated for deglutition.

During chewing, the tongue, cheek, and mandibles move in a coordinated fashion during what are referred to as gape cycles. Gape can be measured as the distance between the tooth rows or, as here, using angular rotation (pitch) of the mandible. Here I define gape cycles as starting and ending at maximum gape. Gape cycles are conventionally divided into four vertical kinematic phases by changes in vertical jaw displacement velocity (second derivative of pitch) (Bramble and Wake, 1985; Crompton and Hiiemae 1970; Reed and Ross 2010; Ross and Iriarte-Diaz, 2019). During the first phase of the gape cycle, fast close (FC), the jaw closes relatively rapidly and yaws toward the working side. The mandible slows down at the transition from FC to slow close (SC), assumed to be the time when the lower molars contact the food bolus and/or upper molars. During SC, the food is compressed and fractured between the teeth as the lower tooth row inverts, everts, and inverts again as it rolls about a longitudinal axis. Slow open (SO) starts when gape distance begins to increase again (i.e., pitch angle decreases) as the molars come out of contact, and the mandibles yaw toward the midline. As the working side mandible nears the midline, the mandibles increase their rate of pitch, defining the start of fast open (FO), which ends at maximum gape.

Definitions of gape cycle phases have changed over time, in part because of changes in methods for measuring jaw kinematics (reviewed by Ross and Iriarte-Diaz 2019). For example, while SC is often assumed to synonymous with earlier kinematic terms such as ‘power stroke’ and ‘rotational grinding stroke’, care should be taken to distinguish the terms defined by jaw vertical kinematics from those describing occlusion or bite force generation. Moreover, as we

show here, the earlier kinematic phases of the gape cycle do not fully capture dynamic changes in roll and yaw during the gape cycle, suggesting that new terminology is needed to capture these variables.

Our choice of *Didelphis virginiana* as a study species is in part based on convenience and in part on its utility as an extant comparative model for the earliest known mammals from the Mesozoic with tribosphenic dentition (Crompton 1971; McKenna 1975; Luo et al. 2001a; Kielan-Jaworowska et al. 2004). Testing hypotheses about kinematics of the extant tribosphenic mammals with a mobile symphysis (Hiiemae and Crompton 1971; Bhullar et al. 2019) is essential to our understanding of the dental function of the Mesozoic mammals with similar teeth, or with an unfused symphysis (Bhullar et al. 2019).

All living mammalian taxa are thought to have evolved from tribosphenic ancestors (Luo et al. 2001a). The tribosphenic molar is a plesiomorphic feature of extant therians (marsupials and placentals) as well as close therian fossil relatives, collectively known as Boreosphenidans (Luo et al. 2001a). The tribosphenic therians have a 'multitool' dentition, with the plesiomorphic shearing surfaces of the trigonid, plus the evolutionarily derived crushing surfaces of the lower talonid that match the protocone of the upper molar, in a system with more versatile occlusal functions for the breakdown of a wide range of foods. The lower molar basin (talonid) occludes with the inner cusp on the upper molar (protocone). The trigonid section is mesial to the talonid and consists of three cusps, two lingual and one buccally (Osborn 1888, Ungar 2010). These cusps interlock with corresponding structures on the upper molars and are spaced in such a way that each upper molar interlocks with a half of each of the two lower molars. The talonid basin is formed by three lower cusps around talonid basin floor, creating a novel crushing surface for the upper protocone. The talonid basin, in combination with the trigonid, is thought to be one of the

key innovations that led to the diversification of Theria (McKenna 1975; Kielan-Jaworowska et al. 2004; Martin 2018). This morphology is hypothesized to have evolved independently in Australosphenida, which have a mesiolingually wrapping cingulid absent in Boreosphenida, have a smaller trigonid to talonid height ratio compared to other Jurassic and Early Cretaceous therians, and a mediodistally short and buccolingually broad talonid (Luo et al. 2001a). The Australosphenida are survived today by Monotremata. In extant Theria, tribosphenic molars are associated with insectivorous and generalized omnivorous species, the latter including *Didelphis virginiana*.

The favored extant models of Boreosphenida are species from the marsupial family Didelphidae, specifically *Monodelphis domestica* used as a developmental biology model (Urban et al. 2017), and *Didelphis virginiana* (the Virginian Opossum). The latter was chosen for this study as it is the only native North American marsupial, locally available, relatively free of zoonotic diseases, of medium size (3 to 5 kg), and thus easily handleable and well-within the imaging limits of XROMM technology. Opossums also have an unfused mandibular symphysis, a relatively long mandible rostrocaudally, and an interlocking tribosphenic dentition (Archer 1987, Szalay 1994, van Nievelt and Smith 2004, Luo et al. 2011, Rowe et al. 2011, Grossnickle and Polly 2013, Rowe 2020). Opossums are much larger than many Mesozoic mammaliaform taxa, including an order of magnitude size difference between *Hadrocodium wui*, estimated to have had a body mass 2 grams (Luo et al. 2001b). *D. virginiana,* like all marsupials, has only one set of ante-molar teeth instead of the two as in most placental mammals, with the exception of the upper and lower p3's (van Nievelt and Smith 2005). Marsupials (including *Didelphis*) have a medially inflected angular process with a more expanded area for insertion of the medial

pterygoid muscle and superficial masseter muscle (Turnbull 1970; Lautenschlager et al. 2017), which may affect the degree of roll and yaw each hemimandible is capable of.

***Goals of thesis chapter 1***

Given the paucity of 3D kinematic data for hemimandibular kinematic systems, the first goal of this project was to describe, quantify and define the chew cycle for an unfused hemimandibular system, using *Didelphis virginiana*. The null hypothesis is that the vertical kinematic phases used in fused mandibular systems will apply to unfused hemimandibles. The second goal was to critically examine the contribution of yaw and roll to the "occlusal phases" of the gape cycle. That is, does the jaw yaw and roll around and during tooth-tooth contact (occlusion) and what is the relative importance of the two?

To make sure I were not measuring something that happened to be unique to a specific type of food, I chose two foods with vastly different mechanical properties that were relatively easily quantifiable: cheddar cheese and California almonds. I predicted that the viscoelastic cheese would be softer and thus easier to chew, while the relatively hard and fibrous almond would require more effort to masticate. I expected that these two foods would result in distinct hemimandibular kinematics.

## Materials and Methods

Bilateral mandibular kinematics were recorded in Virginia opossums using biplanar videoradiography and the XROMM (X-Ray Reconstruction of Moving Morphology) workflow (Brainerd et al. 2010). All experiments were approved by University of Chicago's IACUC (ACUP 72476). Animals were acquired under permits from the Illinois Department of Natural

Resources (Wildlife Capture Permit numbers NH19.6055 (2019), NH20.6055 (2020), and W21.6454 (2021)).

Two male and three female wild-caught opossums were housed at the University of Chicago Animal Resource Center. Each animal had all teeth erupted and present, no obvious gingival wounds or infections, and no cavities exposing the pulp. At least two weeks before data collection each animal was sedated (20-25 mg/kg ketamine), intubated and anesthetized (1-4% isoflurane) for surgical placement of 1 mm tantalum bead markers (CE certified, manufactured by RSA Biomedical for implantation in humans (http://www.umrsa.com/umrsa/marker_insertion.php). Two markers were surgically implanted in each of the right and left zygomatic arches of the cranium, and four were implanted in each hemimandible: two in the symphyseal region, one in the anterior border of the ramus at or above the level of the toothrow, and one on the medially inflected angular process of each mandible. All markers were placed through small incisions, and pressed firmly into 1 mm diameter holes drilled in the bone with a small hand-held drill.

***Data Collection***

Kinematic data were collected at the University of Chicago XROMM Facility and uploaded to the XMA Portal for data storage. Opossums were fasted 12 hours before data collection. Each opossum was placed into an opaque plastic box (40 cm in length, 21 cm in width, and 20 cm in height) positioned next to the image intensifiers and allowed to settle. A small hole at the end of the box allowed a researcher to place a food item inside the box, which the animal could choose to eat or not. Data were then collected at a 200 Hz frame rate, 900 x 900

resolution with radiographic technique of 10 mA and 70-80 kVp, depending on the density of the opossum (see Table 1.1 for individual values). Animals were presented with a single food item and data collected in 10 s bursts until the final swallow. Complete feeding sequences could not usually be collected within the ten second time limit of the x-ray source, but multiple ten second bursts could be collected with only 1-2 seconds between. Trials were selected for upload to XMA Portal if all markers were visible in both frames for the majority of the 10 s interval and not occluded by either the position of the animal or the position of the box.

The animals were fed a range of food items with different material properties. For this study, I chose a relatively soft, deformable food (cheddar cheese) and a brittle food with an internal structure (almonds). Cheddar cheese cubes that were 2 cm on each side were chosen to represent a completely homogenous substance. Cheddar cheese was procured from Dinner Bell Creamery and was 32% fat and 25% protein by weight. Cheese is a viscoelastic material characterized as a biphasic material, with continuous protein gel phase (composed of protein, water, and dissolved minerals), interspersed with fat globules (Gliguem et al. 2009, Rogers et al. 2010). The higher the fat content, the more likely cheese is to form non-spherical globules in a rheological analysis. Rigidity (storage modulus) changes with fat content at lower temperatures (~10 deg C), but is similar across fat contents at biological temperatures (~25 deg C), which is thought to be a product of the fat rigidity decreasing with higher temperature to that of the protein gel network (Gliguem et al. 2009, Rogers et al. 2010). The reported storage modulus (elasticity) of fresh cheddar cheese with a 32% fat and 25% protein content at 25 °C is approximately 200 kPa, loss modulus (viscosity) is around 20 kPa (Rogers et al. 2010).

Full, raw shelled California almonds were used as a relatively hard substance that had to be broken down before being swallowed. Almonds were selected. Almonds are 52% fat by

weight, 2.7% protein, and 5% carbohydrates, 2% mineral, and 11% dietary fiber (Grundy et al. 2016). Almonds have a dry elastic modulus of around 360 +/- 20 MPa, a hardness of 140 +/- 2 KPa, and a rupture force of 8-140 N (depending upon which axis the almond kernel is loaded; Aydin 2002). Almonds are more brittle than cheese and will initially crack into large piece during deformation, then later become a non-homogenous paste where the majority of cells in an almond bolus remain unruptured (Grundy et al. 2016).

***Data Analysis***

Marker coordinates were tracked using auto- and manual tracking functions in XMAlab (version 1.5.5, Knörlein et al. 2016). The rigid body transformations were low pass filtered (20 or 30 Hz cutoff, see Table 1.1), exported from XMA Lab as .csv files and manually merged in Excel (version 2016, Microsoft INC.) before importing into Maya (2019.3.1, Autodesk INC.) following the XROMM workflow (Knörlein et al. 2016). Data were grouped by animal, pre vs. post transection, and food type. STL's for each animal were made using CT scans of either the live animal (Vimago L Base version, Epica) or the animal after death (GE Phoenix v|tome|x 240 kv/180 kv scanner). Specimens were scanned with a voxel size of approximately 80 microns with 170 kVp and 130 uA, 1300 projections, averaging of 3 frames and skipping 1.

A rest position for each animal was defined as a time point in data collection when the animal was not feeding, when the symphysis was in the midline, and gape (pitch) was low (see Table 1.2 for rest position values). In the rest position I set a midline cranial coordinate system and two separate hemimandibular axis systems. Our coordinate system followed that of Orsbon et al. (2018), in which both hemimandibular axes systems had the same positive sign (positive up, forward and right), rather than that of Bhullar et al. (2019) in which the axis systems were

mirrored across the midline. The origin of each hemimandibular coordinate system was set on the superior surface of the condyle at the midpoint between the mediolateral and anteroposterior dimensions (see Figure 1.1 D-F). The z-axis was oriented to pass above the lateralmost and medialmost extrema of the condyle (positive to animal right), the x-axis was oriented along a line from the top of the condyle to the infradentale (positive forward), and the y-axis is the cross-product of x and z (positive upward).

TABLE 1.1. Individuals and Food Type Chew Cycle Number

| *Data Collection Events* | | *Number of Cycles* | | | |
|---|---|---|---|---|---|
| Individuals | Food | Total | Right Working Side | Left Working Side | Filters (Hz) |
| *Opossum Li* | | | | | |
| | *Almond* | 68 | 33 | 35 | 30 |
| | *Cheese* | 41 | 16 | 25 | 20 |
| *Opossum Lu* | | | | | |
| | *Almond* | 68 | 39 | 29 | 30 |
| | *Cheese* | 41 | 21 | 20 | 30 |
| *Opossum W* | | | | | |
| | *Almond* | 35 | 10 | 25 | 20 |
| | *Cheese* | 78 | 45 | 33 | 20 |
| *Opossum M** | | | | | |
| | *Almond* | 43 | 35 | 08 | 30 |
| | *Cheese* | 18 | 10 | 08 | 30 |
| *Opossum A* | | | | | |
| | *Cheese* | 17 | 09 | 08 | 20 |

Measures of translation of points on the hemimandibles were made in a cranial coordinate system, with its origin in the midsagittal plane and level with the top of the two hemimandibular condyles (Figure 1.1 A). The y-axis (yaw) is oriented superoinferiorly, with superior as the positive direction, and the x-axis (roll) is oriented anteroposteriorly, with anterior

as the positive direction, along the midsagittal plane of the cranium. In Maya the ORel (Output of Relative Data) function was used to measure translations, relative to this midline cranial coordinate system, of the left and right lower first molar talonid basins (Figure 1.2 B, Table 1.3), as well as the superiormost point on the midline of each condyle, midway between the mediolateral and anteroposterior dimensions.

TABLE 1.2. Coordinate System Alignment in Rest Position

| | *TX* | *TY* | *TZ* | *RX* | *RY* | *RZ* |
|---|---|---|---|---|---|---|
| *Opossum Li* | | | | | | |
| *RC Midline Sagittal Axis* | 7.694 | -8.863 | 13.866 | -82.938 | -71.55 | 83.239 |
| *Right Hemimandibular Axis* | 5.681 | -8.802 | 13.91 | -59.653 | -70.707 | 49.115 |
| *Left Hemimandibular Axis* | 9.76 | -8.824 | 13.806 | -110.749 | -71.577 | 121.01 |
| *Opossum Lu* | | | | | | |
| *RC Midline Sagittal Axis* | 4.015 | 11.033 | 4.221 | 113.125 | 0.589 | -96.319 |
| *Right Hemimandibular Axis* | 1.832 | 11.349 | 3.224 | 112.638 | -4.884 | -83.403 |
| *Left Hemimandibular Axis* | 6.155 | 10.815 | 5.105 | 112.467 | 5.657 | -108.348 |
| *Opossum W* | | | | | | |
| *RC Midline Sagittal Axis* | 7.225 | 9.443 | 2.45 | 282.223 | -98.583 | 83.103 |
| *Right Hemimandibular Axis* | 4.865 | 9.301 | 2.407 | -6.634 | -76.433 | -0.413 |
| *Left Hemimandibular Axis* | 9.673 | 9.629 | 2.499 | 178.34 | -74.65 | -173.157 |
| *Opossum A* | | | | | | |
| *RC Midline Sagittal Axis* | 4.015 | 11.033 | 4.221 | 113.125 | 0.589 | -96.319 |
| *Right Hemimandibular Axis* | 1.832 | 11.349 | 3.244 | 112.638 | -4.884 | -83.403 |
| *Left Hemimandibular Axis* | 6.155 | 10.815 | 5.105 | 112.467 | 5.657 | -108.348 |
| *Opossum M** | | | | | | |
| *RC Midline Sagittal Axis* | 3.039 | 9.474 | 3.532 | 62.928 | -3.974 | 284.911 |
| *Right Hemimandibular Axis* | 1.208 | 9.002 | 4.509 | 57.142 | 1.674 | 295.687 |
| *Left Hemimandibular Axis* | 4.889 | 9.902 | 2.561 | 68.778 | -9.124 | 632.381 |

*Opossum M was excluded from most analyses because of an undiagnosed cavity found postmortum. Opossum M was left in for final, comparative analysis.

TABLE 1.3. Lower First Molar Coordinates for Helical Axis Centroids

| | *TX* | *TY* | *TZ* |
|---|---|---|---|
| *Opossum Li* | | | |
| *Right Hemimandible* | 7.047 | -11.745 | 19.361 |
| *Left Hemimandible* | 9.108 | -11.75 | 19.228 |
| *Opossum Lu* | | | |
| *Right Hemimandible* | 2.918 | 4.834 | 2.357 |
| *Left Hemimandible* | 4.831 | 4.602 | 3.14 |
| *Opossum W* | | | |
| *Right Hemimandible* | 6.295 | 7.128 | 8.303 |
| *Left Hemimandible* | 8.367 | 7.325 | 8.343 |
| *Opossum A* | | | |
| *Right Hemimandible* | 6.362 | 6.519 | 7.456 |
| *Left Hemimandible* | 8.305 | 6.689 | 7.295 |
| *Opossum M** | | | |
| *Right Hemimandible* | 3.018 | 3.625 | 3.484 |
| *Left Hemimandible* | 4.938 | 4.028 | 2.534 |
| | | | |

Any cycles that obviously contained phase I transport or swallows were excluded from our analyses: I focused on chewing cycles. Relative movement data were exported from Maya as translations and rotations (in .csv format), then imported into Matlab (version R2020b) for analysis. Jaw kinematic data were divided into separate chew gape cycles at maximum gape, i.e., the most negative value of pitch for a given time frame using the 'findpeaks' function in Matlab. Each cycle was then divided into right or left chews using right lateral translation data from the right lower M1 talonid basin. After right of left identification, phase transitions within each chew cycle were identified.

### *Phase and Phase Transition Identification*

Our initial goal was to quantify kinematics using the gape cycle phases described in the literature (Crompton and Hiiemae 1970; Hiiemae 2000; Reed and Ross 2010; Ross and Iriarte-Diaz, 2019). I defined the start of each of the four gape cycle phases using a peak-finding algorithm that identified only the top three negative peaks in the second derivative of pitch (gape angle). Any chew cycle that had fewer or more peaks was excluded. These peaks corresponded to the start of each phase, in order: slow close, slow open, then fast open. The fourth phase, fast close, was defined as the time from maximum gape to onset of slow close. As a first pass, this four-phase system worked out well, as four phases were identified for the majority of the chew cycles in both almond and cheese trials for all individuals. However, when phase cycle transitions were mapped onto a 3D X, Y, and Z coordinate traces of the position of the lower first molar talonid basin, it was clear that the algorithm identified the start of slow close at one of two clusters. Furthermore, when it identified the earlier peak, often the second peak was classified by the 4-phase algorithm as the start of slow open, even though the lower molar was still moving towards the cranium and gape was decreasing. I concluded that the algorithm was switching between two different peaks in the first third of the chew cycle. I decided to subset the chew cycle into two parts before peak identification: a first third and last two-thirds. On a practical level, I used less than 35% as a cutoff for the first third and greater-than 35% for the last two-thirds. I chose this cutoff as it identified the greatest number of cycles with the target number of phase transitions (which was now two for < 35% and two for > 35%). This resulted in better grouping of phase changes when they were plotted with the translation coordinates. The average standard deviations of averaged chew cycle traces within each phase also decreased, suggesting that this method identifies more natural, replicable biological phenomena.

I also sub-divided slow close into two phases because, as reported for *Monodelphis* by Bhullar et al. (2019), many gape cycles in our *Didelphis* individuals exhibited a reversal in roll direction (RX) mid-slow close (Figure 1.1 A, Figure 1.2 F-G). To identify this peak, I used the maximum peak in roll within the timeframe of slow close, which was the most positive peak for the left mandible and the most negative peak of the right mandible (inversion and version in roll having different signs). This divided slow close into two phases: Slow Close 1 (SC1), when the tooth row of the mandible is inverting; and Slow Close 2 (SC2), when the tooth row begins everting.

***Phase Transition Analyses***

Using these phase transition data, phase duration was calculated for each of the six phases in each gape cycle. Phase durations and transition times were then averaged in raw time, as well as expressed as a percent of cycle duration from zero to 100. With the data organized and visualized, we tested if right working, right balancing, left working, and left balancing hemimandibles were temporally different. I also quantified changes in roll and yaw specifically, so I took the difference at the beginning and end of each phase in roll (X-axis rotation) and yaw (Y-axis rotation), and compared this with the difference in mediolateral and anteroposterior translation.

***Helical axis analysis***

I also augmented our study with a helical axis analysis. The helical axis (HA) is an alternative method for analyzing movement data. It calculates the axis of rotation (also known as

a screw axis) for a rigid body between any two time points. In biomechanics it has been applied to modeling of knee and ankle joints (Blankevoort et al. 1990; Sheehan 2010), and human mandibular movement (Gallo et al. 2005, 2006). The most extensive deployment of it in 3D kinematic studies of chewing is the work of Iriate-Diaz et al. (2017) on the location of the instantaneous helical axis of the mandible in three species of primates: baboons, macaques and capuchins. The HA method uses the rigid body coordinates of a reference rigid body (in this case, the cranium) and the rigid body under study (the left or right hemimandibles) at the same time points and calculates a center of rotation, effectively combining the translations of all three axes into one. This calculation, the instantaneous helical axis, can be calculated using differences in rigid body position between any two time points as long as the measurement error is smaller than the rate of change in the position of the rigid bodies.

The HA was calculated using the rigid body transformation matrix exported from XMAlab, loaded into Matlab to apply the HA Matlab code written by JD Laurence-Chasen (JLC) of the Ross Lab (https://github.com/jdlaurence/XROMM_HelicalAxis). The code calculates the helical axis of a given hemimandible relative to the cranium and exports the 3D points of the axis for visualization in Maya. The Matlab code also calculates the shortest distance from the helical axis to the talonid basin of lower M1.

Data, including STL's of the opossum cranium, hemimandibles, and marker positions are available on request; Matlab files and raw data files are available through XMAPortal (https://xromm.rcc.uchicago.edu/).

## Results

Traditional studies of chewing kinematics follow Hiiemae and Crompton (1985) in dividing the gape cycle into four vertical kinematic (VK) gape cycle phases (*sensu* Ross and Iriarte-Diaz 2019). However, as discussed in the Methods, our analysis suggested that 3D hemimandibular kinematics in the opossum are best described using six phases. The traditional FC can be divided into two phases, FC1 and FC2, using distinct peaks in pitch velocity (blue in Figure 1.1), and SC can be divided into SC1 and SC2 on the basis of a negative peak in mandibular roll.

A basic description of kinematics of the working side jaw during chewing is given in Figures 1.1 and 1.2. Figure 1.1 A illustrates movements of the left mandible relative to the cranium during a left-sided chew. This is an anterior view at a coronal section through cranium and mandible at the level of upper and lower M1s. Numbers correspond to numbering in Figure 1C, which gives mandibular pitch (blue), yaw (green), and roll (red), the time of the boundaries between VK gape cycle phases, and our newly proposed six phase model. Rotations in this graph are for the left-handed mandible only.

At the start of fast close (FC1), the mandible is at maximum gape and maximum eversion (Figure 1.1 C, circle 1). From maximum gape the hemimandible pitches upward, yaws buccally, and the toothrow inverts. In Figure 1.1 C, circles 2 and 3 are time points that correspond to noticeable slowing in pitch velocity represented by peaks in the second derivative of pitch. The first of these peaks (FC1-FC2) seems to be associated with negative peaks (maximum inversion) of the balancing side mandible (Figure 1.6). The second of these peaks in Figure 1.1 C (circle 3) corresponds to the start of slow close (SC), likely to be when the upward pitch of the mandible is slowed by the teeth meeting the food, the start of what is often called the power stroke.

SC can also be usefully divided into two phases SC1 and 2. The transition between them (point 4 in Figure 1.1 C) is the time of maximum eversion during SC. As the jaw moves upwards and into SC it is inverting, but around the beginning of SC1 the mandible starts to evert, then reverses roll direction again to invert. This time, when the mandible begins to invert again, is our proposed boundary between SC1 and 2 (Figure 1.1 C, point 4). At this time the mandible also changes yaw direction from a lingual to a buccal yaw and is probably also starting to pitch downwards, i.e., open. However, the exact time of minimum gape is difficult to reliably identify in a hemimandible that is not only pitching, but also rolling. Point (5) is the most replicable time for the start of slow open (SO), during which the mandible pitches negative, continues to yaw lingually, and gradually everts. Point (6) approximates the start of late SO, when the working side mandible more slowly pitches down, everts, and yaws lingually. Point (7) is the end of SO and start of FO, when the midline rapidly pitches down and yaws lingually.

***Change in rotations and translations by phase***

Change in rotations of the working side hemimandible and translations (y-axis values) of the lower working side M1 (for right and left chews) was measured as the difference in the average y-axis value from the start of each phase to the end, with standard deviation calculated as $\text{sqrt}([SD1]^2 + [SD2]^2)$. This metric is useful to characterize the overall change, but can mask small successive increases and decreases within each phase. That is, if a trace increases and decreases repeatedly by amounts between the minimum or maximum value, that change would not be reflected in the bar plot. However, the metric is a good general descriptor to evaluate our novel phase transitions and creates an intuitive baseline for comparison.

***Yaw versus roll***

Bhullar et al. (2019) argue that yaw is important for "positioning the toothrow" (presumably during FC) and roll is a greater contributor to "the mechanism of grinding". Before using *D. virginiana* to test this hypothesis I first evaluated whether jaw kinematics in *Didelphis* are similar to those of *Monodelphis*. In absence of quantitative data on yaw and roll for *Monodelphis* I made qualitative comparisons of our data with graphed data for *Monodelphis* (Bhullar et al., 2019: Fig. 3b). Our data show that, as in *Monodelphis*, the working side mandible of *Didelphis* inverts through the FC-SC transition, then everts and again inverts during SC. (Our point 4 (SC1-2) corresponds to the peak eversion of the working side mandible during SC.) On this basis *Didelphis* is an appropriate model with which to compare the relative importance of yaw and roll. I quantified the magnitudes of yaw and roll and of ML and AP molar translation during each of the six phases of the gape cycle; these data are plotted in Figure 1.3 F. If yaw is important for "positioning the toothrow" I expected greater yaw than roll during FC. However, if roll is more important for grinding, I expected to see greater roll than yaw during SC. All individuals showed significant left-right asymmetry in relative proportions of yaw and roll in different phases, so I present the quantitative data of working sides to test the hypothesis of the relative contribution (thus the importance) of yaw and roll to the hemimandibular kinematics.

Contrary to Bhullar et al. 2019, yaw is not consistently greater than roll during FC1 or 2. During FC1, out of our ten working side data sets, three showed greater yaw than roll, five showed greater roll than yaw, and two were roughly equal. During FC2, four showed greater yaw than roll, four greater roll than yaw, and two were equivocal. Importantly, some individuals show working sides with more yaw than roll in FC1and more roll than yaw in FC2, while the reverse is true for other opossums (Opossum Li, R & L; Opossum Lu, R; Opossum W, R & L; Opossum A, R & L). Thus the new results from *Didelphis* show that both roll and yaw contribute to mandible

kinematics during fast close, but the extent and proportion of the contribution are variable by individuals.

Bhullar et al.'s hypothesis regarding importance of roll and yaw during SC receives only mixed support. During SC1, roll is greater than yaw in working sides of five individuals, yaw is greater than roll in four working sides, and in one case yaw and roll are about equal. The roll > yaw hypothesis receives greater support during SC2, when eight sides show greater roll than yaw and two show greater yaw than roll (Figure 1.3 H). However, the importance of grinding in SC2 appears to be minimal. I quantified lower M1 translation in AP and ML directions during all phases: I focus here on SC1 and 2 (Figure 1.1 C). During SC, transverse translations increase in relative importance, being absolutely and relatively greatest during SC1. ML translations predominate in SC2, but the absolute magnitudes are smaller or even negligible to the point to be indistinguishable from noise sometimes. The fact that transverse components of lower M1 translation are largest during SC1, and that there is no clear predominance of yaw or roll during SC1, calls into question the hypothesis that "grinding" during occlusion is driven primarily driven either by yaw (Grossnickle 2017) or by roll (Bhullar et al., 2019).

It is clear that the *Didelphis* individuals show much wider range of variation in both rotation and translation than previously suspected. Therefore the *Didelphis* kinematics data do not show the same degree of stereotypy mentioned by Bhullar et al. (2019) in their *Monodelphis* study. Long axis rotation (RX) was not symmetrical between the working and balancing sides over the same phase duration (Figure 1.3), in averaged traces of individual variables (Figure 1.6), or in 3D traces (Figures 1.14 and 1.15). For example, the balancing side often reverses direction at the transition from FC1 to 2, while the working side shows a more oblique reversal (Figure

1.3). Working sides were more similar in timing of these reversals, as were balancing sides, than a working-balancing side pair for the same set of trials.

### *Helical axis*

The use of roll, yaw, and molar translation data is one way to quantify hemimandbular jaw kinematics. The helical axis method provides a useful adjunct method that does not depend on the decisions of the researcher when setting up axes of measurement. Instead of decomposing movements into rotations about arbitrary axis systems, a single (helical) axis is calculated using differences in object orientation between two time points. I averaged data across every three time points, i.e., every 0.015 seconds of the chew cycle (see Figure 1.4), and then related helical axis dynamics to the gape cycle phase timing. Data are only presented here for chews on the right side; i.e., the right mandible is the working side.

At the beginning of FC, the helical axis passes through or just posterior to the animal's working-side condyle. The axis is angled antero-laterally, reflecting components of both pitch (gape) and roll, with little or no yaw. During FC1, the axis swings to pass through or just posterior to both condyles, reflecting the dominance of upward pitch; and the HA swings in superior view for the yaw dimension slightly counter-clockwise, in lateral for the roll dimension clockwise (Figure 1.1 D). At the start of FC2 (point 2), the helical axis has shifted from FC1, and it has moved laterally to the working side, initially perpendicular to the long axis of the working side mandible (Figure 1.4 E), and concurrently it swings counter-clockwise in a greater magnitude (than FC1), and is directed anterolaterally and anteroinferiorly during FC2 (2-3) (Figure 1.4 E). The HA is positioned dorsolateral to the mandible itself, so that rotation about this axis yaws the mandible lingually.

At the end of FC2 and start of SC1 (Figure 1.4 E, F, point 3), in right lateral view, the axis is superior and roughly parallel to the posteroventral portion of the mandible. From a dorsal view, the axis is ca. 30-40 degrees off from paralleling the right working mandible. During SC1 the axis moves clockwise in a slightly oblique horizontal plane (Figure 1.4 F). The axis also moves through the teeth, passing through the lower first and second molar, and the first premolar as the axis rotates. By the end of SC1 the direction of the helical axis changes again to move clockwise from the superior view and it reversed the previous counter-clockwise movement in superior view during FC2 (Figure 1.4 E). This change is a reversal of both yaw and roll seen in the averaged rotations (Figure 1.4 A, 'SC1' label). Roll and yaw predominate in SC1, but the pitch change, although noticeable, is much less than the previous FC1 and FC2 phases. This indicates that the axis of rotation is constantly changing in all three dimensions throughout the SC1 phase. By the end of SC1 the axis is parallel to the mandible from the superior view and just lateral to the tooth row. From a right lateral view, the axis is angled so that it appears to go through the canines and incisors and above the posterior molars.

During SC2 (Figure 1.4 F black circle 4, Figure H grey circle 4) the axis is pointing posteriorly, reflecting a major reversal of roll. The part of the axis pointing anteriorly (now the "back" of the axis) continues to rotate in a clockwise direction from the superior viewpoint and inferiorly from a right lateral viewpoint. The part of the helical axis pointing posteriorly (the "front" of the axis) moves medio-inferiorly and remains in front of the condyle. The working hemimandible is inverting at the tooth row and yawing buccally.

In summary, the helical axis changes significantly during the fast close and slow close phases, and reverses during SC 2. This corroborates our newly proposed subdivision of the FC1 vs FC2, and SC 1 vs. SC2.

At the start of SO (Figure 1.4 I) the helical axis continues to rotate clockwise, swinging laterally towards the balancing side (in superior view) and moving into the horizontal plane above the molars from a lateral viewpoint. The axis also moves posterior to or through the right working condyle. SO is a protracted phase relative to the other phases. As SO continues (Figure 1.4 J), the helical axis itself (i.e., not the axis of rotation direction, but the movement of the whole axis) begins to rotate in a counterclockwise direction in the horizontal plane, so that the axis of rotation moves to be just behind and inferior to the condyle. The axis of rotation is pointing toward the balancing side. The end of this portion of the phase (Figure 1.4 J black circle 6) is near circle 6 (Figure 1.4 A). SO continues (Figure 1.4 K) counterclockwise and then clockwise in the horizontal plane. The axis of rotation points laterally toward the working side, posteriorly, and then laterally again by black circle 7 (Figure 1.4 K). At FO (Figure 1.4 L), the axis moves from going through both mandibles to the working side, pointing toward the left of the animal. At the transition of FO to FC, the axis will flip to the animal's right.

***Food Type***

The smallest effect of food type was on gape angle (pitch) (Figure 1.5); the greatest effect was on roll, with cheese chew cycles being more variable than almond cycles, especially during SO. Maximum gape for almonds is consistently smaller than maximum gape for cheese, with a difference of 5-10 degrees depending on the individual. Minimum gape is reached at or within slow close 1 and there is no clear, defined "peak" of minimum gape for any of the opossums. The beginning of fast open has the most distinctive change in slope. Opossum W, which had a wider range of maximum gape for cheese on the right and left working sides, with both sides showing more variation at maximum gape and consequently FC1. The right working (and left

balancing) side also show more variation at the end of slow open and the start of fast open. The major exception to these trends is Opossum M especially on its left side, which had a cavity (infected tooth) in the left teeth. Eating almonds, Opossum M had a shallow maximum gape on the left working side, with a total gape range of only a few degrees, and a right working side maximum gape of -10 degrees.

For roll (Figure 1.6) cheese trials always had a larger standard deviation than almond trials. The phases with the largest difference between cheese and almond were FC1 and 2, and FO, which is consistent with the changes seen in gape. SC1 and 2 show less inversion and eversion for both working and balancing sides. SO has the widest standard deviation and thus the most variable movement. In Opossum M, there was less roll for the left working and balancing sides for almond. However, movement is equivalent to the other individuals for cheese.

There was also slightly less or equivalent yaw (Figure 1.7) for cheese trials relative to almond trials. The greatest change is seen in the SC phases, with less lingual yaw in SC1 and less buccal yaw in SC2.

Supero-inferior translation (Figure 1.9) was more variable for cheese than for almond. Cheese trials also consistently had a greater minimum value (inferior direction) at the start of FC (i.e., cheese trials always showed more superoinferior movement). Cheese cycles were more variable from FC2 through SC1 and again from either mid or late SC2 through SO. Opossum W showed more variation for both almond and cheese at FC and FO. Opossum M has ~5 degree supero-inferior translation for almond left working side data, while the minimum value for cheese shows ~25 deg of variation. Opossum M cheese trial data is also the only data set where the right mandibular kinematic traces match and left mandibular kinematic traces match,

regardless if they are balancing or working. All other traces are correlated more tightly with either working/balancing state or by right-left hemimandibular pairs.

Mediolateral translation (Figure 1.10) showed the most variation for cheese and almonds out of all three translation dimensions. There was consistently more variation for cheese than in almond. The working side and balancing side averaged traces were very similar, as expected with the connected symphysis. The most variation was seen at slow open. FC 1 and 2 also showed variation. SC 1 and 2 had the most consistency. Opossum M showed very little change in medio-lateral translation for the left working condition.

Anteroposterior translation (Figure 1.10) changed the most in FC and FO for all individuals, decreasing in value and thus moving anteriorly. FC1 showed a positive change. FC2 slope is still decreasing, but at a slower rate. SC 1 and 2 change was either negligible or showed small decrease (i.e., small anterior movement) relative to the FC phases. SO would always begin to decrease (posterior movement) at the end of the phase, but would sometimes have a separate decrease at the start of SO as well. FC showed a steep decrease equivalent to FO.

***Phase Timing Change and food type***

In general, giving an animal two different food types changed phase duration, but this response was different for every animal (Figure 1.13). When the SC cycles are combined to make one phase, SC as a whole was longer for almonds than for cheese and the combined FC cycles were longer. FO was also almost always longer for cheese, and the SO to FO transition had the least amount of variation.

### *3D Traces and food type*

Antero-posterior, mediolateral, and supero-inferior coordinates of movement at the right and left lower molar talonid basins were mapped out for each chew cycle by animal, food type, working side, and right or left mandible (Figures 1.14 and 1.15). The traces are oriented as if the opossum is facing the reader, with right hemimandibles on the reader's left and the left hemimandible on reader's right. The cycles were then labeled with molar location at phase transitions, augmenting our understand of where in space each transition occurred. Overall, no opossum had averaged traces that were indistinguishable from another individual, as is to be expected with biological variation. Balancing sides followed the paths of the working sides, but often smaller gape and mediolateral translation. Almond traces formed an elongated bean shape that was concave toward the working side and convex toward the balancing side.

Each trace starts at maximum gape (darker blue dot) and moves laterally to the opossum's right for right working side and left for left working side. For almond traces, FC2 (Figure 1.14, red dots) initiates approximately half way through jaw closing and was not easily visible on the trace without the phase transition data. Opossum W and A initiated FC2 closer to the superiormost portion of the cycle when compared to the other opossums (Figure 1.14 G-J). SC1 (Figures 1.14-15, yellow dots) initiates towards the superior part of the trace, as the trace inflects medially, away from the working side. It is difficult to say where tooth-food-tooth or tooth-tooth contact initiates, as this was not directly measured. Despite their proximity, yellow and red dots do not often overlap (but see Figure 1.14 H). The superiormost position is reached at the start of SC2 (Figure 1.14, purple dots), the start of SO (Figure 1.14, green dots), or some time point in-between. There was no definitive correlation between a specific phase, phase transition, and the superior-most excursion of the lower mandible. SO (Figure 1.14, green dots to

blue dots) had the greatest amount of directional change within a phase, tracing a superomedial "bump" that was not reflected in a phase transition. FO (Figure 1.14, light blue dots) begins just after the "bump" and runs inferiorly and slightly lateral to maximum gape and the start of the next fast open.

3D traces for cheese cycles (Figure 1.15) were more variable and less consistent than almond cycles. In general, the chew cycles had a flattened bean shape, with more abrupt superior and inferior maximum excursion points. Phase cycle changes were more mediolaterally variable and the start of FC1 was more variable superioinferiorly. Like almond, the starts of SC1, SC2, and SO converge on a small area superiorly, showing the likely area where the lower first molar is contacting the upper. SO is also mediolaterally variable and often doesn't have that distinct "bump" (see discussion). FO often begins moving toward the working side, but again this was not consistent as in almond.

Even opossum M (Figure 1.14 K-L), which was pathological and had a cavity on the left side, showed consistent phase transitions and a bean-shaped trace on the right working side. However, in comparison with the other individuals gape was reduced on both sides, causing the trace to have a "squished" appearance.

## Discussion

This chapter presents the most detailed 3D quantification of hemimandibular kinematics in a mammal to date. The data in this study show that hemimandibular kinematics during mastication are more complex than those reported for fused mandibles of e.g., macaques, although more detailed analyses of macaque mandible kinematics are clearly needed. The traditional sequence of vertical kinematic phases of the gape cycle (FC, SC, SO, FO) does not

fully capture the complexity of hemimandibular kinematics in opossums. In particular, division of SC into two phases is needed to fully understand the complexities of roll kinematics during food breakdown.

Hemimandibular kinematics are also more variable than previously suggested in the literature (Bhullar et al., 2017), varying by individual, left versus right side (working or balancing), and food type. The SC phases took up the greatest amount of time relative to the distance traversed, about a quarter of each chew cycle for the distance of a couple millimeters (Compare the yellow and purple bars in Figure 1.13 with the distances from the yellow to green dots in Figure 1.14). The greatest variation in timing was seen in the FC and SC cycles. Minimum gape position was also more variable than expected and could not be easily or consistently used as a criterion for transition from SC to SO. Working sides were more similar to each other than their balancing side counterparts (with the same for balancing side).

### *Yaw vs. Roll*

Bhullar et al. (2019, 2020) and Grossnickle (2017, 2020) express differing opinions regarding the relative importance of yaw and roll during the power stroke of mastication in opossums. Grossnickle used 2D morphometrics of the mandible and lever mechanical analyses, as well as a deep understanding of morphology early mammal fossils, to conclude that yaw is a key kinematic function in the early tribosphenic therian evolution. Bhullar et al. used a novel visualization method and actual kinematic data to show that mandibular roll is an important and prevalent component of jaw movement during SC, and presumably the power stroke.

The data from this thesis work show that both yaw and roll (like pitch) are essential aspects of jaw kinematics during FC2 and SC. During SC1, when the lower molar talonid shows

the greatest translations, yaw and roll seem to be equally important, although can vary depending on the chew side and the individual animal. During SC2, when roll shows greater magnitudes than yaw, molar translation is minimal. If "grinding" is defined to include translation, then the grinding functioning of the tribosphenic molar during SC1 can be achieved by either roll or yaw.

Thus the new data of rotational movement, translation of molars, and helical axes of *Didelphis virginiana* do not support the premise of a binary question whether yaw is the prevalent driver, or the roll is the prevalent driver of molar grinding (Bhullar et al. 2019; 2020; Grossnickle 2017; 2020). In FC2 and SC, yaw and roll are both contributing to overall kinematics of hemimandibles. Our results show that the greatest magnitude of yaw rotation and the anteroposterior translation occurs during the fast close, and then yaw and A-P translation decrease rapidly during SC1. These results are consistent with the interpretation that yaw plays a major role in manipulating the mandible to ready the jaw for (although prior to) the actual occlusion, as suggested by Bhullar et al. (2019).

***Food Type***

Food type matters. Differences in food toughness and viscoelasticity greatly influence the magnitude of rotation and yaw, but the overall kinematic movements in roll (Figure 1.6) and yaw (Figure 1.7) were both present at the same averaged time points for the majority of animals. Timing in the combined SC1 + 2 phase was significantly (in the statistical sense) longer for cheese chew cycles, but by parsing out the phase into SC1 and SC2, the correlation between longer timing in SC and cheese went away (Figure 1.13). Cheese cycles were more difficult to side using the mediolateral (TZ) criterion that worked well for almond cycles. This can be seen most easily when comparing 3D traces for SO (Figures 1.14 and 1.15). Many cycles did not fit

easily into either classic right working or left working chews, which likely accounts for a lot of variation in SO phases during cheese chewing. A few possible explanations for these results need to be examined. One could be that the tongue is moving a lot at SO. The viscoelastic property of cheese could be causing the cheese to stick to the teeth and thus require more work to adjust. However, masticated almond particles mixed with saliva are also known to stick to teeth (Grundy et al. 2016). Another possibility is that the opossum is using both sides of the hemimandibles at the same time and there is no one dominant working side. To discriminate among these possible scenarios, it requires further examination of how much the balancing side is contributing to mastication.

Food type effects may also be obscured by averaging. Foods are known to change physical properties over the course of the chew cycle. In capuchins, foods of high toughness had less variable cycle durations throughout the sequence, while foods of low toughness had shorter chew cycles at the beginning of a chew sequence and longer cycles at the end, primarily due to increases in SO and FO, and concurrent decreases in SC phases (Reed and Ross 2010). After cycle fifteen, the initial starting state of the food (the toughness) appeared not to matter, which was hypothesized to be because the now homogenized particles were being moved by the tongue to the oropharynx for deglutition. Low toughness foods also had greater horizontal excursion and smaller average gape. I also saw a smaller gape with the low toughness food used in this study (cheese). The mediolateral translation was the opposite of capuchins, with the high toughness food (almonds) showing more mediolateral excursion during SC. This could be because capuchin teeth are bunodont and do not ‘lock’ into place the same way tribosphenic molars do during SC. There are also the added differences of a fused vs. unfused symphysis. Sequence order was not considered for this initial study. I opted to average all chew cycles by a given

individual and food type. Recording complete chew sequences was not possible due to the ten second limit of the UC biplanar radiography machine. This could have led to a homogenization of chew sequence, where the pre-first swallow chews are partially or wholly obscured by the later chews, which are hypothesized to match across food types. Chew sequence duration could be measured, giving an estimate of the number of chews missed between 10 second radiation bursts (approximately 1 second elapses between bursts), and then chew sequence number could be estimated with the given data. I could then test intra-sequence variation, and I expect there to be a greater number of total chew cycles before the first swallow for the tougher almond data. I also expect that the post-swallow chews for both almond and cheese would become more similar to each other later in the chewing sequence.

***Slow Close vs Occlusal Phase vs Centric Occlusion vs The Power Stroke***

The end of SC and the start of SO are historically defined by minimum gape. However, for opossums there were many traces where minimum gape seemed to happen at multiple points during SC. This is likely due to a combination of the occlusal morphology of the tribosphenic molar and hemimandibular movement. This phenomenon and other variabilities in opossum mastication warrant further study in light of the conclusions made about tribosphenic dentition and diet. Paleontologists and functional morphologists have been using microwear and tooth occlusal surface morphology studies to infer masticatory function, or even the dietary ecologies for 150 years (Ryder 1878, Osborn 1903; Wilson et al. 2012; Gill et al. 2014; Martin et al. 2020; Grossnickle et al. 2021). An important and looming question in mammal paleontology and human orthodontics is to what degree the occlusal surfaces of the teeth act as guides for jaw kinematics during mastication (Schultz et al. 2017; Jäger et al. 2019; 2020), independent of

muscular control. What exactly is 'precise occlusion', if minimum gape and the transitions of occlusal phases are variable and inconsistent?

Paleontologists studying mammalian mastication often infer relative tooth movement from tooth occlusal morphology. Osborn (1908) meticulously described the interlocking cones and basins of tribosphenic teeth (which he termed 'tritubecular teeth'), and suggested that *functionally* the occlusal surfaces could crush, shear, and slice. Simpson (1933) stated that there were four main types of interactions between opposing occlusal surfaces: alternation, opposition, shearing, and grinding. During 1960's and 1970's, tooth morphology especially the wear facets became useful indicators of occlusal direction through macro- to microwear striation patterns (Mills 1967; Crompton and Jenkins 1968; Crompton 1971; Mills 1971; Kay and Hiiemae 1974). As early as 1970's, Gorniak (1977) described *Mesocricetus auratus* (golden hamster) occlusion "The interlocking molar cusps of hamsters restrict protrusive, retrusive and true transverse movements" (measured in a dead individual) in the same paper where he meticulously describes muscle control of mastication in live individuals. Over the last 10 years, the occlusal contact surfaces have been used to model the movement trajectories of the teeth and jaw in simulation studies of Occlusal Fingerprint Analysis (OFA) (Kullmer et al. 2009, 2010; Schultz et al. 2017; Jäger et al. 2020). The shape of the tooth was thought to impose a hard limit on how the mandibles could move. Tooth morphology, especially the molar occlusal configuration are determinants of the biomechanical limits of mandibular movement.

However, it is also clear that there are severe limits on the degree to which dental morphology informs mandibular kinematics. For example, Scapino (1965) used molar and canine occlusion to argue that mandibular symphysis was mobile, while Mills (1966) used similar data to argue the opposite. More recently, electromyographic (EMG) signals from the

muscles of mastication have been used to infer masticatory phases, such as EMG pattern of the masseter as an indication of power stroke onset (Komuro et al. 2001). Orsbon et al. (2020) use 'intercuspal phase' and define it as the time when mathematical planes overlying the cusps of the upper and lower molars overlap. All these are valid ways that can measure different aspects of mouth form or function. However, these are proxies, and they do not directly measure the tooth-tooth, or tooth-food-tooth contact during the *in vivo* kinematic movement of the teeth and mandibles.

There is an obvious need to establish more detailed comparisons of the kinematic measurements of FC2, SC1 and SC2 to metrics of occlusion in live animal experiments. Such *in vivo* kinematic data on metrics of mandible in synchrony with metrics of molar occlusion would be valuable to determine to what extent chewing behavior can be estimated reliably from occlusal morphology and wear facets. Data from *in vivo* study could be used to *infer* contact from proximity of the occlusal surfaces of the opposing upper and lower teeth, and the change in speed itself. Biplanar videoradiography is just now at an accuracy level where tooth-tooth contact is measurable. The tooth-tooth or tooth-food-tooth contact is a very fast behavior on very small scale that happens over a few millimeters, and a challenge to accurate measurement of such contact is that it requires high resolution of the videoradiography. In addition, foods under mastication are constantly changing, and difficult to digitize and quantify in kinematics, even if these can be made radio-opaque. Often, the physical limits of the oral cavity and oropharynx are used as proxies to estimate the bolus size and constraints of movements (for example, see Mayerl et al. 2020). Perhaps a machine learning algorithm that can identify food particles as they change shape and consistency over the course of the food cycle, perhaps with an algorithm like

application by Laurence-Chasen et al. (2020) of DeepLabCut (Mathis et al. 2018, Mathis and Mathis, 2020).

### *Comparison with Fused Symphysis Biomechanics*

Hylander (1984, 1985; Hylander and Johnson, 1994) studied patterns of stress and strain during mastication in the fused symphysis of *Macaca fascicularis*. He found that the mandible was minimally loaded at jaw opening, with medially directed force from the lateral pterygoid muscles. During the power stroke, the jaw experiences the highest loads, with dorsoventral shear from the balancing side adductor force and 'wishboning' due to laterally directed forces during the bite as well as the adductor muscles. Hylander (1985) argued that the most efficient solution to decreasing strain in the symphyseal region during the power stroke is to add bone to the lingual aspect of the symphyseal region. Hylander et al. (2000) found that galagos (which have an unfused symphysis) had greater working side superficial and deep masseter mm. firing activity than anthropoid primates with fused symphyses. This leads to several questions about the movements and limits of unfused symphysis. Does a lack of symphyseal fusion lead to a lower limit for the amount of stress and strain a jaw can experience before failure? Are there clade-specific adaptations to unfused symphyses that experience high loads?

It is tempting to label the mirrored mediolateral movements in the opossum chew cycle 'wishboning', as in Hylander (1984, 1985) and assume that increased loads would cause increased movement of the hemimandible in the direction of the load, as the symphyses are semi-independent. However, I do not yet have the simultaneous strain or electromyographic data needed to analyze what is controlling and limiting hemimandibular movement. It is even unclear if the symphyseal ligament itself limits movement, or if it never reaches its full length during a

chew cycle. Therefore, in this study I purposefully did not use any terms associated with strain or load from the previous studies on mandibles with fused symphysis. I look forward to further work on this question.

***Slow Open***

Although this thesis mostly focuses on the "occlusal phases", that is, FC2-SC, slow open (SO) also displayed a variation worth of investigation. The 3D trace (Figures 14 and 15) and helical axis data (Figure 1.4) showed that there was a great deal of hemimandibular movement during SO. SO also takes up about a third of each chew cycle phase. In the helical analysis, the axis reversed direction twice, which can be seen in both roll (Figure 1.5) and yaw (Figure 1.6). Pitch (Figure 1.5) often shows a notable change in slope a little more than half-way through SO, which is why researchers in the past have suggested dividing slow open into two phases. Despite all this movement, pitch never shows a sharp change in acceleration. Thus, by our definition of using the second derivative of gape for the majority of our phases, there was no evidence for a phase transition in SO. Gape has a continuous acceleration at SO despite the (inferred) large amount of tongue movement and bolus re-adjustment going on. Just as I concluded that the second derivative of gape was not sufficient for describing hemimandibular kinematics at SC, perhaps the same is true for SO. Also, slow open phase is here shown to be more variable among individuals, even without much change in excursions in roll and yaw of the same individuals over multiple chewing cycles, in response to chewing cheese, a food type with softer, more deformable and viscoelastic properties.

### *Fast Open*

The most surprising aspect of fast open in opossums was that the mandible begins moving toward the working side before maximum gape. This can be seen in both the 3D traces (Figures 1.14 and 1.15) and by the helical axis (Figure 1.4). For cheese this was more apparent on the working side (Figure 1.15). This gives us another way to classify working-side chews. It also tells us that the decision to switch working sides (or not to switch and stay) is made before FO. It is possible that there may be some biomechanical advantage to moving over to the working side before maximum gape.

## Conclusion

This thesis work has measured the kinematics of six individuals of *D. virginiana* using biplanar videoradiography and found that hemimandibular mastication is fundamentally different from the condition of the fused condition. Such differences warrant an augmented set of phase definitions, as a refined framework better for kinematic analyses of hemimandibles. Each hemimandible is semi-independent from the other, allowing for novel rotations and translations not seen in fused mandibular system. The chew cycle in the hemimandibular system of *Didelphis virginiana* can be divided into six phases: fast close 1, fast close 2, slow close 1, slow close 2, slow open, and fast open. Jaw yaw decreases significantly from fast open 1 to fast open 2 and slow close, but there is only mixed support for a hypothesis of greater roll magnitude during the phases associated with occlusion (FC2, SC1, SC2, and the beginning of SO). A new observation is that food type has a significant effect on chew cycle kinematics. Cheese cycles were more variable among individuals of *D. virginiana* especially during SO, but showed less excursion for roll and yaw. The smallest effect of food type was on pitch (gape) angle and the greatest effect was on roll. When average traces are compared, balancing side chews were more similar to each

other than to their working side counterparts. The same can be said for the working side, showing that there is a degree of stereotyped patterning for working side and balancing side across most individuals of *D. virginiana*, no matter if it is left or right. Furthermore, roll and yaw, as measured by a joint coordinate system, impose limitations on phase interpretation. When a helical axis (HA) analysis was applied to find the axis of rotation of the mandible, the helical axis is determined to be outside the working side hemimandible for the majority of the chew cycles. The HA constantly changes over the course of the chew cycle and is superolateral to the working side hemimandible at the start of SC1. The axis then rotates in a clockwise direction, passing through the first molar with a movement that involves all three dimensions of rotation. I hypothesize that full utilization of the tribosphenic molar simply could not happen without pitch, yaw, and roll. It requires the biomechanical function in both roll and yaw of the hemimandible for a unique set of hemimandibular and dental morphologies to impact the diversification of therians with tribosphenic dentition in early mammalian history.

# CHAPTER 1

# FIGURES

FIGURE 1.1.

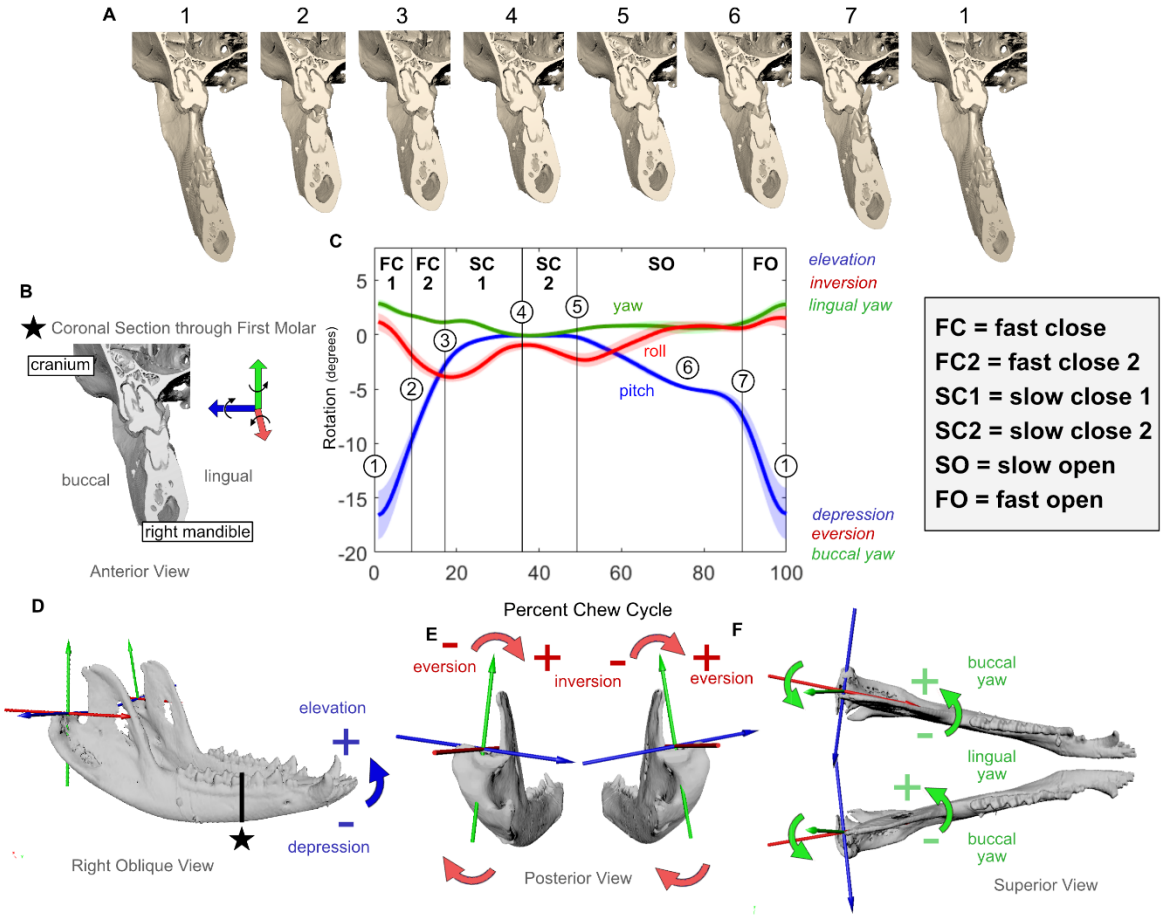


**Figure 1.1. Definitions of gape cycle phases, coordinate systems, and kinematic terminology.** (A) Movements of right mandible relative to the cranium during a right-sided chew; anterior view at a coronal section through cranium and mandible at the level of upper and lower M1s. Numbers correspond to numbering in (C). (B) Anatomical terminology on a coronal section through cranium and left mandible. (C) Mandibular pitch (blue), yaw (green), and roll (blue), and vertical kinematic gape cycle phases (*sensu* Ross and Iriarte-Diaz, 2019). Traces are averages +/- 1 S.D. for n = 39 chews on almond by individual Li normalized to a gape cycle duration of 100%. Numbers correspond to jaw positions in (A). Rotations in this graph are for the right mandible only. See (D, E, F) for definition and polarity of rotations. (1) Beginning of fast close 1 (FC1), the mandible is at minimum pitch (maximum gape), maximum lingual yaw, and maximum inversion. (1)-(2), FC1, hemimandible pitches upward, yaws buccally, and everts. (2) start of FC2, pitch often slows prior to SC, sometimes associated with a shift from buccal to lingual yaw.

**Figure 1.1, continued.** (3) Start of slow close (SC), time of largest decrease in rate of pitch during closing and usually of maximum eversion. (4) Time of maximum inversion during SC and often maximum buccal yaw; mandible begins to evert and yaw lingually. (5) Start of slow open (SO), as mandible pitches down, it continues to yaw lingually, but roll switches from eversion to inversion. (6) Early slow SO, the working side mandible is pitching down, inverting, and yawing lingually. (7) end of SO, mandible slows down, then in FO rapidly pitches down as it yaws buccally and everts. (D) Oblique view of mandibular axes, highlighting pitch. In both mandibles negative pitch is jaw depression (opening), and positive pitch is jaw elevation (closing). (E) Posterior view of left and right mandibles and mandibular axes, highlighting roll conventions for left and right mandibles. Positive roll follows the right-hand rule (clockwise in posterior view), corresponding to eversion of right mandibular tooth row and inversion of left mandibular tooth row. Negative roll is the reverse. (F) Superior view of the left and right mandibles and mandibular axes, highlighting yaw. Positive yaw is lingual for right mandible and buccal for left; negative yaw is buccal for right mandible and lingual for left. Origin of mandibular axis system is positioned at the highest point near the middle of the condyle, with the positive roll (X) axis (red) oriented to pass over infradentale at the level of the condyle; the positive yaw (Y) axis (green) oriented superoinferiorly (superior is positive); the positive pitch or gape (Z) axis (blue) is the cross-product of the two other axes, positive to animal right. Axis systems of left and right mandibles are similarly oriented (positive is anterior for roll, superior for yaw, and to animal's right for pitch).

FIGURE 1.2.

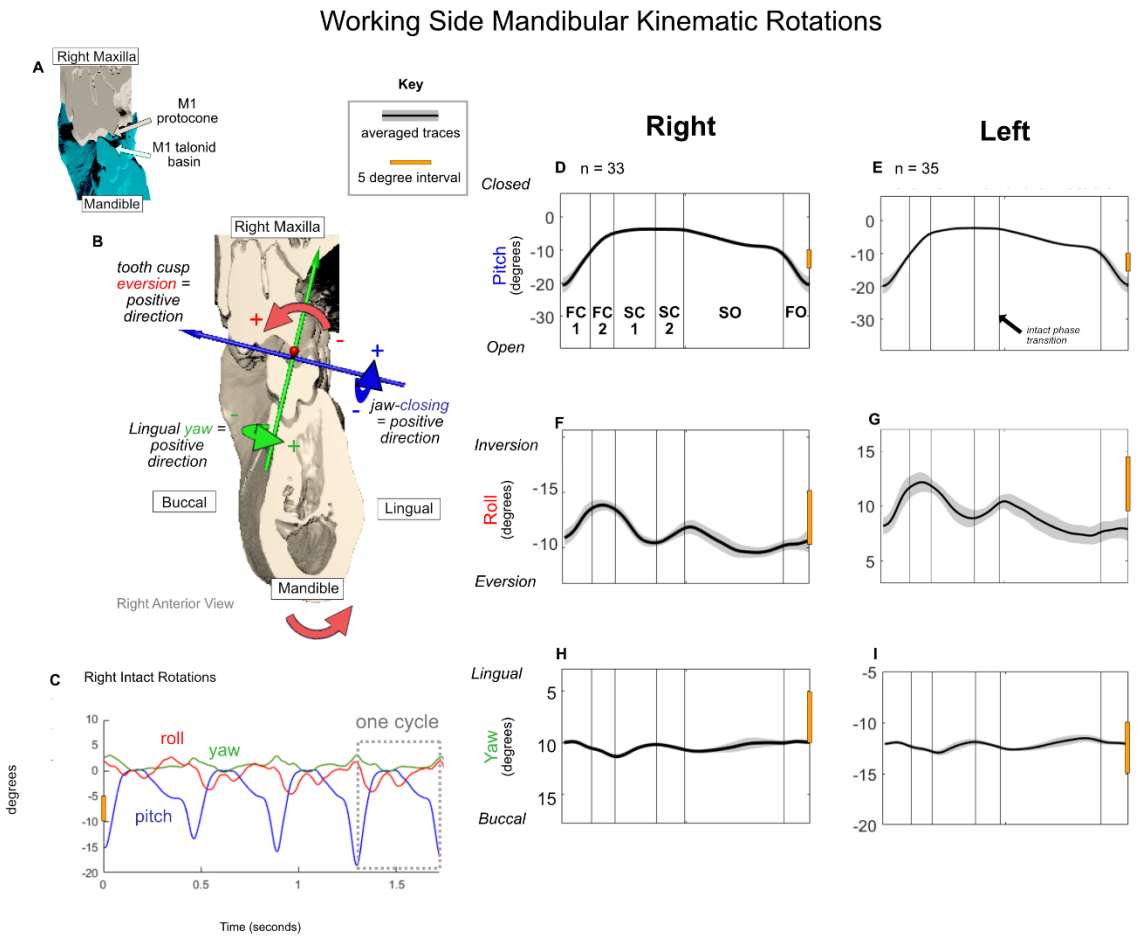


**Figure 1.2. Working side mandible kinematic rotations.** Food is almond, animal is Opossum Li. (A) Coronal section through right cranium and mandible showing focal molar cusps. Key for kinematic traces. Black solid lines represent kinematic traces; gray, +/- 1 S.D. (B) Anterior view of right molar with rotation coordinate system positioned (arbitrarily) at right first lower molar talonid basin. Arrows and descriptions indicate positive rotations for right mandible (cf. Figure 1.1D, E, F) (C) Plot of average right mandible rotations in an almond feeding sequence for intact condition. (D-I) Right and left mandibular working side rotations (black line). Black vertical lines mark phase transitions. The yellow bar on the right of each graph indicates a five-degree increment, highlighting different y-axis scales. FC = fast close, SC = slow close, SO = slow open, FO = fast open. The y-axes in (F) and (H) are inverted so that inversion/eversion and buccal/lingual yaw have the same polarity in the graphs for right and left mandibles; i.e., data for right mandible presented as if for left mandible.

FIGURE 1.3.

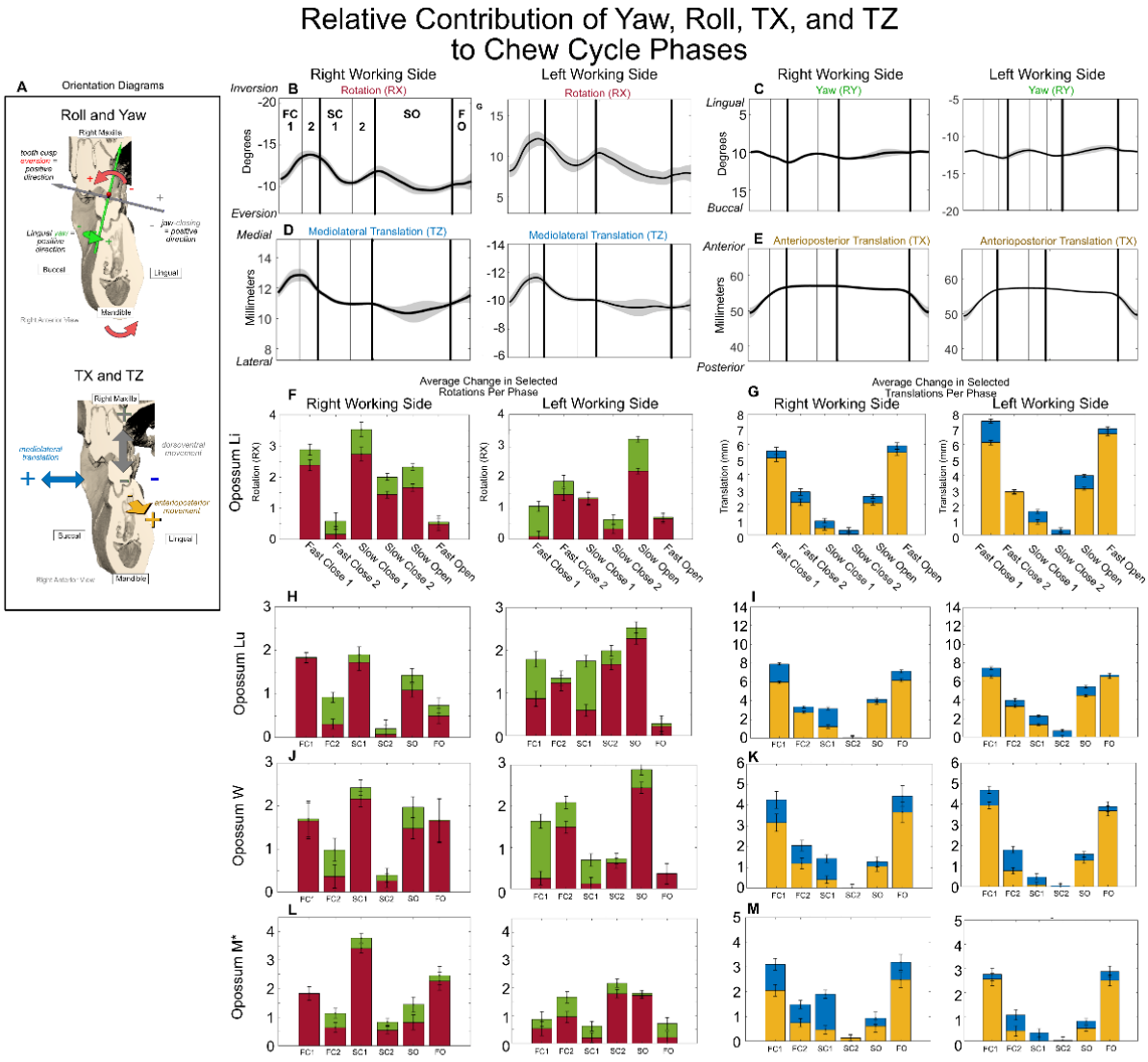


**Figure 1.3. Contributions of roll and yaw to mandibular kinematics, and proportions of anteroposterior versus mediolateral translation during each phase.** Food is almond, animal is Opossum Li for (A-G). (H-I) Opossum Lu, (J-K) Opossum W, and (L-M) Opossum M*, asterix indicates pathological cavity on the left lower M4. (A) Orientation diagrams for the rest of the figure. Both top and bottom figures show an anterior view of right molar. The top diagram shows the rotation coordinate system; arrows and descriptions indicate positive rotations for right mandible (cf. Figure 1.1 D, E, F). Yaw and roll are in color; pitch is in grey (not presented in this figure). The lower diagram shows the three translation axes at the right lower M1. Anteroposterior translation is yellow; mediolateral translation is blue. NB. rotation will be the same anywhere in the mandibular rigid body, the translations differ depending on the location of the point on the rigid body. (B) Right and left working side average gape cycle rotation for almond. The right working trace's y-axis is reversed. Black vertical lines mark phase transitions.

**Figure 1.3, continued.** Thicker black vertical lines divide the four main phase transitions: FC = fast close, SC = slow close, SO = slow open, FO = fast open. (C) Right and left working side average gape cycle yaw. (D) Right and left working side average gape cycle mediolateral translation. The left working trace's y-axis is reversed. (E) Right and left working side average gape cycle anteroposterior translation. (F, H, J, L) Bar graph showing the average total change in roll (red) and yaw (green) for each phase of the chew cycle, with standard error of the mean for each value. (G, I, K, M) Bar graph of average change in anteroposterior (yellow) and mediolateral (light blue) translation for each phase of the chew cycle (+/-standard error of the mean).

FIGURE 1.4.

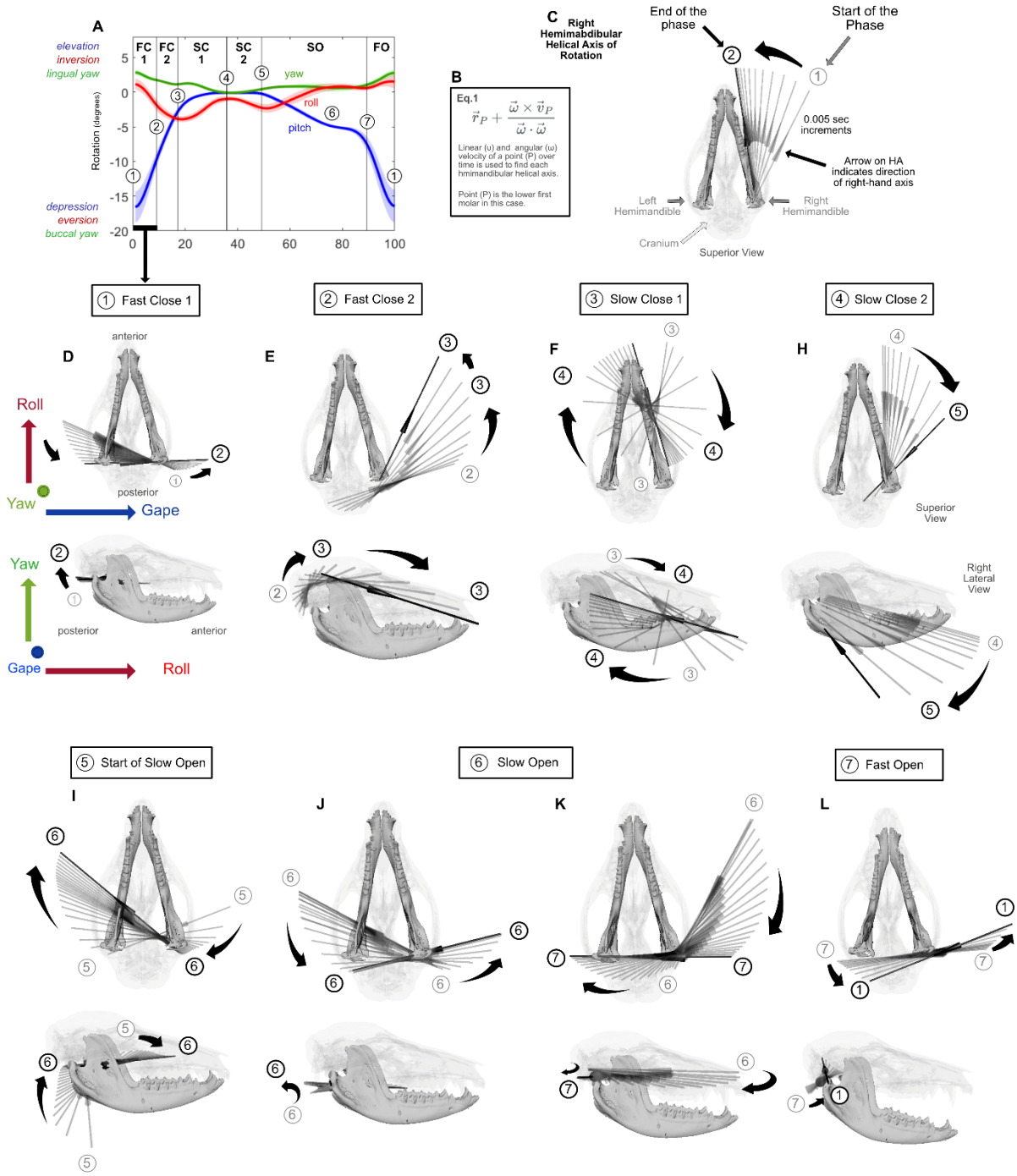


**Figure 1.4. Orientation and location of helical axes during gape cycle phases.** Opossum Li. Right side almond chew cycles. Figure shows an exemplar right working side chew cycle and correlates the timing of the chew cycle with the gape cycle phases in Figure 1.1. (A) Average right working side almond chew cycle. Red = roll, Green = yaw, Blue = gape, with +/- 1 SD. Zero position is when the animal was at rest and the mandibles were centered on the midline. Positive values on the y-axis correspond to a upwards pitch, toothrow inversion, and lingual yaw.

**Figure 1.4, continued.** Negative values on the y-axis correspond to negative pitch (jaw depression), toothrow eversion, and buccal yaw. The x-axis, time, is normalized to a 0:100 scale. Circled points on the graph indicate phase changes that correspond with the helical axis figures except for 6A and 6B, which were divided to show the movement of the helical axis at this stage in greater detail. The circled numbers in (A) correspond to the numbers in (D-K). (B) Equation (Eq.1) used to calculate the changing axis of rotation of the hemimandible over the course of the chew cycle, a.k.a. the helical axis (HA). HA calculated over 0.15 second time steps with a 0.2 degree minimum rotation value allowed. Superior and right-lateral views of semi-transparent cranium and two opaque mandibles. The helical axis at the numbered time point is represented as a black axis, with the preceding 14 time points shown in grey. The arrow in the middle of the axis shows the direction of rotation using the 'right-hand rule', with the size of the arrow representing the relative magnitude of rotation. Pure pitch (blue), yaw (green), and roll (red) are indicated schematically with arrows or a dot if the axis is pointing at the reader. The length of the helical axis is arbitrary. (D) FC1. The HA at start of FC1 is indicated with the grey circled (1) and grey bars, the start of FC2 with a black axis (black circle 2). At the beginning of FC, the helical axis passes through or just posterior to the animal's working-side condyle. The axis is angled antero-laterally, indicating components of both pitch (gape) and roll. There is very little or no yaw. During FC, the axis rotates so that by FC2 it is predominantly transverse, just posterior to both condyles. (E) Start of Fast Close 2. As FC2 progresses, the axis becomes more anteriorly oriented (indicating increasing eversion roll) and is positioned dorsolateral to the mandible. (F) Slow Close 1. The helical axis rotates counterclockwise in a slightly oblique horizontal plane, passing through the lower first and second molar, and first premolar as it rotates. By the end of SC1 the direction of the helical axis has reversed and passes through the toothrow. (H) Slow close 2. At the start of SC2 the HA points posteriorly along the toothrow, indicating eversion, then swings to point posterosuperiorly and just anterior to the condyle. During SC2 the working hemimandible everts and yaws lingually. (I) Start of SO. The HA continues to rotate clockwise in superior view, swinging towards the balancing side and moving into the horizontal plane above the molars. The axis also moves posterior to or through the right working condyle. (J) Mid SO. The HA begins to rotate in a counterclockwise direction in the horizontal plane, so that the axis of rotation moves to be just behind and inferior to the condyle. The axis of rotation is pointing toward the balancing side. (K) Slow Open continues counterclockwise and then clockwise in the horizontal plane. The axis of rotation points laterally toward the working side, posteriorly, and then laterally again by black circle 7. (L) Fast Open. The axis moves from going through both mandibles to the working side, pointing toward animal left.

FIGURE 1.5.

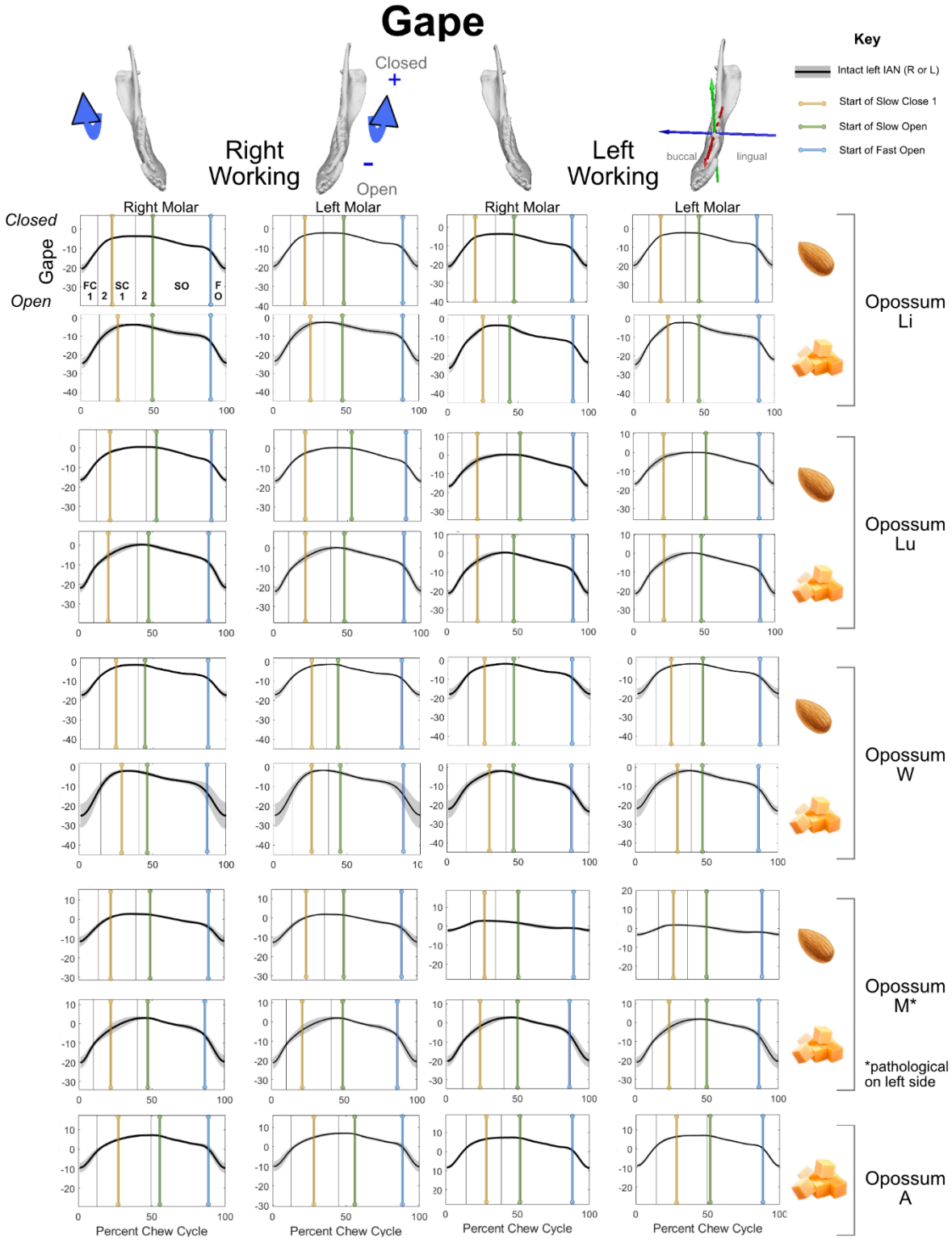


**Figure 1.5. Mandibular pitch by side, individual, and food type.** Right and left mandibular working and balancing side averaged gape cycle rotations (black line) for all opossums in the study; gray, +/- 1 S.D. Gape is represented schematically at the top of each column.

**Figure 1.5, continued.** Black vertical lines mark phase transitions. FC = fast close, SC = slow close, SO = slow open, FO = fast open.

FIGURE 1.6.

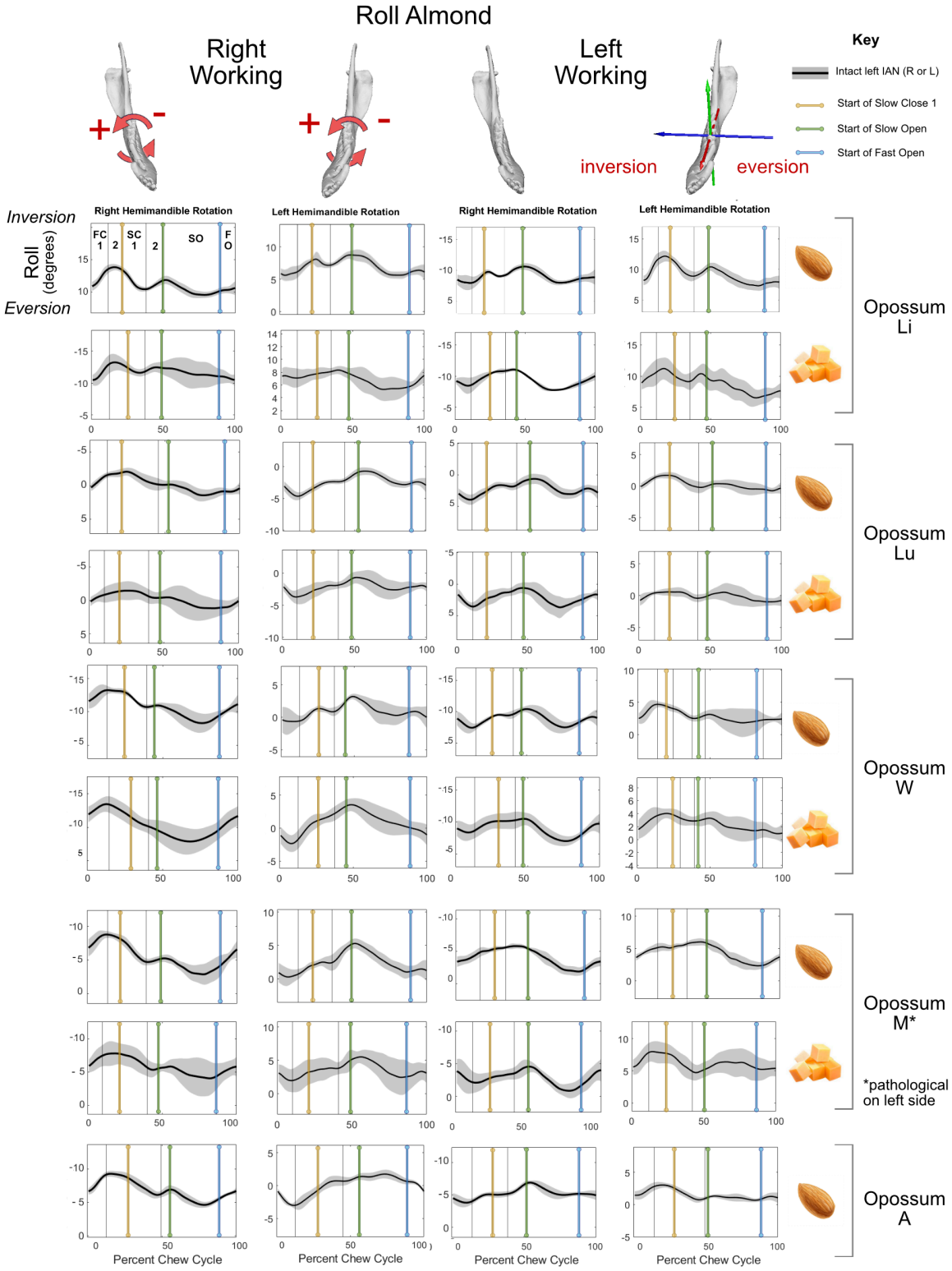


**Figure 1.6. Mandibular roll by side, individual, and food type.** Right and left mandibular working and balancing side averaged roll (black line) for all opossums in the study.

**Figure 1.6, continued.** Gray area is +/- 1 S.D.. Roll is represented schematically at the top of each column. Black vertical lines mark phase transitions. FC = fast close, SC = slow close, SO = slow open, FO = fast open.

FIGURE 1.7.

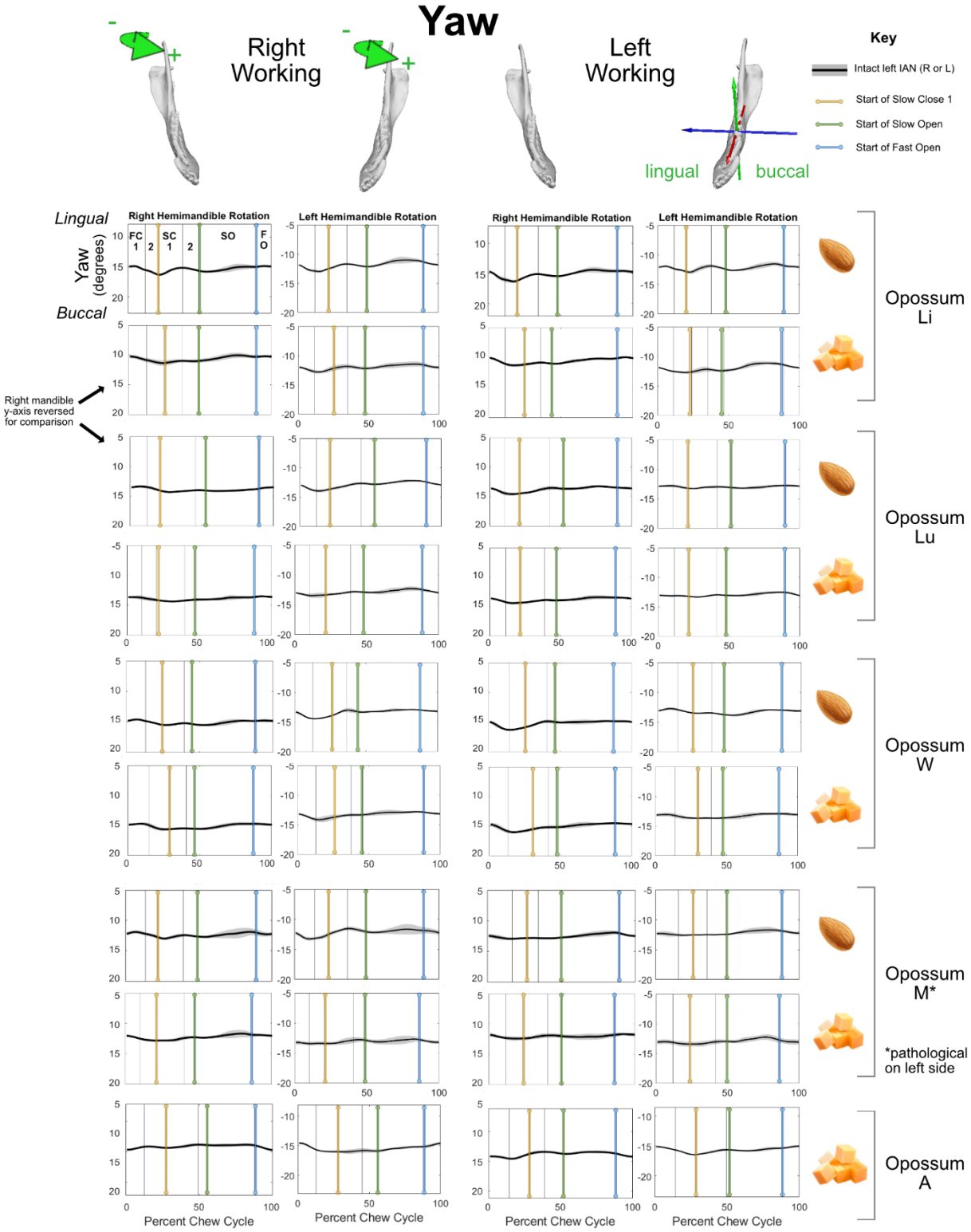


**Figure 1.7. Mandibular yaw by side, individual, and food type.** Right and left mandibular working and balancing side averaged gape cycle rotations (black line) for all opossums in the study gray, +/- 1 S.D. Yaw is represented schematically at the top of each column.

**Figure 1.7, continued.** Black vertical lines mark phase transitions. FC = fast close, SC = slow close, SO = slow open, FO = fast open.

FIGURE 1.8.

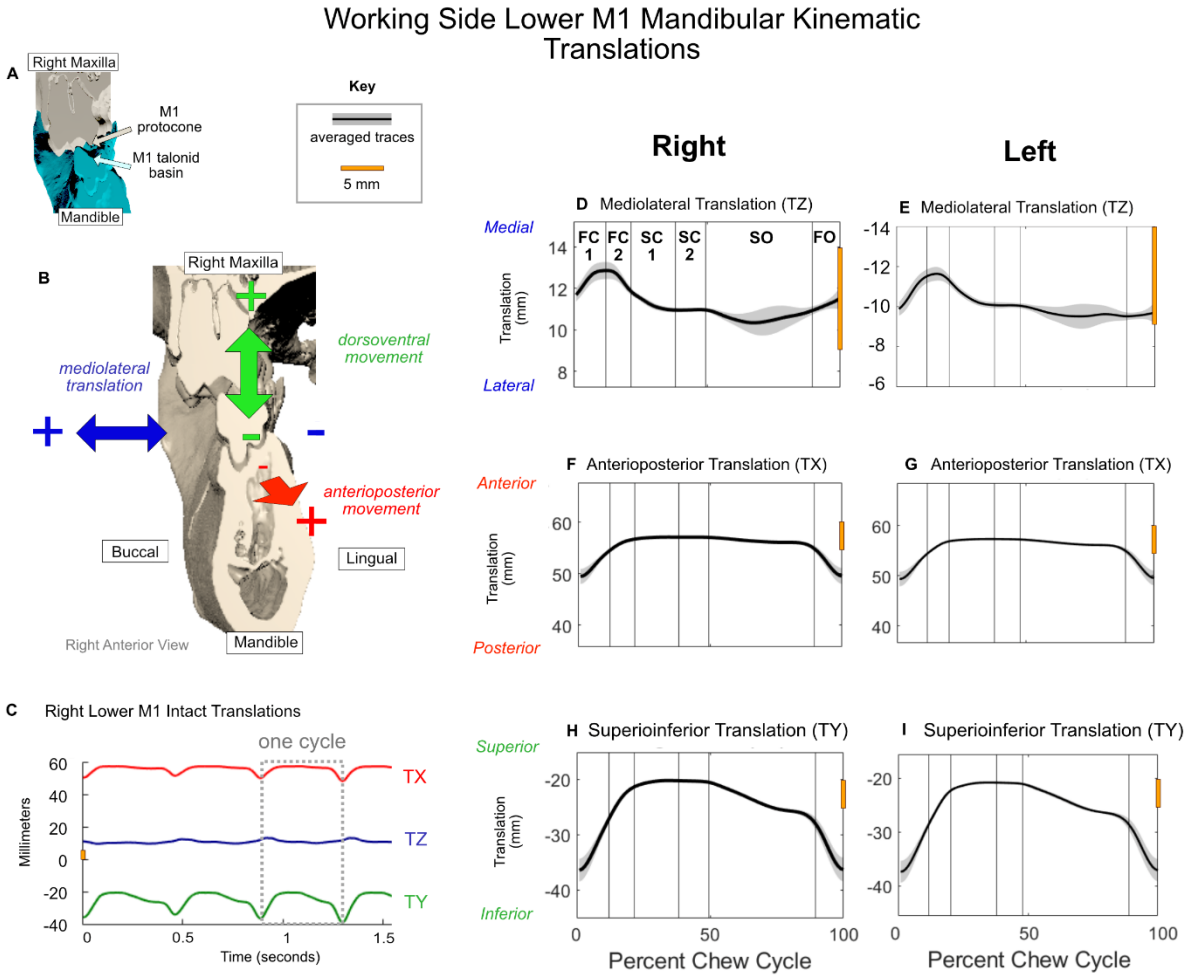


**Figure 1.8. Working side lower M1 translations.** Food is almond, animal is Opossum Li. (A) Coronal section through right cranium and mandible showing cusps for which translational movement at the lower M1 was calculated, relative to a midline axis. Key for kinematic traces. Black solid lines, mean kinematic traces; gray, +/- 1 S.D. (B) Anterior view of right molar with translation coordinate system positioned at right molar point. Arrows and descriptions indicate positive translations for right mandible. (C) Plot of right mandible translation at the M1 talonid basin in an almond feeding sequence for intact condition. Colors correspond with axes in 2B. (D-I) The yellow bar on the right of each graph indicates a five-degree increment, highlighting different y-axis scales. FC = fast close, SC = slow close, SO = slow open, FO = fast open. The y-axis in (E) is inverted so that mediolateral traces have the same polarity in the graphs for right and left mandibles; i.e., data for right mandible presented as if for left mandible zero position is when the animal was at rest and the mandibles were centered on the midline.

FIGURE 1.9.

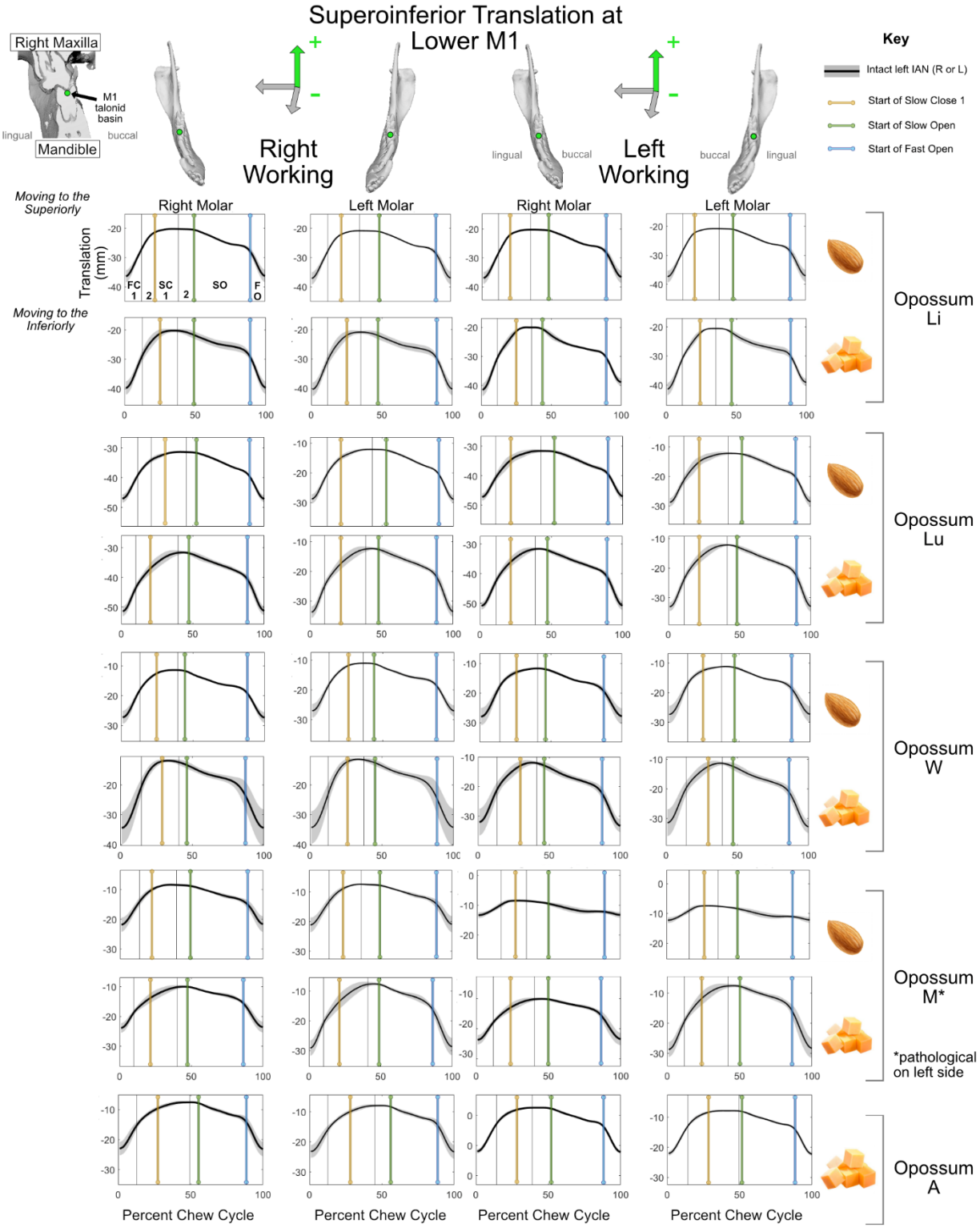


**Figure 1.9. Working side lower M1 superoinferior translations by individual, side and food.** Right and left mandibular working and balancing side averaged gape cycle translations (black line) for all opossums in the study; gray, +/- 1 S.D.

**Figure 1.9, continued.** Superioinferior translation is represented schematically at the top of each column. FC = fast close, SC = slow close, SO = slow open, FO = fast open.

FIGURE 1.10.

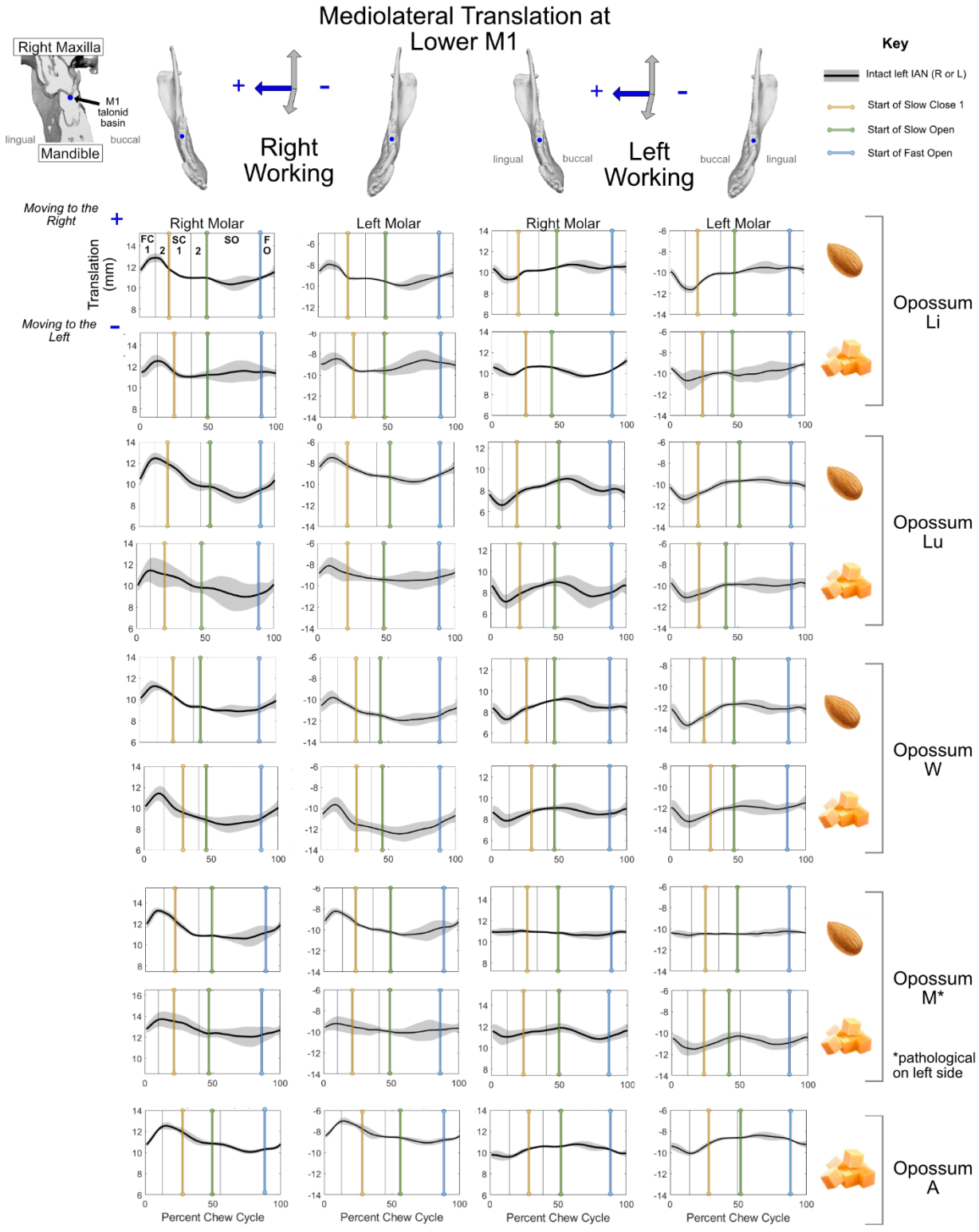


**Figure 1.10. Working side lower M1 mediolateral translations by individual, side and food.** Right and left mandibular working and balancing side averaged gape cycle translations (black line) for all opossums in the study; gray, +/- 1 S.D.

**Figure 1.10, continued.** Mediolateral translation is represented schematically at the top of each column. FC = fast close, SC = slow close, SO = slow open, FO = fast open.

FIGURE 1.11.

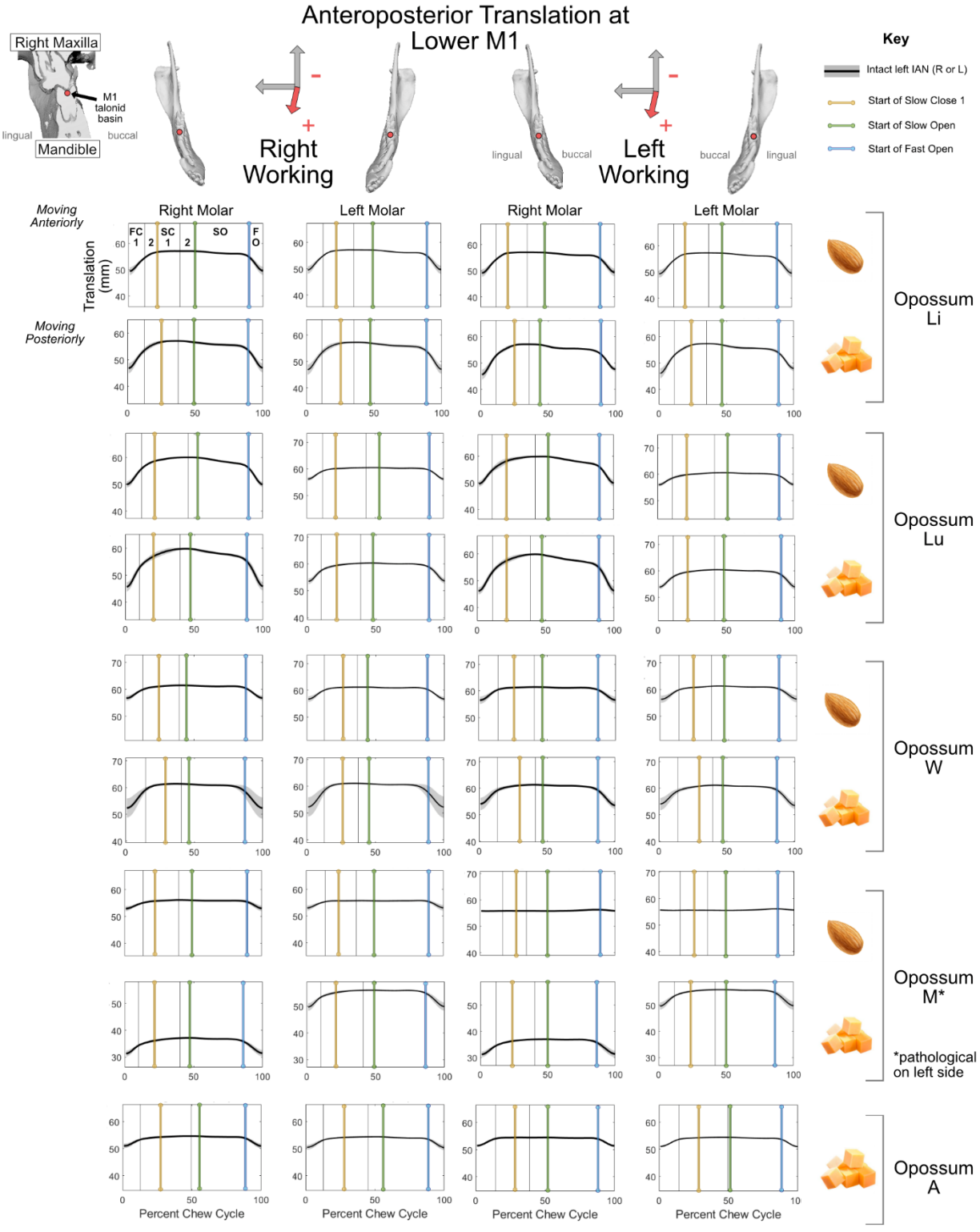


**Figure 1.11. Working side lower M1 anteroposterior translations by individual, side and food.** Right and left mandibular working and balancing side averaged gape cycle translations (black line) for all opossums in the study; gray, +/- 1 S.D.

**Figure 1.11, continued.** Mediolateral translation is represented schematically at the top of each column. FC = fast close, SC = slow close, SO = slow open, FO = fast open

FIGURE 1.12.

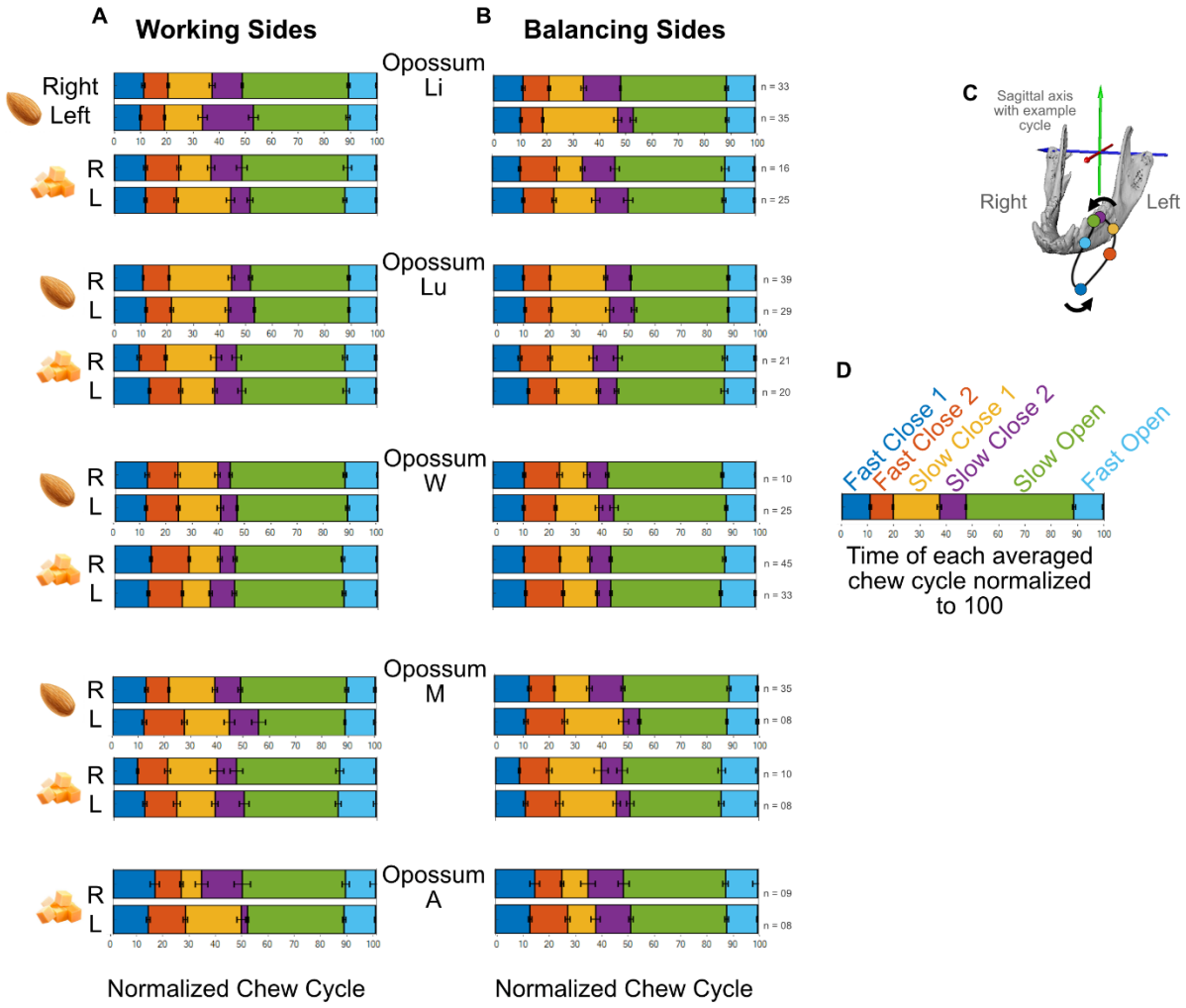


**Figure 1.12. Gape Phase Timing Variation in Right and Left Hemimanibles and by Individuals and Food Types.** Right and left average chew cycle phase times for all opossums, food types, and right and left working and balancing sides. (A) Food type is indicated by a symbol on the left of the figure with an almond or cheese cubes. Next to each food type is the R (right) or L (left) working side phase timing. (B)The right column contains all working sides, with R and L following the same order as the left column. The data is then grouped by individual. All individuals have both almond and cheese data except for opossum A, which only has data for cheese. Each bar plot is normalized to a 0:100 scale. n = total cycle number. (C) 3D trace of an example averaged left working side chew cycle color-coded to match the start of each phase represented in the bar graph. The opossum mandible is at an oblique view, facing slightly to the right and laterally and slightly inferiorly. Arrows indicate the direction of the chew cycle. Axis is the mid-sagittal cranial axis that all right and left kinematic data is measured relative to. (D) Example bar plot with phase labels, going from left to right temporally.

FIGURE 1.13.

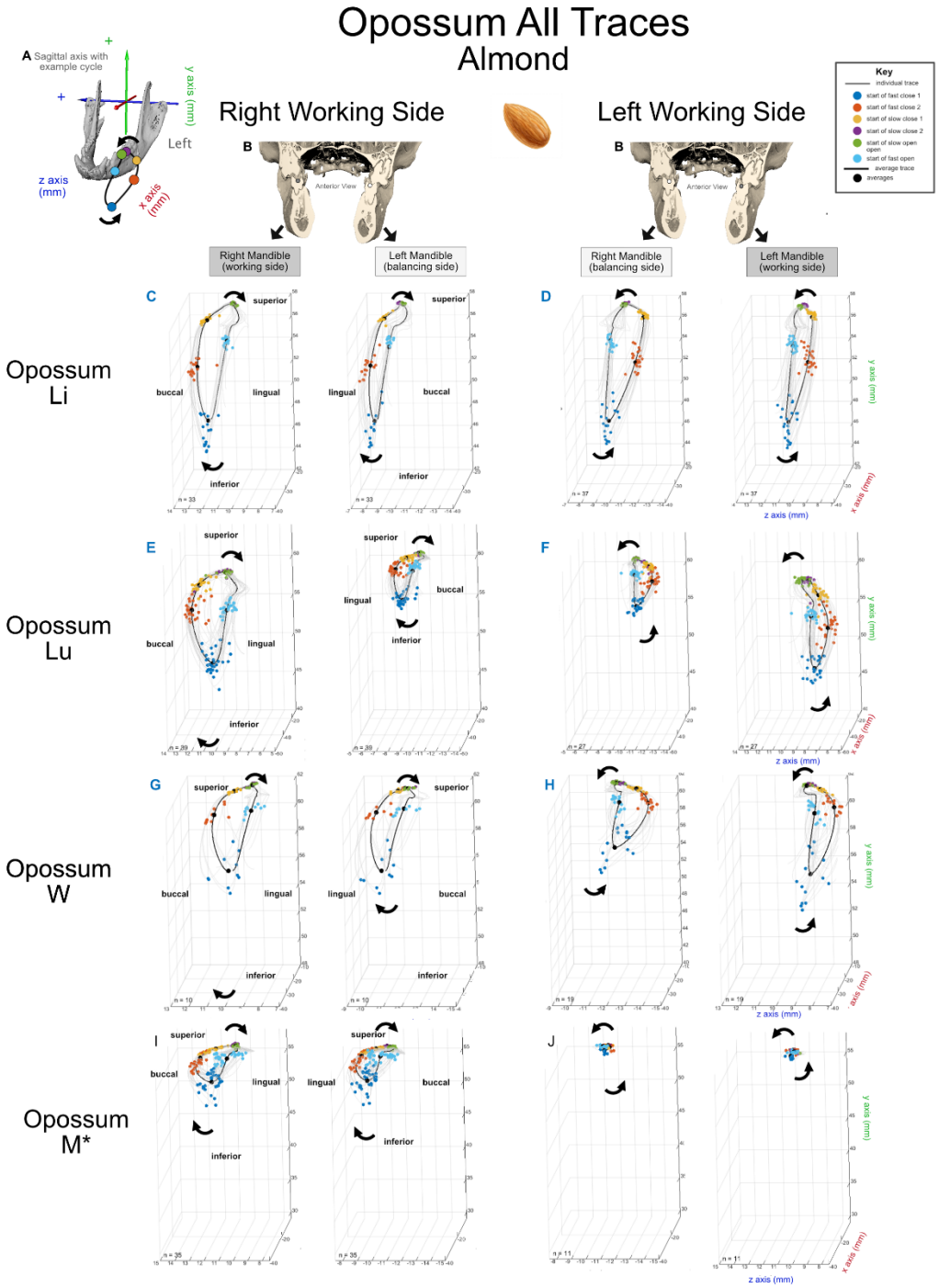


**Figure 1.13. Summary of Phase Transitions at the Lower First Molar Visualized by Major Axes and in 3D for all almond trials by individual.** Traces were calculated in Maya relative to mid-sagittal cranial axis seen in (A) and graphed in Matlab. Each right and left mandible group have the same data, graphed for the right and left sides, respectively. The data was divided into right or left working sides by individual, and then all four states (right working, left balancing, left working, and right balancing) were graphed separately. Therefore, all the data in one row has come from the same group of data collection events.

**Figure 1.13, continued.** Note that dimensions are the same for each individual, but not between individuals. (A) Orientation diagram: 3D trace of an example averaged left working side chew cycle color-coded to match the start of each phase represented in the bar graph. The opossum mandible is at an oblique view, facing slightly to the right and laterally and slightly inferiorly. Arrows indicate the direction of the chew cycle. Axis is the mid-sagittal cranial axis that all right and left kinematic data is measured relative to. (B) There are two (B) figures, one for each right and left diagram. The figure is a ct scan of an opossum facing the reader and sectioned at the first molar talonid basin, from which the traces were exported. The mandibles match the corresponding labels in (C) and (D) In (B) a dot can be seen at each talonid basin. The darker grey dot is the working side hemimandible, while the lighter grey dot is the balancing side mandibles (also corresponding to their respective labels). The (key) details the colors for the start of each phase. Individual cycle traces are shown in grey, with colored phase transitions, while the averaged chew cycle is shown in black, with black averaged phase transitions. (C) Right working and left balancing trace for Opossum Li. Arrows indicate the direction of the chew cycle. (D) Right balancing and left working trace for opossum Li. (E) Right working and left balancing trace for Opossum Lu. (F) Right balancing and left working trace for opossum Lu. (G) Right working and left balancing trace for Opossum W. (H) Right balancing and left working trace for opossum W. (I) Right working and left balancing trace for Opossum M. (J) Right balancing and left working trace for opossum M. Asterix indicates that the left mandible had a cavity.

FIGURE 1.14.

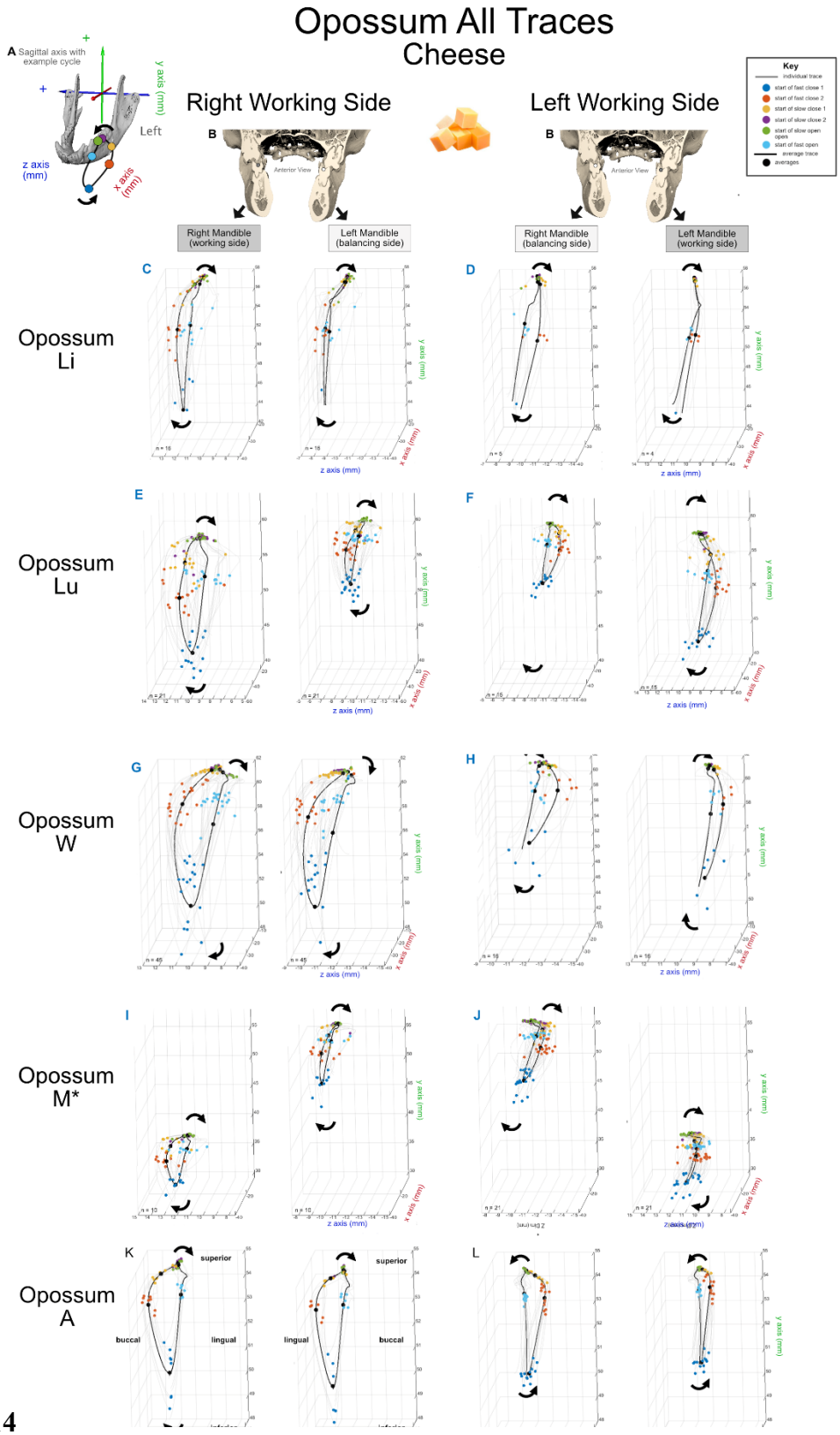


**Figure 2.14**

**Figure 1.14, continued. Summary of Phase Transitions and Kinematic Translations Visualized by Major Axes and in 3D for all cheese trials by individual.** Traces were calculated in Maya relative to mid-sagittal cranial axis seen in (A) and graphed in Matlab. Each right and left mandible group have the same data, graphed for the right and left sides, respectively. The data was divided into right or left working sides by individual, and then all four states (right working, left balancing, left working, and right balancing) were graphed separately. Therefore, all the data in one row has come from the same group of data collection events. Note that dimensions are the same for each individual, but not between individuals. (A) Orientation diagram: 3D trace of an example averaged left working side chew cycle color-coded to match the start of each phase represented in the bar graph. The opossum mandible is at an oblique view, facing slightly to the right and laterally and slightly inferiorly. Arrows indicate the direction of the chew cycle. Axis is the mid-sagittal cranial axis that all right and left kinematic data is measured relative to. (B) There are two (B) figures, one for each right and left diagram. The figure is a ct scan of an opossum facing the reader and sectioned at the first molar talonid basin, from which the traces were exported. The mandibles match the corresponding labels in (C) and (D) In (B) a dot can be seen at each talonid basin. The darker grey dot is the working side hemimandible, while the lighter grey dot is the balancing side mandibles (also corresponding to their respective labels). The (key) details the colors for the start of each phase. Individual cycle traces are shown in grey, with colored phase transitions, while the averaged chew cycle is shown in black, with black averaged phase transitions. (C) Right working and left balancing trace for Opossum Li. Arrows indicate the direction of the chew cycle. (D) Right balancing and left working trace for opossum Li. (E) Right working and left balancing trace for Opossum Lu. (F) Right balancing and left working trace for opossum Lu. (G) Right working and left balancing trace for Opossum W. (H) Right balancing and left working trace for opossum W. (I) Right working and left balancing trace for Opossum M. (J) Right balancing and left working trace for opossum M. (K) Right working and left balancing trace for Opossum A. (L) Right balancing and left working trace for Opossum A. Asterix indicates that the left mandible had a cavity.

FIGURE 1.15.

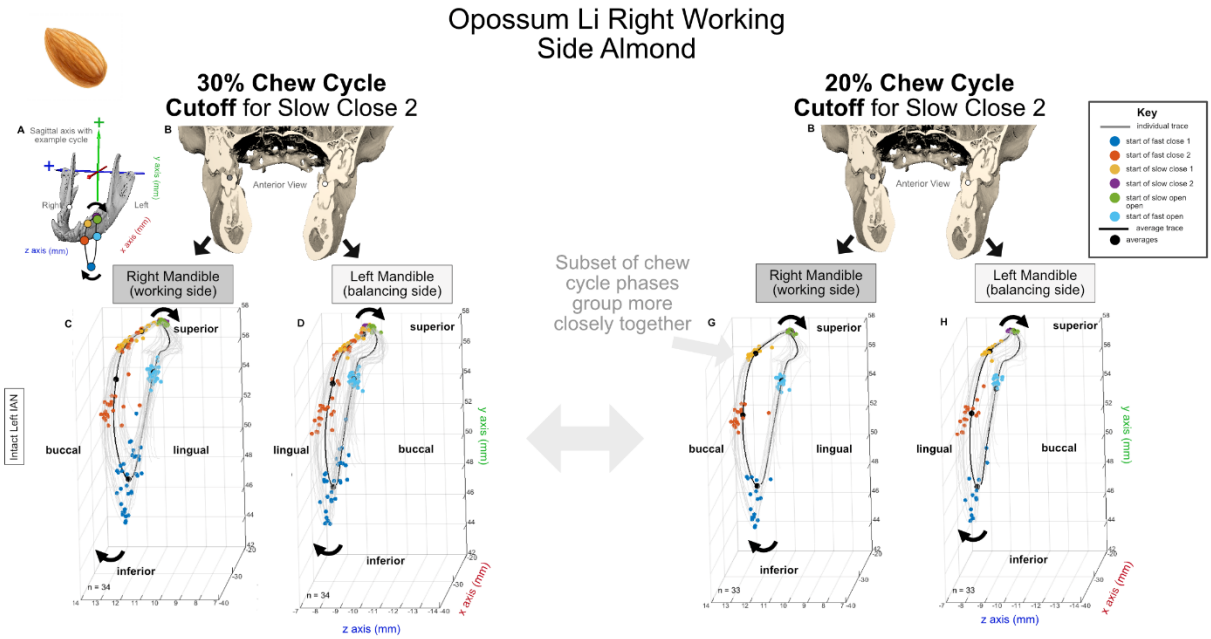


**Figure 1.15. Comparison of different sorting parameters for Phase Transitions and Kinematic Translations Visualized by Major Axes and in 3D for Opossum Li Right Side Working Almond Trials.** Traces were calculated in Maya relative to mid-sagittal cranial axis seen in (A) and graphed in Matlab. The two graphs under each letter have the same data, graphed for the right and left sides, respectively. The data was divided into right or left working sides by individual, and then all four states (right working, left balancing, left working, and right balancing) were graphed separately. (A) Orientation diagram: 3D trace of an example averaged left working side chew cycle color-coded to match the start of each phase represented in the bar graph. The opossum mandible is at an oblique view, facing slightly to the right and laterally and slightly inferiorly. Arrows indicate the direction of the chew cycle. Axis is the mid-sagittal cranial axis that all right and left kinematic data is measured relative to. (B) There are two (B) figures, one for each right and left diagram. The figure is a CT scan of an opossum facing the reader and sectioned at the first molar talonid basin, from which the traces were exported. The mandibles match the corresponding labels in (C) and (D) In (B) a dot can be seen at each talonid basin. The darker grey dot is the working side hemimandible, while the lighter grey dot is the balancing side mandibles (also corresponding to their respective labels). The (key) details the colors for the start of each phase. Individual cycle traces are shown in grey, with colored phase transitions, while the averaged chew cycle is shown in black, with black averaged phase transitions. (C) Right working and left balancing chew cycle phases for almond where the peak finding algorithm could only look at the second derivative of gape (RZ) in the first 30% of each chew cycle. (D) Right working and left balancing chew cycle phases for almond where the peak finding algorithm could only look at the second derivative of gape (RZ) in the first 20% of each chew cycle, showing a subset of identified peaks.

# CHAPTER 2:

Mastication in *Didelphis virginiana* before and after inferior alveolar nerve transection: Implications for the evolution and function of the mammal dentoalveolar neurofeedback system.

## INTRODUCTION

Chapter 1 examined the chew cycle in the hemimandibular system of *Didelphis virginiana* and defined the phases of the chew cycle, including two new fast close phases and two slow close phases. Special attention was paid to these phases in particular, as they are the phases of the mastication cycle expected to be involved in neurofeedback of mastication through the teeth. This second chapter describes experiments in which I disrupted this feedback by a unilateral cut of the inferior alveolar nerve (IAN). I quantify the impact of this nerve transection on 3D hemimandibular kinematics.

## BACKGROUND

### *Morphology of the Sensor*

Teeth are extremely sensitive structures that are regularly subjected to high loads while simultaneously encoding the orientation of forces acting on them. Teeth are primarily composed of enamel, dentine, and pulp. Enamel is the hardest, least organic, portion and surrounds the crown of the tooth (Berkovitz et al. 2009). Only a strong acid (e.g., lemon juice or large amounts of soda) or an abrasive material can erode dentine (Hargreaves and Berman 2011, Haggard and de Boer 2014). Under the enamel is dentine, a hard material that forms the majority of the tooth. Dentine is not completely solid, but is perforated by microscopic, fluid-filled tubules which

radiate outward from the pulp-dentine junction and may or may not be plugged by overlying enamel (Berkovitz et al. 2009). Pulp fills the inner cavity and is composed of blood vessels, nerves, and various maintenance cells. The root of each tooth can be divided into three parts: the cervical region closest to the crown, the body of the tooth which forms the majority of the root, and the apex, or lowest part of the tooth root. The apex of the tooth root closes off most of the pulp cavity in many adult mammalian teeth, including *Homo sapiens*. Nerves, veins, and arteries enter through the apex and also surround the tooth root structure as part of the dentoalveolar complex described below.

As bite force is applied to the tooth during any of the phases from FC2 to the start of SO, the tooth moves relative to its alveolar socket, causing mechanoreceptors within the periodontal ligament to fire. Molars are likely to be loaded primarily supero-inferiorly during puncture/crushing cycles (Type I chew cycles; Thexton and Crompton 1998) and obliquely during SC (Type II Chew; Thexton and Crompton 1998). Movement of the tooth relative to the socket is dependent upon the angles of the tooth occlusal surface, the kinematics of the mandible, and the food itself. Recent loading studies have shown that the roots of molars actually rotate in the alveolar socket, even when simply superioinferiorly loaded (Lin et al., 2013; Naveh et al. 2012; 2013, Pal et al., 2017, Bemmann et al., 2021). This movement of the tooth relative to the socket stimulates mechanoreceptors interleaved with the periodontal ligaments (PDLs) anchoring the tooth to the alveolar socket. The PDL connects cementum surrounding the roots of the teeth to Sharpey's fibers entering the alveolar bone of the mandible. The fibers of the PDL can extend straight from the tooth to the alveolar bone, or wrap around the tooth in many different directions (Hargreaves and Berman 2011, Haggard and de Boer 2014). Mechanoreceptors interleave with the PDL and fire when the PDL is pulled taught. Specifically, A-α fibers are interdigitated with

the PDL and are associated with proprioception. Meissner corpuscle-like and Ruffini-like nerve endings are also found between PDL fibers and are thought to encode the amount and direction of force applied to the teeth (Linden and Scott 1989, Haggard and de Boer 2014). Pacinian corpuscle-like structures have also been observed, which are thought to encode vibration (Haggard and de Boer 2014). Trulsson (2006) showed directional sensitivity of human PDL afferents by applying variable pressure, in different directions, to human incisors and premolars. The type of mechanoreceptor, its placement within the PDL, the orientation of fibers within the PDLs, and the morphology of the tooth are all thought to influence mechanoreceptor stimulation.

***Connection to the Central Nervous System***

All of the structures described so far are found in the dentoalveolar complex. The information still has to be transferred to ganglia and the central nervous system for further processing. There are two known sets of afferent nerve populations in the PDL: the trigeminal ganglion primarily innervates the middle portion (body) of the PDL, and the mesencephalic nucleus of CN V (MesV) (also called the supratrigeminal nucleus) primarily innervates the apical region PDL (Naftel et al.1999, Piancino et al. 2017). Both these areas also process information relating to mastication, including muscle control, salivation, and proprioceptive feedback in the mouth.

The trigeminal ganglion contains most of the cell bodies for nerves innervating the orofacial region, including most orofacial proprioception, tactile input, and nociception. The ophthalmic (V1) and maxillary divisions (VII) of the trigeminal nerve are sensory, while the mandibular branch has both sensory and motor components. V3 contains efferent motor neurons for the muscles of mastication: medial pterygoid m., lateral pterygoid m., masseter m.,

temporalis m., anterior belly of digastric m., and mylohyoid m. As far as teeth are concerned, activity in the trigeminal ganglion is associated with molar tooth loading, force and rate of change, and there is some evidence that they fire primarily at the start of slow close phase (Lund 1991).

The second set of sensory nerves in the PDL supplies the apical region and their cell bodies are located in MesV, which is found at the mesopontine junction of the midbrain. MesV contains the only set of primary afferent cell bodies within the central nervous system (CNS), instead of in dorsal root ganglia in the PNS. MesV contains unipolar proprioceptive afferent cell bodies from the masseter m., temporalis m., as well as the lateral and medial pterygoid mm. (the jaw closing muscles, although there can be some anatomical variation), as well as the extraocular muscles of the eye in placentals (Helms 1979, Wang and May 2008, Morquette et al. 2012). Activity in MesV PDL mechanoreceptors has been reported throughout the slow close phase and fire with increased pressure (Lund 1991). They also fire in response to tapping. The jaw opening response occurs when concentrated pressure or vibration are applied to the teeth, causing the jaw opening muscles to fire. The jaw jerk reflex also travels via MesV and induces masseter firing (jaw closing). MesV PDL mechanoreceptors are hypothesized to provide positive feedback to increase masticatory pressure during jaw closing (Morquette et al. 2012). The faciliatory masseteric response (FMR) is seen when masseter muscle electromyographic activity increases prior to contact with the food, indicating an anticipatory response to food property in FMR disappeared after lesioning MesV.

MesV appears to be highly regulated as the MesV soma receive input from cortical, midbrain, and trigeminal dendrites (Morquette et al. 2012). MesV synapses primarily with the trigeminal motor neuron pool as well as other brainstem areas. Caudal to the MesV in the

midbrain is the trigeminal motor neuron pool, which contains the cell bodies of the efferent neurons supplying the jaw muscles used for mastication (Lavigne et al. 1987, Piancino et al. 2017). The trigeminal motor neuron pool receives ipsilateral input from MesV, as well as input from the trigeminal nucleus, premotor areas within the brainstem, and the cortical masticatory area, and is believed to be the central pattern generator for mastication. Anesthetized or decerebrate animals are still able to rhythmically chew when the pyramidal tract is electrically stimulated (Komuro et al. 2001). MesV also synapses with the cerebellum, nucleus ambiguus, peritrigeminal area, trigeminal spinal nucleus, trigeminal sensory nucleus, and the hypoglossal nucleus (Morquette et al. 2012). Horseradish peroxidase tracer studies have shown that nerves carrying information from PDL mechanoreceptors crosses to the contralateral side (as well as staying ipsilateral) in the premotor areas of the trigeminal area (Piancino et al. 2017). This shows that a great deal of filtering and calculation to modify the central pattern generator output can be done before the information ever reaches the cortex.

***Cortical Pathways***

PDL sensation is bilaterally represented in the primary somatosensory cortex, as well as the insular and supplementary motor cortices (Piancino et al. 2017; Avivi-Arber and Sessle 2018). In the somatosensory cortex, the oral region is partially separated into tooth, gingiva, palate, tongue, and teeth. Input and output, therefore, appear to be constantly sorting and reorganizing through the neural hierarchy, but oral regions never completely lose their identity. Lund and Kota (2006) describe this system as a series of modifiable and interacting central pattern generators. One of the ways that this rhythmic pattern is modified is thought to be through dental neurofeedback (Rossignol et al. 1988, Lanenbach and van Eijden 2001). When

the somatosensory cortical response was measured in humans using magnetoencephalography, the latency of stimulation to cortical response time was significantly faster bilaterally for molars (approximately 47 ms) than canines (approximately 62-65 ms) (Hihara et al. 2020).

### *Implications for specific chew phase control*

Given all the above information, it might be surprising to learn that decerebrate animals are still able to chew and swallow food (Lund 1991, Van der Bilt et al. 2006). Stimulation in the oral region of the motor cortex also elicits a chewing cycle (Van der Bilt et al. 2006). However, these cycles are stereotyped and cannot respond to novel stimuli beyond single synapse midbrain reflex arcs such as the jaw opening reflex (Yamada et al. 2013). Here, I propose that the tooth mechanosensory system is maintained not just for tooth protection, but to respond to the properties of foods that animals ingest and which vary between and during chewing sequences. Maintaining airway patency is key to an animal's and a lineage's survival.

## *Evolution of Masticatory Control*

Intraoral food breakdown is widespread in Vertebrata (Sibbing, 1982; Reilly et al. 2001; Gidmark et al., 2014; Laurence-Chasen et al. 2019); mammalian mastication is characterized by chewing sequences that are rhythmic (low variance in chew cycle duration; Ross et al., 2007). Jawed vertebrates all share a MesV, which is the first trigeminal structure to develop in the brain (Stainier and Gilbert 1990). The nerves of MesV, however, do not reach the periodontium until after birth in mice. In caimans (*Caiman sclerops*) MesV activity was recorded when the masseter m. was stretched (Desole et al. 1970). In fact, MesV is found in all jawed vertebrates. In

placentals, MesV sends information up to the cortex as well as the trigeminal motor neuron pool, with which it forms a monosynapic connection for the jaw closing reflex.

Mammalia have a large number of afferent nerves from the oral cavity to the brain, and novel connections to distinctly mammalian neocortical brain structures, including the sensorimotor cortex (Kaas 2016, Rowe 2020). Mammalia also chew to pre-digest food rapidly and efficiently; as a part of this evolutionarily innovative function, mammals have chew sequences that can be divided sub-sequences or phases (see Chapter 1). Mammals have a novel temporomandibular joint populated with joint receptors (Anthwal and Tucker 2020), increased occlusal complexity, and tooth replacement reduced to one or two generations (Luo et al. 2004, Langenbach and van Eijden 2005; Ungar 2010).

The dentoalveolar complex is distinctly important for mastication in the best-studied mammalian system: humans. Substantial tooth loss (e.g., an entire upper or lower tooth row) often occurs in geriatric individuals (Kumar et al. 2018). Tooth loss is associated with substantial maxillary and mandibular bone loss, which can contribute to difficulty in eating, even cognitive impairment and a lower quality of life (Lexomboon et al. 2012, Peres et al. 2015, Saito et al. 2018, Arce-McShane 2021). Tooth loss and degeneration of tooth bearing bones can be potentially related to locus coeruleus degeneration and loss of norepinephrine (Goto et al. 2020, Grigoriadis et al. 2020). The locus coeruleus sits anatomically next to MesV and is thought to degenerate when MesV degenerates from substantial tooth loss (Goto et al. 2020). If teeth are lost or pulled, dentures that attach to screws embedded in maxillary or mandibular bone have to been shown to be more effective for mastication than dentures that only sit on the gums (Grigoriadis et al. 2015). It is thought that even the small amount of proprioceptive feedback given by the bone screws likely allows for an easier mastication and thus a greater quality of life

(Ravi et al. 2020, Dhall et al. 2021). Feedback itself may be worth the risk of tooth loss, infection, gum retraction, and pain that come from maintaining a PDL instead of fusing the tooth to the bone.

FEA analyses have shown that presence or absence of a PDL does not significantly change the stress and strain patterns of the whole mandible, although some argue this can affect the tooth roots (Sulej et al. 2020). Gomphoses, or socketed teeth, are therefore probably not adaptations reducing stresses and strains of the mandible or hemimandibles per se. The stress and strain patterns of the bone that composes and surrounds the alveolar socket, however, does change when tooth root fusion to the mandible is modeled (Panagiotopoulou et al. 2011, McCormack et al. 2014; 2017, Mehari Abraha et al. 2019; Sulej et al. 2020), meaning that local stresses and strains are important to the alveolar complex. This points to the mammalian dentoalveolar complex as a sensory component of mastication and other oral functions, and not a significant structural component of mastication.

***Goals of thesis chapter 2***

The goal of this chapter is to test hypotheses about the function of the dentoalveolar feedback system for control of jaw kinematics during mastication. How important is dentoalveolar feedback, really, to mastication? How important is dentoalveolar feedback for a hemimandibular masticatory system? As a first pass, I opted to remove the key tooth sensory feedback by cutting the nerve that innervates the mandibular dentoalveolar complex, the inferior alveolar nerve, on just one side. In this case, I arbitrarily chose to cut the nerve leading to the teeth on the left mandible and complete a sham surgery on the right side. Biplanar videoradiography of almond and cheese mastication was then collected on the pathological

condition. Chew cycle data were then analyzed using the framework developed in Chapter 1. There, I divided the chew cycle into 6 phases: fast close (FC1), fast close 2 (FC2), slow close 1 (SC1), slow close 2 (SC2), slow open (SO), and fast open (FO). Each of these kinematic phases is expected to respond differently to dentoalveolar neurofeedback. The kinematic phases of the chew cycle where the teeth are not likely to occlude, FC1 and FO, are expected to incorporate little information from the teeth, while the parts of the cycle where tooth-food-tooth or tooth-tooth contact is inferred is expected to be highly dependent on neurofeedback.

There are several different ways I can develop and test the hypotheses of how the kinematic chew cycle phases could be affected. Our first hypothesis was that only the hemimandible with the transected nerve would be affected. That is, after unilateral transection of the left inferior alveolar nerve, only the same left mandible deprived of dentoalveolar neurofeedback would be affected kinematically and the greatest change would be seen and measurable at SC2-SO. Although information is known to cross at the level of the pons and/or the somatosensory subnucleus of the thalamus (Piancino et al., 2017), I predicted that dentoalveolar neurofeedback would be integrated unilaterally. Using a condylar axis to define the dimensions of pitch, yaw, and roll (following Olson et al. 2020), I expect to see the inversion-eversion-inversion pattern seen in the first chapter to be present in the healthy opossum, but significant loss of these movements, or a total disappearance after transection, only on the transected side, for both working and balancing conditions.

The second hypothesis was that both sides would be equally affected after unilateral transection. If both sides are equally affected, this suggests that the opossum integrates information from both the working and balancing hemimandibiles to control jaw movements, and that unilateral nerve transection disturbs that balance.

The third hypothesis was that neurofeedback might affect individual opossums differently. However, even this would be informative, as it would show the degree of plasticity in the neurofeedback between individuals. If some individuals are greatly affected, while others only marginally, then this would show that different individuals might rely on different parts of the feedback system to produce a mastication behavior.

## MATERIALS AND METHODS

Bilateral mandibular kinematics were recorded in opossums before and after left inferior alveolar nerve (IAN) transections using biplanar videoradiography and the XROMM (X-Ray Reconstruction of Moving Morphology) workflow (Brainerd et al. 2010). All experiments were approved by University of Chicago's IACUC (ACUP 72476). Animals were acquired under Illinois Department of Natural Resources (Wildlife Capture Permit numbers NH19.6055 (2019), NH20.6055 (2020), and W21.6454 (2021)).

Two male and three female wild-caught opossums were housed at the University of Chicago Animal Resource Center. Each animal had all teeth erupted and present, no obvious gingival wounds or infections, and no cavities exposing the pulp. At least two weeks before data collection each animal was sedated (20-25 mg/kg ketamine), intubated and anesthetized (1-4% isoflurane) for surgical placement of 1 mm tantalum bead markers (CE certified, manufactured by RSA Biomedical for implantation in humans (http://www.umrsa.com/umrsa/marker_insertion.php). Two markers were surgically implanted in each of the right and left zygomatic arches of the cranium, and four were implanted in each hemimandible: two in the symphyseal region, one in the anterior border of the ramus at or above the level of the toothrow, and one on the medially inflected angular process of each mandible.

All markers were placed through small incisions, and pressed firmly into 1 mm diameter holes drilled in the bone with a small hand-held drill.

After collection of pre-nerve transection data (see Chapter 1) the animals were anesthetized for a second, nerve-transection surgery. The oral cavities of each individual were sterilized with iodine and chlorhexidine. On animal left, an incision was made in the oral mucosa just lateral to the left palatoglossal arch and a pathway to the nerve was blunt dissected between the medial pterygoid and the mandibular ramus. This technique was the most parsimonious way to reach the inferior alveolar nerve at the location where the nerve enters the mandibular foramen. The nerve could not be cut more proximally as the nerve to mylohyoid is often running with the inferior alveolar nerve and I wanted to maintain the function of the mylohyoid muscle. After the inferior alveolar nerve was identified, it was cut with straight iris scissors, taking care not to cut the inferior alveolar artery and vein. If possible, a portion of the visible nerve was removed to prevent reattachment. The mucosa was sutured closed with 4-0 Vicryl. The same procedure was repeated on the right side, with the exception that the nerve was not cut. Little swelling was observed during recovery and all animals ate *ad libitum* within hours of waking up. One animal, Opossum A, had a sham performed on both sides to test if sham sidedness was an issue. Animals recovered for 72 hours before data were collected every-other day for 10 days. All animals ate 4-6 hours after surgery and did not show signs of distress or infection. At the end of data collection, the animals were euthanized and dissected to confirm the success of nerve transection.

### *Data Collection*

Kinematic data were collected at the University of Chicago XROMM Facility and uploaded to the XMA Portal for data storage. Opossums were fasted 12 hours before data collection. Each opossum was placed into an opaque plastic box (40 cm in length, 21 cm in width, and 20 cm in height) positioned next to the image intensifiers and allowed to settle. A small hole at the end of the box allowed a researcher to place a food item inside the box, which the animal could choose to eat or not. Data were then collected at a 200 Hz frame rate, 900 x 900 resolution with radiographic technique of 10 mA and 70-80 kVp, depending on the density of the opossum. Animals were presented with a single food item and data collected in 10 s bursts until the final swallow. Complete feeding sequences could not usually be collected within the ten second time limit of the x-ray source, but multiple ten second bursts could be collected with only 1-2 seconds between. Trials were selected for upload to XMA Portal if all markers were visible in both frames for the majority of the 10 s interval and not occluded by either the position of the animal or the position of the box.

The animals were fed the same foods as in Chapter 1: a relatively soft, deformable food (cheddar cheese) and a harder and brittle food with an internal structure (almonds). Cheddar cheese cubes that were 2 cm on each side were chosen to represent a completely homogenous substance. Full, raw shelled California almonds were used as a relatively hard substance that had to be broken down in oral cavity before being swallowed.

### *Data analysis*

Marker coordinates were tracked using auto- and manual tracking functions in XMAlab (version 1.5.5, Knörlein et al. 2016). The rigid body transformations were low pass filtered (20

or 30 Hz cutoff, see Table 2.1), exported from XMA Lab as .csv files and manually merged in Excel (version 2016, Microsoft INC.) before importing into Maya (2019.3.1, Autodesk INC.) following the XROMM workflow (Knörlein et al. 2016). Data were grouped by animal, pre vs. post transection, and food type. STL's for each animal were made using CT scans of either the live animal (Vimago L Base version, Epica) or the animal after death (GE Phoenix v|tome|x 240 kv/180 kv scanner). Specimens were scanned with a voxel size of approximately 80 microns with 170 kVp and 130 uA, 1300 projections, averaging of 3 frames and skipping 1.

**TABLE 2.1.** Individuals and Food Type Chew Cycle Number

| *Data Collection* ***Events*** | | *Number of Cycles* ***Intact*** | | ***Transected*** | | |
|---|---|---|---|---|---|---|
| Individuals | Food | Right Working Side | Left Working Side | Right Working Side | Left Working Side | Filters (Hz) |
| *Opossum Li* | | | | | | |
| | *Almond* | 33 | 35 | 37 | 46 | 30 |
| | *Cheese* | 16 | 25 | 5 | 28 | 20 |
| *Opossum Lu* | | | | | | |
| | *Almond* | 39 | 29 | 27 | 30 | 30 |
| | *Cheese* | 21 | 20 | 15 | 16 | 30 |
| *Opossum W* | | | | | | |
| | *Almond* | 10 | 25 | 19 | 20 | 20 |
| | *Cheese* | 45 | 33 | 16 | 31 | 20 |
| *Opossum M** | | | | | | |
| | *Almond* | 35 | 08 | ~ | ~ | 30 |
| | *Cheese* | 10 | 08 | 10 | 08 | 30 |
| *Opossum A* | | | | | | |
| | *Cheese* | 09 | 08 | ~ | ~ | 20 |

A rest position for each animal was defined as a time point in data collection when the animal was not feeding, when the symphysis was in the midline, and gape (pitch) was low (See

Table 1.2 for alignment values). In the rest position I set a midline cranial coordinate system and two separate hemimandibular axis systems. Our coordinate system followed that of Olson et al. (2019), in which both hemimandibular axes systems had the same positive sign (positive up, forward and right), rather than that of Bhullar et al. in which the axis systems were mirrored across the midline. The origin of each hemimandibular coordinate system was set on the superior surface of the condyle at the midpoint between the mediolateral and anteroposterior dimensions (see Figure 2.1 D-F). The z-axis was oriented to pass above the lateralmost and medialmost extrema of the condyle (positive to animal right), the x-axis was oriented along a line from the top of the condyle to infradentale (positive forward), and the y-axis is the cross-product of x and z (positive upward).

Measures of translation of points on the hemimandibles were made in a cranial coordinate system with its origin in the midsagittal plane and level with the top of the two hemimandibular condyles (Figure 2.14 A). The y-axis (yaw) is oriented superoinferiorly, with superior as the positive direction, and the x-axis (roll) is oriented anteroposteriorly, with anterior as the positive direction, along the midsagittal plane of the cranium. In Maya the ORel (Output of Relative Data) function was used to measure translations, relative to this midline cranial coordinate system, of the left and right lower first and fourth molar talonid basins, as well as the superiormost point along the midline of each condyle, midway between the mediolateral and anteroposterior dimensions.

Any cycles that obviously contained phase I transport or swallows were excluded from our analyses: I focused on chewing cycles. Relative movement data were exported from Maya as translations and rotations (in .csv format), then imported into Matlab (version R2020b) for analysis. Jaw kinematic data were divided into separate chew gape cycles at maximum gape, i.e.,

the most negative value of pitch for a given time frame using the 'findpeaks' function in Matlab. Each cycle was then divided into right or left chews using right lateral translation data from the right lower M1 talonid basin. After right of left identification, phase transitions within each chew cycle were identified.

### *Phase Transition Analyses*

Using the phase transition method developed in Chapter 1, I divided each chew cycle into six phases: fast close 1 (FC1), fast close 2 (FC2), slow close 1 (SC1), slow close 2 (SC2), slow open (SO) and fast open (FO). Phase duration was calculated for each of the six phases in each gape cycle. Phase durations and transition times were then averaged in raw time, as well as expressed as a percent of cycle duration from zero to 100. With the data organized and visualized, I decided to test if right working, right balancing, left working, and left balancing hemimandibles were temporally different before vs. after nerve transection. I also wanted to quantify changes in roll and yaw specifically, so I took the difference at the beginning and end of each phase in roll (X-axis rotation) and yaw (Y-axis rotation), and compared this with the difference in mediolateral and anteroposterior translation.

Data, including STL's of the opossum cranium, hemimandibles, and marker positions are available on request; Matlab files and raw data files are available through XMAPortal (https://xromm.rcc.uchicago.edu/).

# RESULTS

Kinematics in all three rotational axes and translational dimensions were significantly affected by the left unilateral nerve transection. For rotations, roll was the most affected, showing a loss in the magnitude of roll, to the point sometimes where roll during FC2, SC1, SC2, and the start of SO was effectively lost. Yaw showed dramatic changes in one individual and showed the most difference in SO, but in general only changed a few degrees, much less than the impact on roll. Gape (pitch) became more variable post-transection, with the most change seen in the FO1 and FC phases. Predictably, superoinferior translation at the lower M1 followed the same pattern as gape. Mediolateral translation changed the most for FC1, FC2, and SO. Anteroposterior translation only showed minor changes. As with intact nerve chew cycles, cheese post-transection chew cycles were more difficult to side.

### *Averaged Chew Cycle Data*

Gape (RZ) was the least effected of the rotations (Figure 2.2 D-E and Figure 2.3). Gape during almond cycles (Figure 2.3) was affected less than cheese cycles and closely resembled the pre-transection data. For cheese cycles (Figure 2.3), most opossums showed greater variance in FC1 and FO. Opossums Li, W, and M also changed to a shallower (less negative) gape post-transection. All opossums except for opossum W eating almonds showed either a smaller or larger gape at FC2 through SC1. The degree of gape change appears to be related to working side. That is, if the gape is shallower on one side (both hemimandibles of left working side for opossums Li and Lu, and both hemimandibles of right working side for opossum W), then it did not change on the other side. The only exception that this did not hold true is for Opossum M, which had a cavity on the left hemimandible. In fact, as we will see below, transection actually

made Opossum M's chew cycles less pathologic. In Opossum M's case, the gapes on both the right and left working conditions changed. The right working side gape was wider (more negative) while the left working side gape was more narrow (maximum was more positive).

For roll (RX), eversion was often greatly reduced or lost in FC2 to SO (Figure 2.4). Roll in these phases is completely different for Opossum Li for both food types. The right hemimandible in Opossum Li is also being held at a more everted angle for the entire cycle, so the transected trace (blue in Figure 2.4) looks "higher" for both the almond and cheese treatments. The left hemimandible for Opossum Li shows less overall mandible angle translation and a bit more roll, while massively inverting during SO no matter if it is the working or balancing side. Opossums Lu and Win Figure 2.4 show more left hemimandibular angle change. For Opossum Lu almond condition, the left working eversion at SC1 to SC2 is almost entirely lost, while it is the right hemimandible that shows less roll in both working and balancing conditions for cheese. Opossum W shows more eversion for the right side hemimandible during FC1 and FC2, while the left side hemimandible shows more inversion for the working side only. Opossum M has right and left side chews that look very similar to one another for both the working and balancing conditions.

Yaw (RY) was very similar for all individuals (Figure 2.5). The most change from the healthy to transected condition was seen in Opossum Li, who showed a lack of lingual yaw during SC1, SC2, and SO. There was more change in the right hemimandible than the left hemimandible. All opossums showed less yaw during SO, but usually this was only by a few degrees. Opossum W again had very similar left and right working side chews in the post transection condition.

Superoinferior translation (TY) was most variable in FC and FO (Figure 2.6). The greatest amount of variability is seen in opossum Lu for the cheese condition. Opossum W had less negative superoinferior translation in gape for the right side. Opossum M was the only opossum that showed statistically significant change in SC1, where superoinferior translation decreases more (i.e., moves more superiorly) than it did for the intact condition. This is true for both hemimandibles and working conditions.

For mediolateral translation (TZ), in general there was a post-transection reduction of mediolateral movement for cheese, and a greater reduction than in almond trials (Figure 2.7). The almond condition showed very little post-transection change overall. There was a loss of medially-directed movement for the right working side in opossum Li, and the right mandible moved laterally when the left mandible was the working side. Opossum Lu shows slightly more lateral translation on the left side. For cheese chewing my opossums Li, Lu, and W, the right side translation was more affected at FC1 to FC2 than the left side, for both the working and the balancing conditions. Opossum M shows more right working side lateral translation and left working side medial translation.

Anteroposterior translation (TX) showed the least amount of variation of the translations (Figure 2.8). Of the non-pathologic individuals, opossum Lu showed the most variation. For both almond and cheese, both mandibles moved more anteriorly in the post-transection condition. The entire mandible was translated more anteriorly for the cheese condition, but this was not the case for almond. Opossum M holds the right mandible in an entirely new position after the transection (only cheese cycles are available post-transection), becoming equivalent in anteroposterior position to the left hemimandible.

***Phase Comparisons***

Change from healthy to transected chew cycles for each individual and treatment (food) was calculated as the difference in the average x (time) and y (rotation or translation) axis value from the start of each phase to the end, with standard deviation calculated as sqrt($[SD1]^2$ + $[SD2]^2$ ). I then compared the difference of this change in timing (Figure 2.9) and translation/rotation (Figure 2.10) between the intact and transected conditions, for each food type. For the y-axis data, if the value is positive, then there was more change in that dimension before transection. If the value is negative, then there was more change in that dimension for a given individual and treatment after transection. This metric is useful to assess the overall change, but masks small successive increases and decreases within each phase, and is ultimately the difference of two differences. However, the metric is a good general descriptor to evaluate changes in phase transitions and creates an intuitive baseline for comparison.

When relative chew cycle phase timing was compared (Figure 2.9), timing was highly variable in how much FC1, FC2, SC1, SC2, and the start of SO changed. However, the transition from SO to FO was very regular, always occurring at around the 90% mark of the cycle. The pathological individual with a cavity in the left fourth molar, opossum M, showed the same amount of post-transection variation as healthy individuals.

When difference in rotations and translations was taken for each phase of each individual and food type (Figure 2.10), it became obvious that the greatest determinant in the amount of phase change was not working or balancing side or even roll vs yaw, but whether the data was being measured from the right or left hemimandible. For example, Opossum Li (Figure 2.10 A-B) shows the most change in the roll dimension (red bars) for the right hemimandible for both almonds and cheese. The change is negative, meaning there is less of it in the transected

condition than the healthy condition. In the left hemimandible, there is less roll and more translation (green bars) for almond, but relatively little rotational change during cheese feeding. Note that there is a consistent amount of change in yaw (orange bars) in both working and balancing sides for cheese, except for left working side cheese, where very little change in yaw is observed.

Opossum Lu (Figure 2.10 C-D) shows a similar pattern, but with translations dominating on the right mandible and positive or negative roll for the left mandible. A positive change in roll is associated with the balancing sides, while a negative change in roll is associated with the working sides. Opossum W (Figure 2.10 E-F) also shows the greatest amount of rotational change in roll in all conditions except for right hemimandible cheese. There, little difference is observed except for in FC1 and SO. For opossum Mi (Figure 2.10 G) the only pre and post data available was for the cheese condition. Changes in anteroposterior translation (TX; green bars) dominates the right hemimandible, with significant changes in superoinferior translation (TY, blue bars) and gape (RX; yellow bars) as well when the y-axis range is considered. The left mandible has significant changes in roll, superoinferior translation, and gape. It is also noteworthy that superoinferior translation (TY) and gape (TZ) change from pre to post transections were consistently greatest during FC1 and FO for the majority of sides and individuals, consistent with the fast opening and closing of the hemimandibles.

***3D Traces and food type***

As in Chapter 1, anteroposterior, mediolateral, and superoinferior coordinates of movement at the right and left lower molar talonid basins were mapped out for each chew cycle by individual animal, food type, working side, and right or left mandible (Figures 2.10 to 14),

this time with both the pre and post-transection conditions. The traces are oriented as if the opossum is facing the reader, with right hemimandibles on the reader's left and the left hemimandible on reader's right. The cycles were then labeled with molar location at phase transitions, to illustrate our understanding of where in space each transition occurs. Each trace starts at maximum gape (darker blue dot) and moves laterally to the opossum's right for right working side and left for left working side. Overall, 3D kinematic traces were often skinnier post-transection, indicating less mediolateral movement overall (Figure 2.11 D-F) or there was a mediolateral change in the shape of excursion envelop (Figure 2.12 K-N). Superoinferior excursion was also more variable (Figure 2.13 O-R).

## DISCUSSION

### *Bilateral Feedback*

These new data from multiple individual animals reveal evidence for bilateral dentoalveolar feedback during mastication. Even though feedback was lost for the dentoalveolar system in the left lower quarter of oral space, the system was not unilaterally affected. Right side chews, which were receiving full neurofeedback from the intact right side, were just as affected as the left side chews, no matter if the left side was in the working or balancing condition. In fact, often the right hemimandible showed more change (Figure 2.5, Opossum Li) or 'complimentary change'. That is, if roll everted more on the left side, for the same phases the right mandible would be more inverted than the intact nerve transition (Figure 2.5, Opossum W cheese right working).

Mediolateral translations (Figure 2.7) were smaller after transection, especially for the right hemimandible for the cheese treatment (Opossums Li and Lu). Right side pitch (Figure 2.3)

and superoinferior translation (Figure 2.6) was altered for Opossum W post-transection. Changes in rotation or translation from the pre to post transection condition were highly correlated with hemimandibular side (Figure 2.10), but there were correlations in working vs balancing side as well. For instance, compare working and balancing sides for Opossum Lu data in Figure 2.10 for FC2 and SC1. Some of the changes in the rotations and translations may be a result of an overall shift in the angles at which the two hemimandibles were held, throughout the cycle. For example, Opossum Li's averaged right hemimandible translations are often translated superiorly or inferiorly relative to the intact condition trace on all the averaged chew cycle graphs (see Figures 2.4 and 2.5).

The question is, are these changes a byproduct of mechanical connections between the hemimandibles, or are they solely the result of the one-sided interruption of neurofeedback? If these changes were a result of only being a semi-connected system, I would expect the changes to occur in only one side or the other. Instead, I see that sometimes the transected side is more affected and sometimes the non-transected side is more affected. It is also telling that all the opossums still chose to chew on the transected left side, even without feedback from the mandibular teeth. Like a person with dentures, they chewed on the afflicted side with the neurofeedback information they could get. To get more answers, I turned to Opossum M.

***Opossum M***

Opossum M turned out to be an exception that proved the rule and provided useful information on animal pain management. After all data was collected, the head of Opossum M was scanned and I found that this individual had a cavity on the left fourth molar. When I mapped out the chew cycles (Figure 2.14) I found that the animal rarely chewed on the left

working side even in the “healthy” condition and the animal had a very small cycle for almond, as shown by the very small 3D traces envelop (Figure 2.14). Notably, the animal still tried to eat on the left side even though the small envelop of the 3D traces and evidence of tooth infection indicate that the animal was in pain. The right working side chew cycle was larger for almond, with distinct phase transitions, but was still smaller than the equivalent cycles in Opossum Li (Figure 2.11), a similarly sized individual. For cheese cycles Opossum M had similarly oddly small cycles in 3D traces, with only the balancing sides occluding and the working sides held open. None of the other opossums showed these behaviors in the healthy working condition, or transected condition. This also told us that none of the other opossums were likely in pain after the nerve transections.

After the left inferior alveolar nerve transection, Opossum M’s chew cycles became more like the other opossum’s healthy conditions, relative to Opossum M’s “healthy” chew cycles. That is, for cheese cycles both the right and left working side hemimandibles were equal in height to the balancing side chews and appeared to be occluding. This also explains the difference in the right mandible seen for Opossum M in Figure 2.10. The right working side chews were an elongated bean shape and showed a clustering of the chew cycle phases similar to other healthy individuals. Left working side chews, however, showed a kinematic trace similar to a left side chew and were not elongate. This suggests that, even though Opossum M didn’t feel the pain from the tooth infection anymore after the transection, it had been around long enough that she did not have any left working side stereotyped feeding behaviors to fall back on when there was no feedback.

Opossum M’s chew cycles both before and after transection points to feedback from both the working and balancing sides that relies on a combination of learned behavior and

neurofeedback, with a part of that neurofeedback coming from the dentoalveolar feedback. Taken in combination with the significant changes in roll and mediolateral translation, as well as the evidence that all the opossums showed evidence of favoring one side or the other, bilateral feedback from both the working and balancing mandibles appears to be necessary for the chew phases associated with occlusion.

***The significance of roll***

Unilateral transection resulted in a significant reduction in roll, with shallower slopes during both eversion and inversion. This is most evident in Opossum Li (Figure 2.5), but can be seen in all the opossums. Translation only changed by a few degrees, if present at all. This suggests that the roll is the dominant kinematic component influenced by feedback of the dentoalveolar system. Yaw may be either a more stereotyped behavior that doesn't rely on feedback. Another possibility is that the yaw dimension is influenced by feedback from a different set of mechanosensors than those of inferior alveolar nerve network. For example, nerves in the temporomandibular joint could be involved.

Given the debate outlined in Chapter 1, I suggest that a further helical axis analysis is needed to assess if roll is the dimension most significantly affect by neurofeedback, relative to yaw and pitch. As mentioned in the previous chapter, using a pre-set coordinate system on individuals that grow allometrically can cause amplifications of some dimensions and diminish others. It's worth taking a second look at the effects of nerve transection with a different type of analysis.

### *Timing of Phases*

For most of the phases, the overall timing of phase transition was variable and did not alter in a systematic way from pre to post-transection conditions. However, the transition from SO to FO was very regular, always occurring at around 90% of chew cycle duration. This is consistent with the hypothesis that the transection is primarily affecting the "occlusal" phases (FC2, SC1, SC2, and the start of SO). The differences in phases may be due to individual effects, but this will require further analyses to begin to pick apart the system. Additionally, timing may be affected by chew cycle order and intra-cycle variation (see Discussion in Chapter 1), which needs to be tested in a future analysis.

### *Other functions of IAN*

Up until this point, the IAN has only been considered in terms of tooth sensory functions, but the IAN can also provide sensation to a number of other structures after it enters the mandibular foramen (i.e., the portion that was transected in this study). In humans, the majority of the nerve passes through the mandibular canal and gives off branches to the teeth (Carter and Keen 1971). A subset continues anteriorly to exit the mandible through the mental foramen to become the mental nerve, which provides sensation to a portion of the gums, the lower lip, and chin. These small nerves often insert into the lower incisal dentoalveolar complexes from cervix of the root. In other animals this nerve also innervates sensitive chin vibrissae (Hiroshima et al. 1998, Reep et al. 1998, Pyenson et al. 2020). Portions of the IAN may also exit on the medial portion of the body of the mandible and communicate with the nerve to mylohyoid or exit around the area of the mental spines. In fact, the nerve to mylohyoid as well as the lingual nerve may

sometimes extend anteriorly to innervate the lower incisal teeth through retromental foramen (Frommer et al. 1972, Rood 1977,Wilson et al. 1984, Moodley 2017, Kini et al. 2020). Finally, the left and right IAN meet anteriorly as the incisal nerve in to create a nerve plexus and/or anterior loop at the midline in fused mandibles (Carter and Keen 1971). In animals with unfused mandibles, blood vessels and nerves from the incisal n., mental n., and possibly the nerve to mylohyoid all innervate the symphyseal region, but, for the majority of animals, it is largely unknown if the innervation is just sympathetic afferents associated with vasculature or if there is a sensory feedback component. Rorqual whales have a sensory organ found within the fibrous ligament of the unfused symphysis that is innervated by the incisal nerve and is thought to respond to jaw movement and ventral groove blubber expansion (Pyenson et al. 2012) and there are nerves found in the symphyseal joint of carnivorans such as *Canis familiaris* (Scapino 1965). However, there are no studies explicitly studying the symphysis as a sensory system beyond cetaceans. There is also evidence that edentulous mammalian species still maintain an IAN for sensory feedback during feeding. Myrmecophageous anteaters, armadillos, aardvarks, and filter-feeding baleen whales show dorsal canaliculi connecting the IAN to the edentulous regions, which are often covered in a keratin pad (anteaters) or baleen (whales), in place of teeth (Ferreira-Cardoso et al. 2019).

The nerve transection in this study could have cut off feedback to structures innervated distally to the teeth, such as feeling to the lower lip, chin vibrissae, and even the mylohyoid muscle. In fact, the nerve to mylohyoid itself could be innervating some of the lower incisors. Although these are interesting confounding factors, these variations in innervation are more likely to affect ingestion and stage 1 transport than the chew cycles, which are localized primarily on the molars. Chew cycle kinematics might be affected by the degree of innervation

(or loss of innervation after the unilateral transection) in the mandibular symphysis, but this has yet to be directly tested in any animal. If the opossums receive sensory feedback from the mandibular symphysis, then a unilateral transection would only cut off part of this feedback system, and the amount would be dependent upon the degree of innervation from the left IAN. This could be tested with local anesthesia to the mandibular symphyseal region.

## CONCLUSION

Overall, these changes show that the kinematics measured during post-transection mastication are likely a mix of individual learned responses to nerve transection, and a change to the entire stereotyped system. Individual responses include the average change in a dimension, if almond or cheese is more difficult to chew, or even what phase cycle is changed. But three important patterns emerge:

(1) Both hemimandibles show changes in kinematics, even when the healthy right side is the working side.

(2) Transected individuals preferentially evert either their right or left hemimandible for the entire cycle.

(3) Roll is the rotational dimension with the most change, while mediolateral translation is the movement at the M1 talonid basin with the most change.

The results reported in this chapter strengthen the hypothesis that the phases of the chew cycle where tooth-tooth or tooth-food-tooth contact are likely to occur (end of FC2, SC1, SC2, and start of SO) are controlled bilaterally through dentoalveolar neurofeedback. Transecting the inferior alveolar nerve unilaterally does not entirely inhibit mastication, but limits the ability of the animal to respond to changes in food physical properties in all dimensions, primarily roll.

This has important implications for early evolution of tooth occlusion coupled with changes to the jaw joint in the earliest-known mammalian form, and for how to infer functional change in that morphological transition. Almost certainly the neurofeedback, as seen in *Didelphis virginiana*, is implicated in the early tribosphenic therian mammals. An early therian mammal with tribosphenic molars would also need a similar neurofeedback system for such complex occlusal surfaces of tribosphenic molars to function, as demonstrated here in the in vivo experimental studies of *Didelphis virginiana*.

# CHAPTER 2:

# FIGURES

FIGURE 2.1.

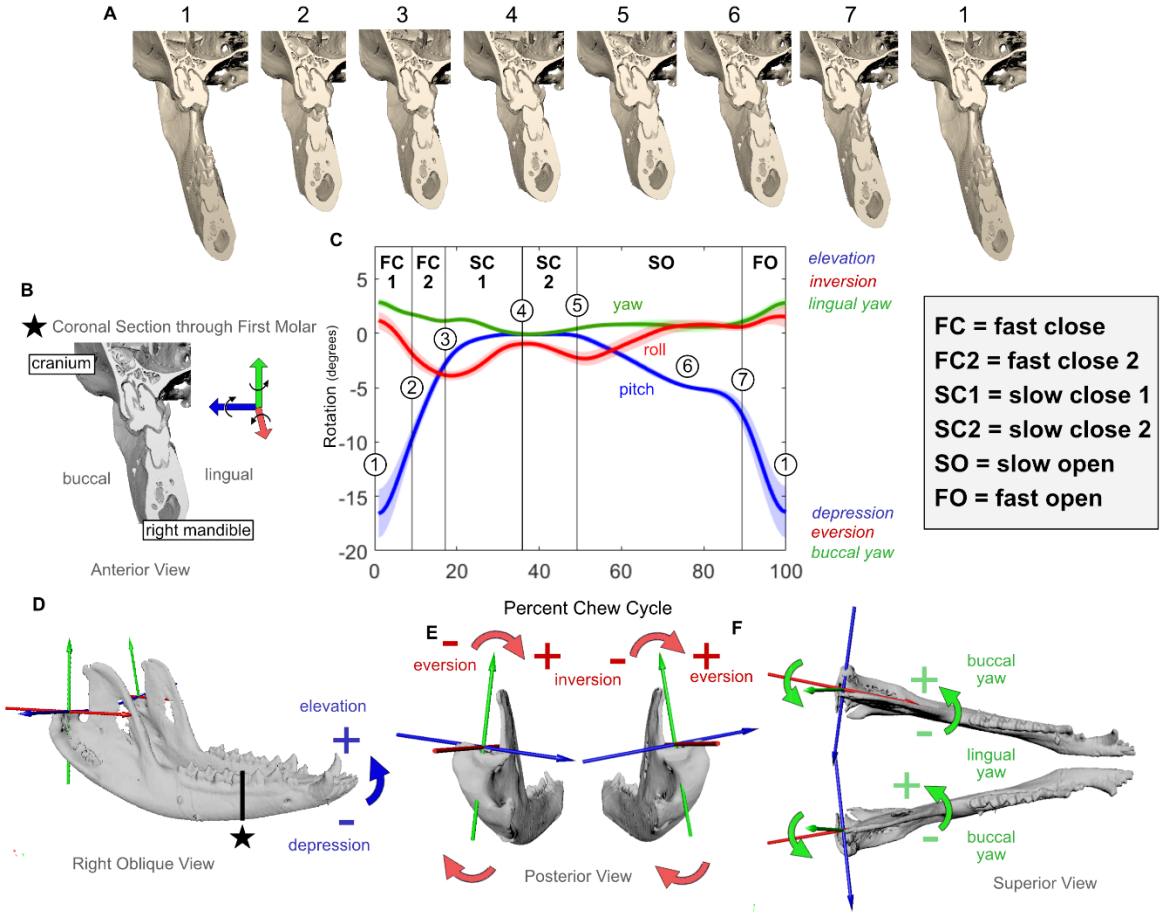


**Figure 2.1. Definitions of gape cycle phases, coordinate systems, and kinematic terminology.** (A) Movements of right mandible relative to the cranium during a right-sided chew; anterior view at a coronal section through cranium and mandible at the level of upper and lower M1s. Numbers correspond to numbering in (C). (B) Anatomical terminology on a coronal section through cranium and left mandible. (C) Mandibular pitch (blue), yaw (green), and roll (blue), and vertical kinematic gape cycle phases (*sensu* Ross and Iriarte-Diaz, 2019). Traces are averages +/- 1 S.D. for n = 39 chews on almond by individual Li normalized to a gape cycle duration of 100%. Numbers correspond to jaw positions in (A). Rotations in this graph are for the right mandible only. See (D, E, F) for definition and polarity of rotations. (1) Beginning of fast close 1 (FC1), the mandible is at minimum pitch (maximum gape), maximum lingual yaw, and maximum inversion. (1)-(2), FC1, hemimandible pitches upward, yaws buccally, and everts. (2) start of FC2, pitch often slows prior to SC, sometimes associated with a shift from buccal to lingual yaw. (3) Start of slow close (SC), time of largest decrease in rate of pitch during closing and usually of maximum eversion.

**Figure 2.1, continued.** (4) Time of maximum inversion during SC and often maximum buccal yaw; mandible begins to evert and yaw lingually. (5) Start of slow open (SO), as mandible pitches down, it continues to yaw lingually, but roll switches from eversion to inversion. (6) Early slow SO, the working side mandible is pitching down, inverting, and yawing lingually. (7) end of SO, mandible slows down, then in FO rapidly pitches down as it yaws buccally and everts. (D) Oblique view of mandibular axes, highlighting pitch. In both mandibles negative pitch is jaw depression (opening), and positive pitch is jaw elevation (closing). (E) Posterior view of left and right mandibles and mandibular axes, highlighting roll conventions for left and right mandibles. Positive roll follows the right-hand rule (clockwise in posterior view), corresponding to eversion of right mandibular tooth row and inversion of left mandibular tooth row. Negative roll is the reverse. (F) Superior view of the left and right mandibles and mandibular axes, highlighting yaw. Positive yaw is lingual for right mandible and buccal for left; negative yaw is buccal for right mandible and lingual for left. Origin of mandibular axis system is positioned at the highest point near the middle of the condyle, with the positive roll (X) axis (red) oriented to pass over infradentale at the level of the condyle; the positive yaw (Y) axis (green) oriented superoinferiorly (superior is positive); the positive pitch or gape (Z) axis (blue) is the cross-product of the two other axes, positive to animal right. Axis systems of left and right mandibles are similarly oriented (positive is anterior for roll, superior for yaw, and to animal's right for pitch).

FIGURE 2.2.

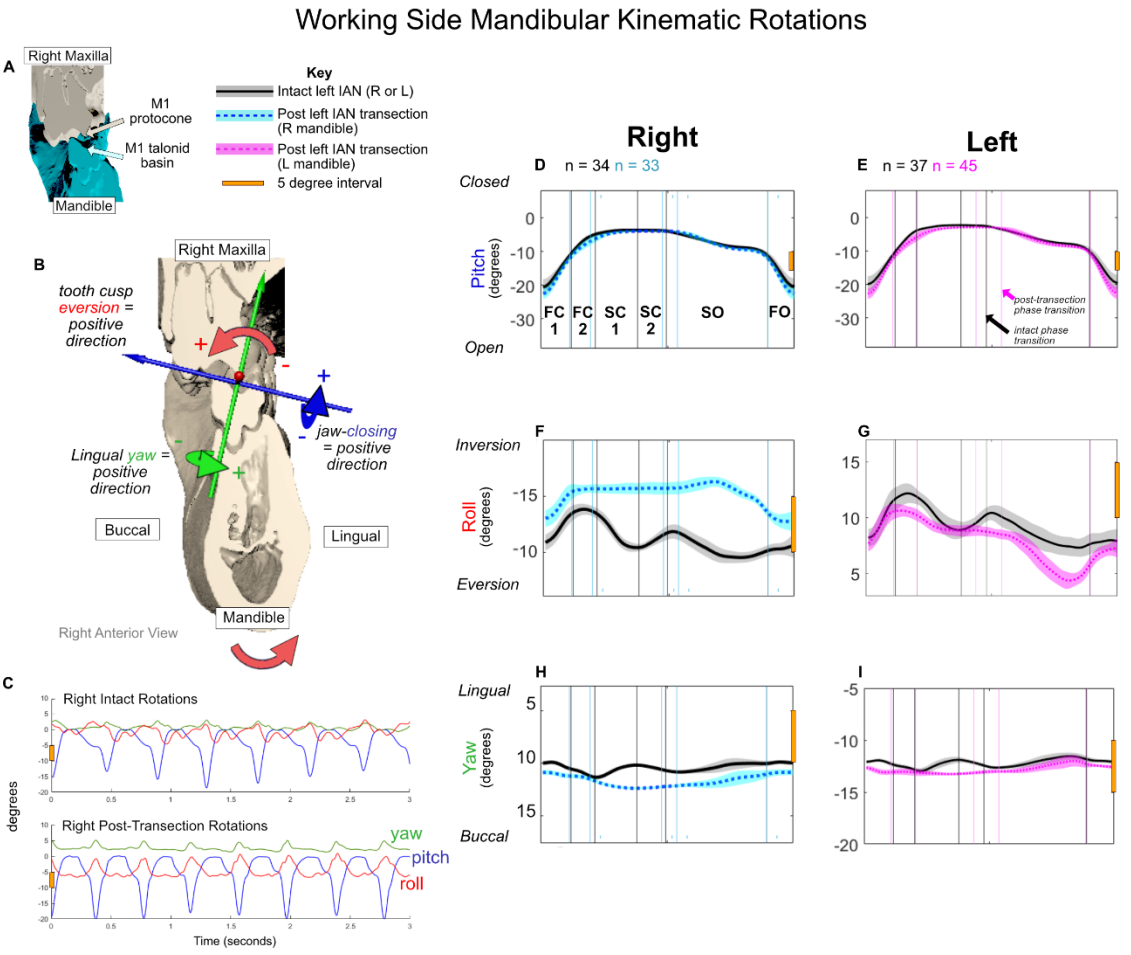


**Figure 2.2. Working side hemimandibular rotations before and after nerve transection.** Food is almond, animal is Opossum Li. (A) Coronal section through right cranium and mandible focal molar cusps and key for kinematic traces. Black solid lines, mean kinematic traces with intact left inferior alveolar nerve (IAN) condition (control); gray, +/- 1 S.D. Aqua, right mandibular kinematics post-left IAN transection; magenta, left mandibular kinematics post-left IAN transection. (B) Anterior view of right molar with rotation coordinate system. Arrows and descriptions indicate positive rotations for right mandible (cf. Figure 1D, E, F). (C) Plot of right mandible rotations in an almond feeding sequence for intact and transected conditions. Colors correspond with axes in 2B. (D-J) Right and left mandibular working side rotations before (black line) and after (aqua or magenta dotted line) left IAN transection. Black vertical lines mark phase transitions in the intact condition; aqua or magenta vertical lines mark phase transitions in the post-left IAN transection condition. The yellow bar on the right of each graph indicates a five-degree increment, highlighting different y-axis scales. FC = fast close, SC = slow close, SO = slow open, FO = fast open. The y-axes in (F), (H) and (J) are inverted so that inversion/eversion and buccal/lingual yaw have the same polarity in the graphs for right and left mandibles; i.e., data for right mandible is presented as if for a left mandible.

FIGURE 2.3.

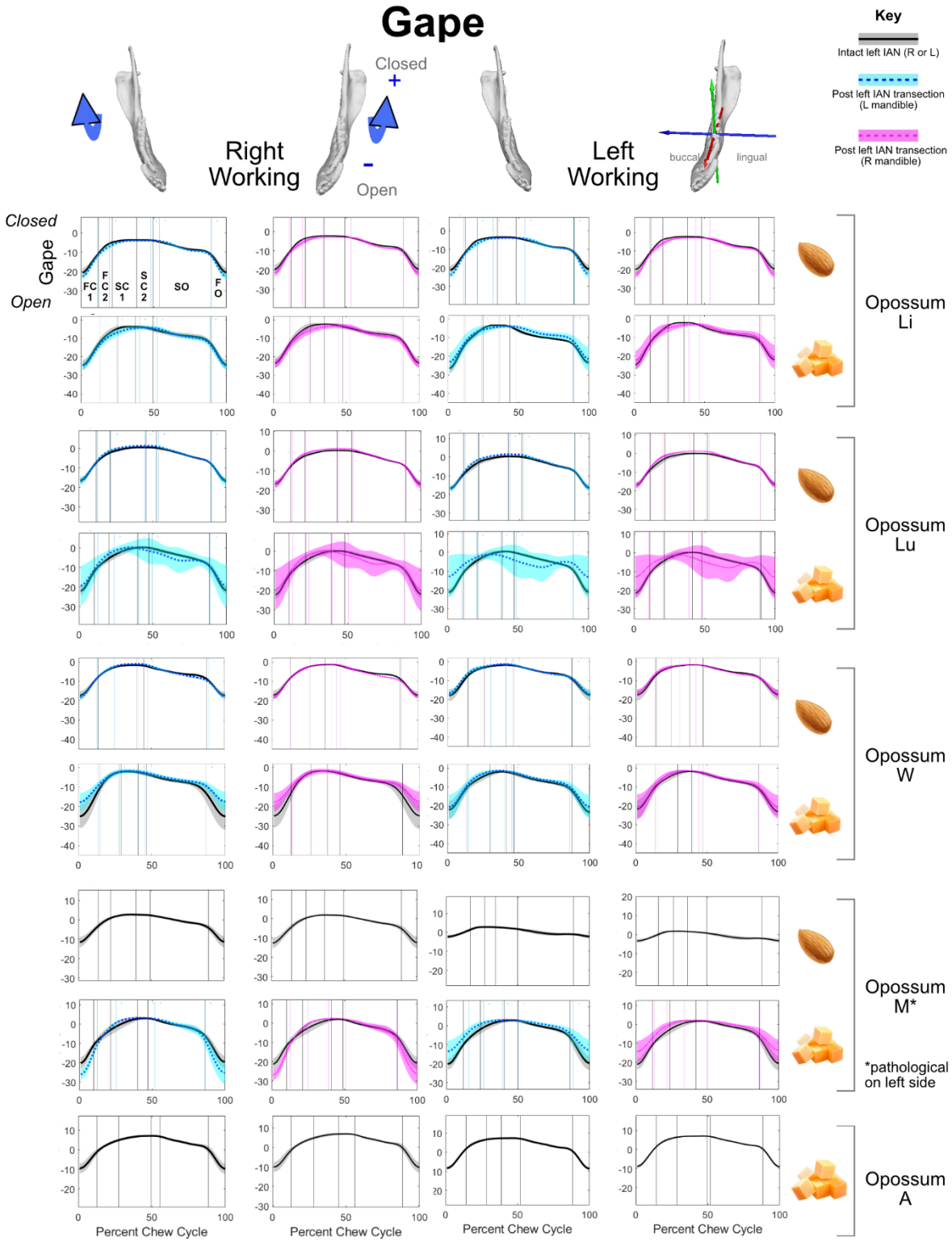


**Figure 2.3. Mandible pitch (gape) by side, individual, and food type.** Right and left mandibular working and balancing side averaged gape cycle rotations (black line).

**Figure 2.3, continued.** Gape is represented schematically at the top of each column. Black vertical lines mark phase transitions. Black solid lines represent kinematic traces with intact left inferior alveolar nerve (IAN) condition (control); gray, +/- 1 S.D. Aqua, right mandibular kinematics post-left IAN transection; magenta, left mandibular kinematics post-left IAN transection. FC = fast close, SC = slow close, SO = slow open, FO = fast open.

FIGURE 2.4.

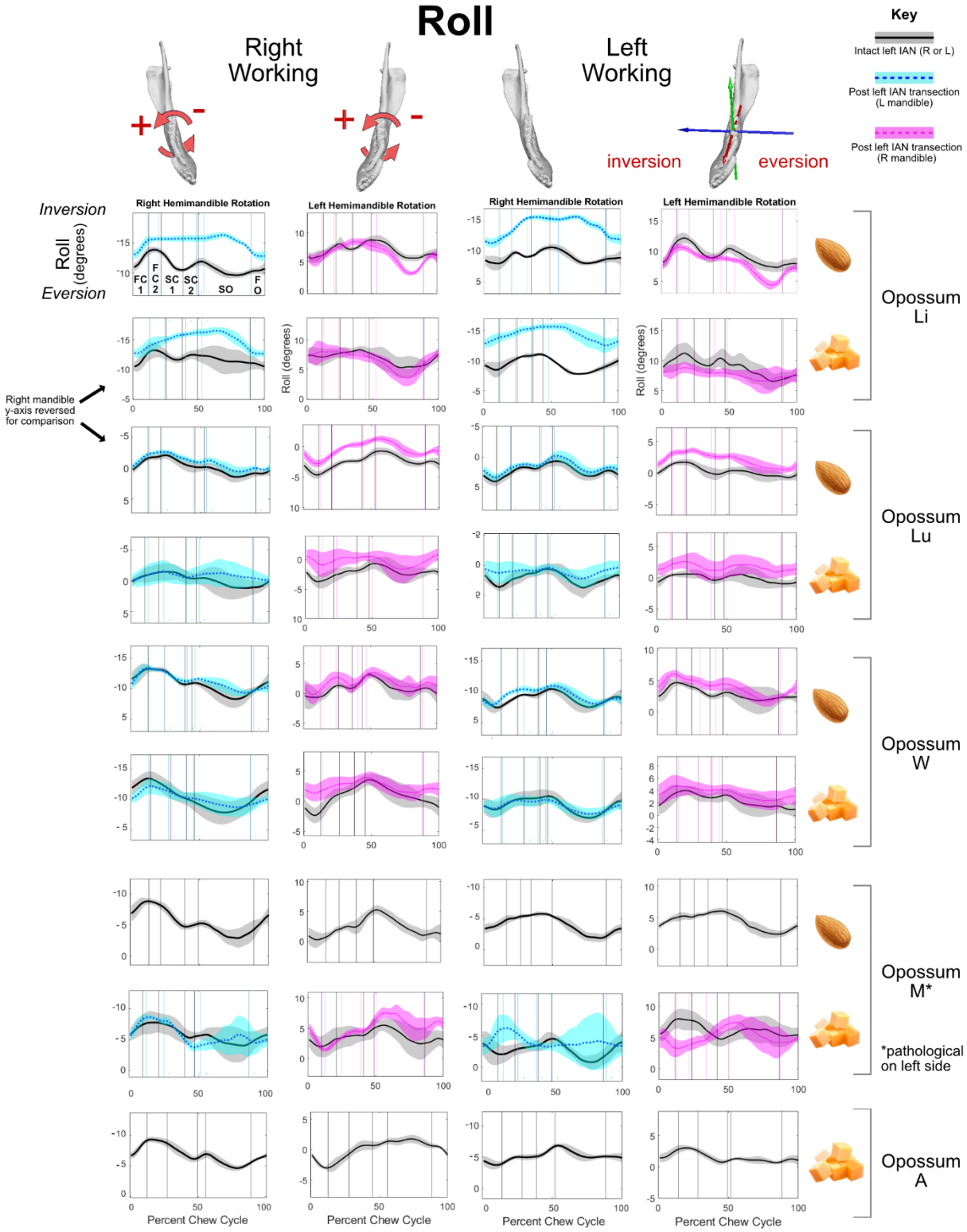


**Figure 2.4. Mandible roll by individual, food type, and hemimandibular side.** Right and left mandibular working and balancing side averaged gape cycle rotations (black line) for all opossums in the study. Roll is represented schematically at the top of each column.

**Figure 2.4, continued.** Black vertical lines mark phase transitions. Black solid lines represent kinematic traces with intact left inferior alveolar nerve (IAN) condition (control); gray, +/- 1 S.D. Aqua, right mandibular kinematics post-left IAN transection; magenta, left mandibular kinematics post-left IAN transection. FC = fast close, SC = slow close, SO = slow open, FO = fast open.

FIGURE 2.5.

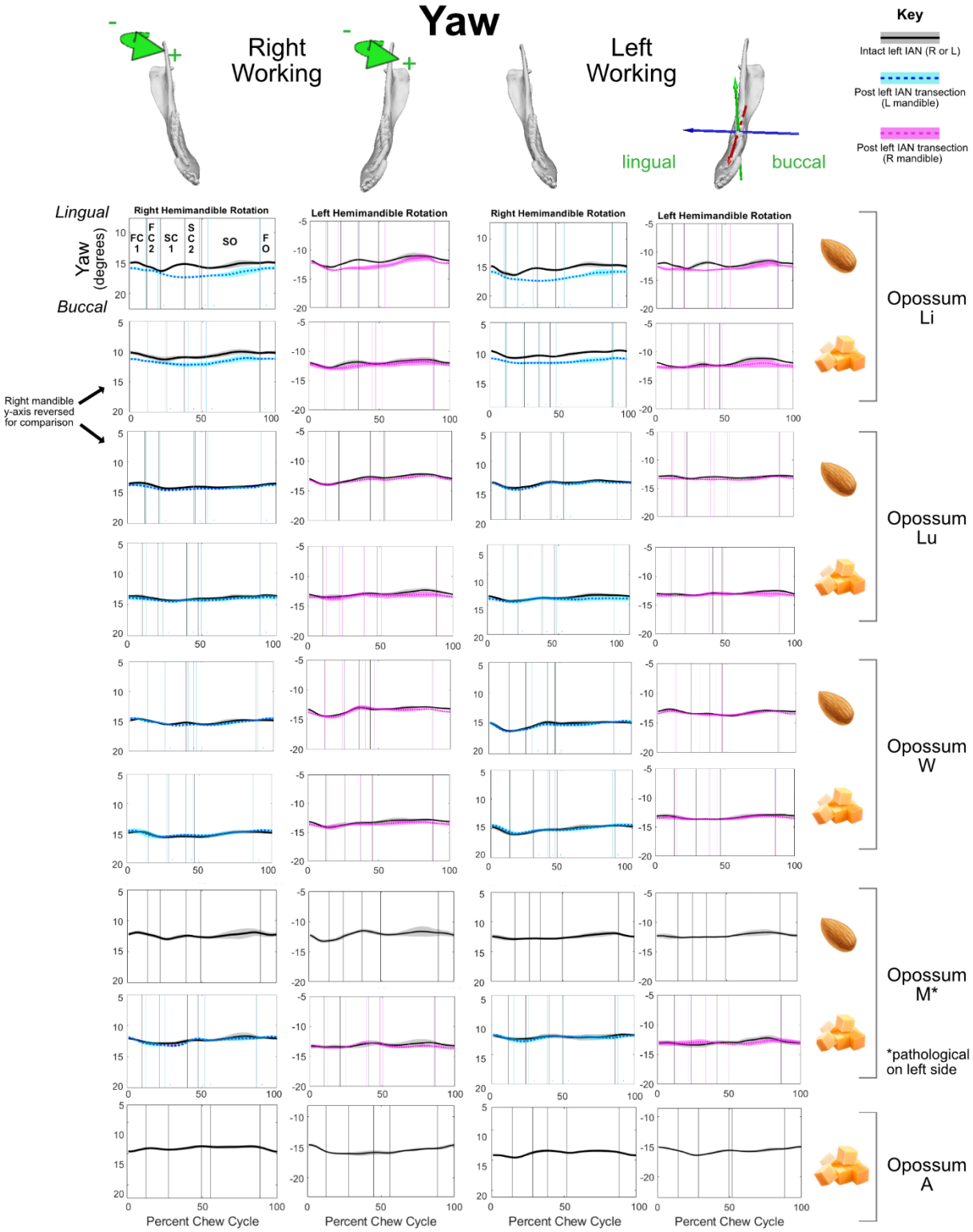


**Figure 2.5. Mandibular yaw by individual, food type, and hemimandibular side.** Right and left mandibular working and balancing side averaged gape cycle rotations (black line) for all opossums in the study. Yaw is represented schematically at the top of each column.

**Figure 2.5, continued.** Black vertical lines mark phase transitions. Black solid lines represent kinematic traces with intact left inferior alveolar nerve (IAN) condition (control); gray, +/- 1 S.D. Aqua, right mandibular kinematics post-left IAN transection; magenta, left mandibular kinematics post-left IAN transection. FC = fast close, SC = slow close, SO = slow open, FO = fast open.

FIGURE 2.6.

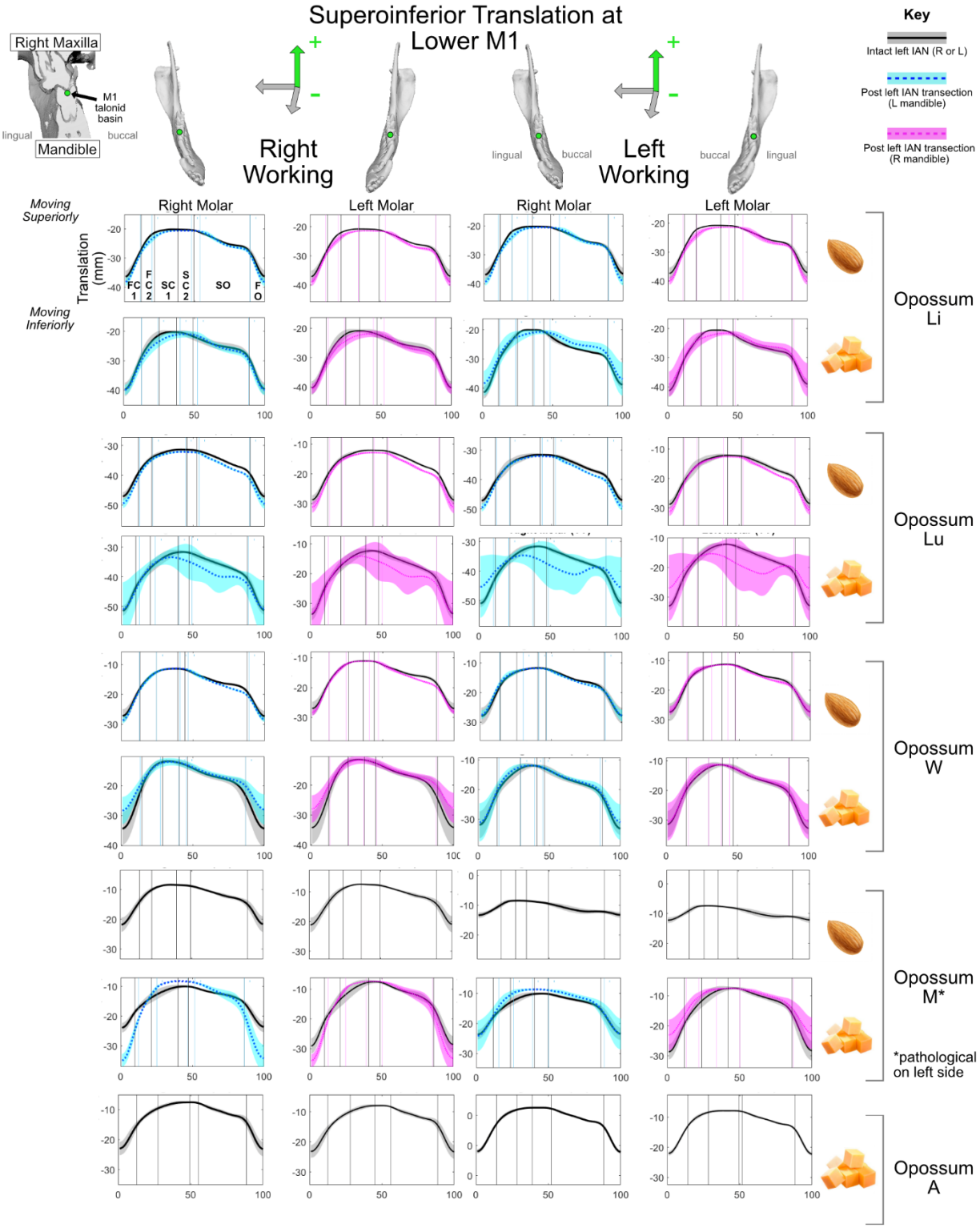


**Figure 2.6. Superoinferior translation of lower M1 by side, individual and food type variation.** Right and left mandibular working and balancing side averaged gape cycle translations (black line) for all opossums in the study.

**Figure 2.6, continued.** Superorinferior translation is represented schematically at the top of each column. Black vertical lines mark phase transitions. Black solid lines represent kinematic traces with intact left inferior alveolar nerve (IAN) condition (control); gray, +/- 1 S.D. Aqua, right mandibular kinematics post-left IAN transection; magenta, left mandibular kinematics post-left IAN transection. FC = fast close, SC = slow close, SO = slow open, FO = fast open.

FIGURE 2.7.

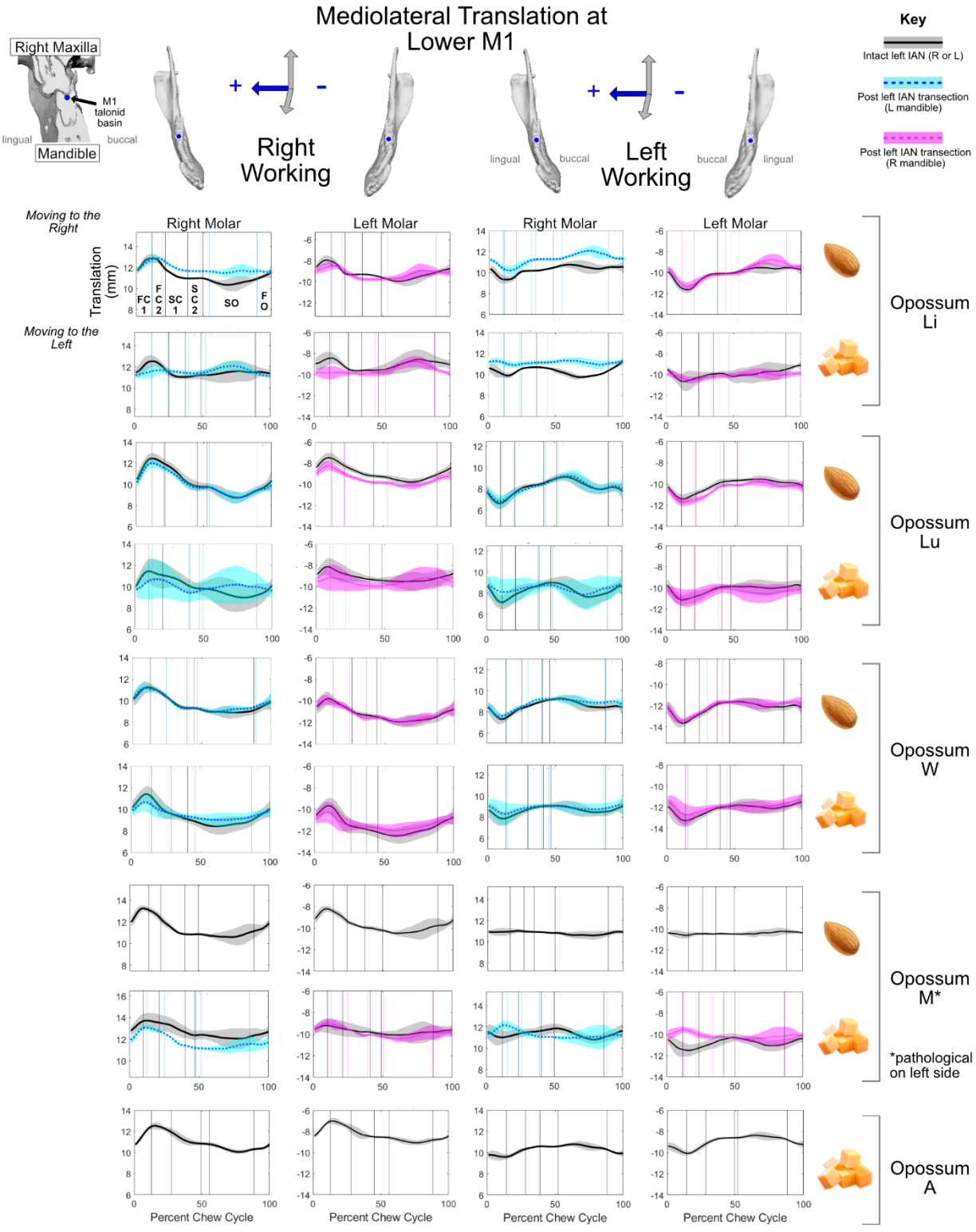


**Figure 2.7. Mediolateral translation of the Lower M1 by individual, food type, and hemimandibular side.** Right and left mandibular working and balancing side averaged gape cycle translations (black line) for all opossums in the study.

**Figure 2.7, continued.** Mediolateral translation is represented schematically at the top of each column. Black vertical lines mark phase transitions. Black solid lines represent kinematic traces with intact left inferior alveolar nerve (IAN) condition (control); gray, +/- 1 S.D. Aqua, right mandibular kinematics post-left IAN transection; magenta, left mandibular kinematics post-left IAN transection. FC = fast close, SC = slow close, SO = slow open, FO = fast open.

FIGURE 2.8

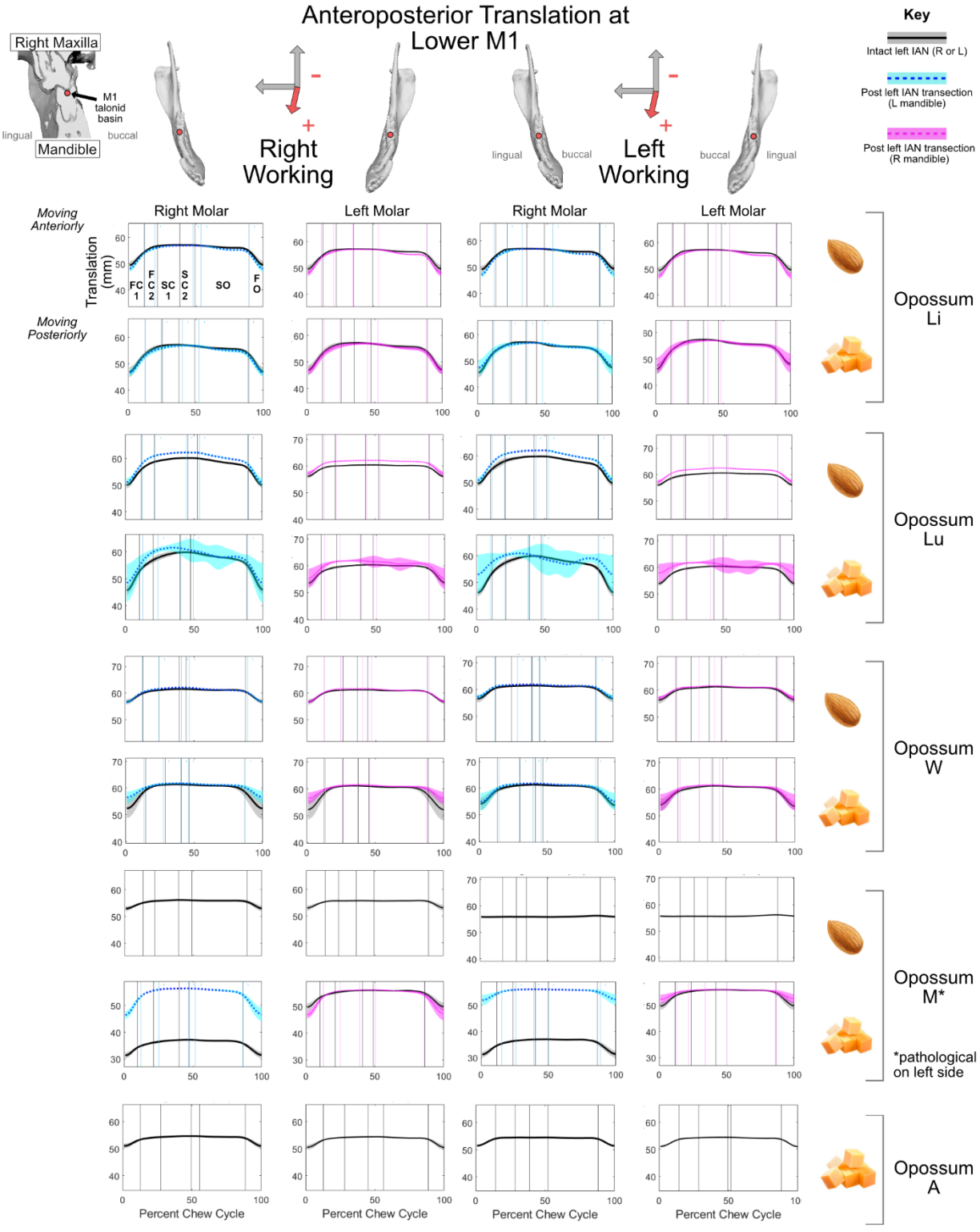


**Figure 2.8. Anteroposterior translation of the lower M1 by individual, food time, and hemimandibular side.** Right and left mandibular working and balancing side averaged gape cycle translations (black line) for all opossums in the study.

**Figure 2.8, continued.** Anteroposterior translation is represented schematically at the top of each column. Black vertical lines mark phase transitions. Black solid lines, mean kinematic traces with intact left inferior alveolar nerve (IAN) condition (control); gray, +/- 1 S.D. Aqua, right mandibular kinematics post-left IAN transection; magenta, left mandibular kinematics post-left IAN transection. FC = fast close, SC = slow close, SO = slow open, FO = fast open.

FIGURE 2.9.

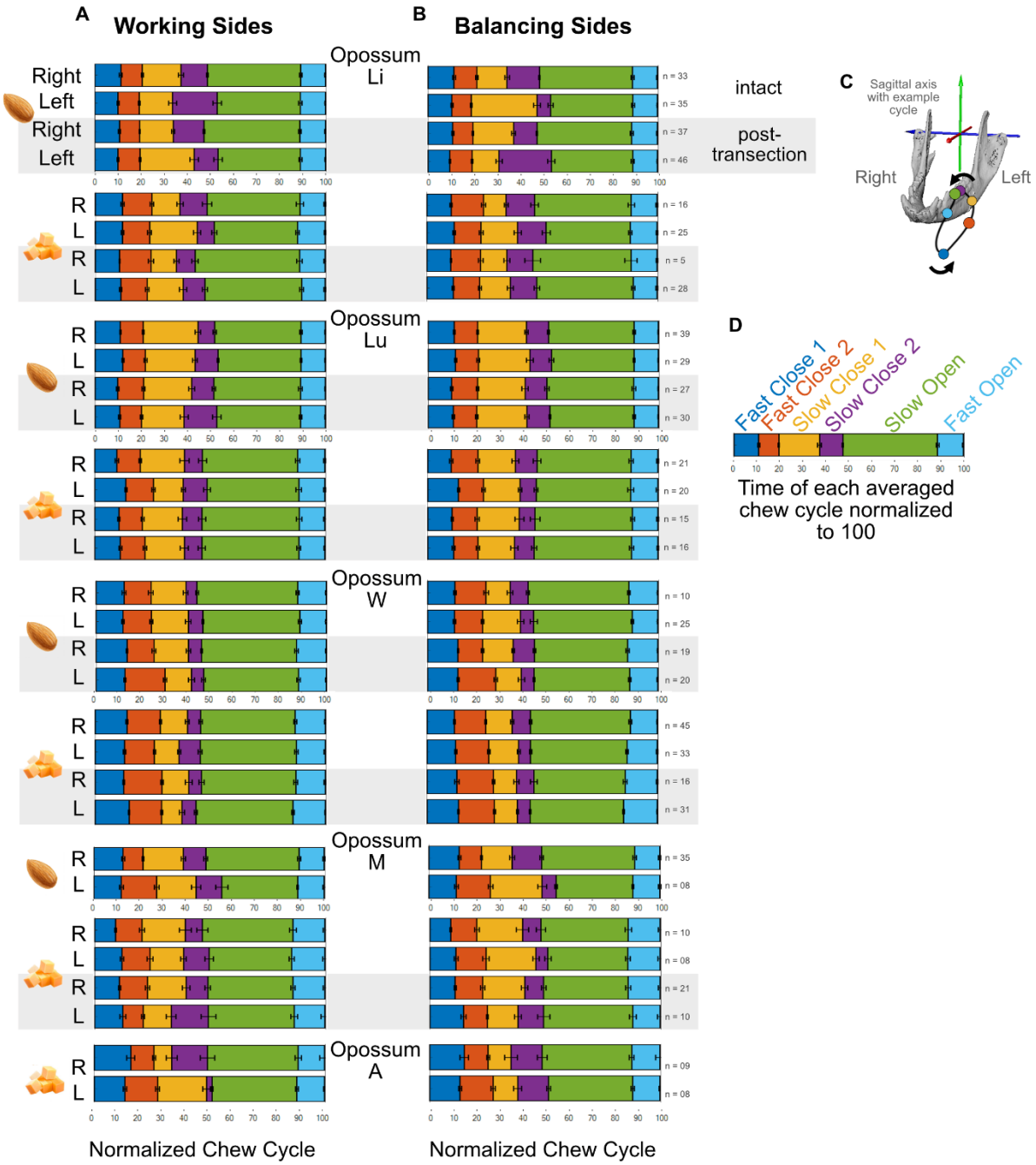


**Figure 2.9. Gape phase timing in right and left hemimandibles by individual and food type.** Right and left average chew cycle phase times for all opossums, food types, and right and left working and balancing sides. (A) Food type is indicated by a symbol on the left of the figure with an almond or cheese cubes. Next to each food type is the R (right) or L (left) working side phase timing. Grey bars indicate a post-transection condition. (B)The right column contains all working sides, with R and L following the same order as the left column. The data is then grouped by individual. All individuals have both almond and cheese data except for opossum A, which only has data for almonds.

**Figure 2.9, continued.** Each bar plot is normalized to a 0:100 scale. n = total cycle number. (C) 3D trace of an example averaged left working side chew cycle color-coded to match the start of each phase represented in the bar graph. The opossum mandible is at an oblique view, facing slightly to the right and laterally and slightly inferiorly. Arrows indicate the direction of the chew cycle. Axis is the mid-sagittal cranial axis that all right and left kinematic data is measured relative to. (D) Example bar plot with phase labels, going from left to right temporally.

FIGURE 2.10.

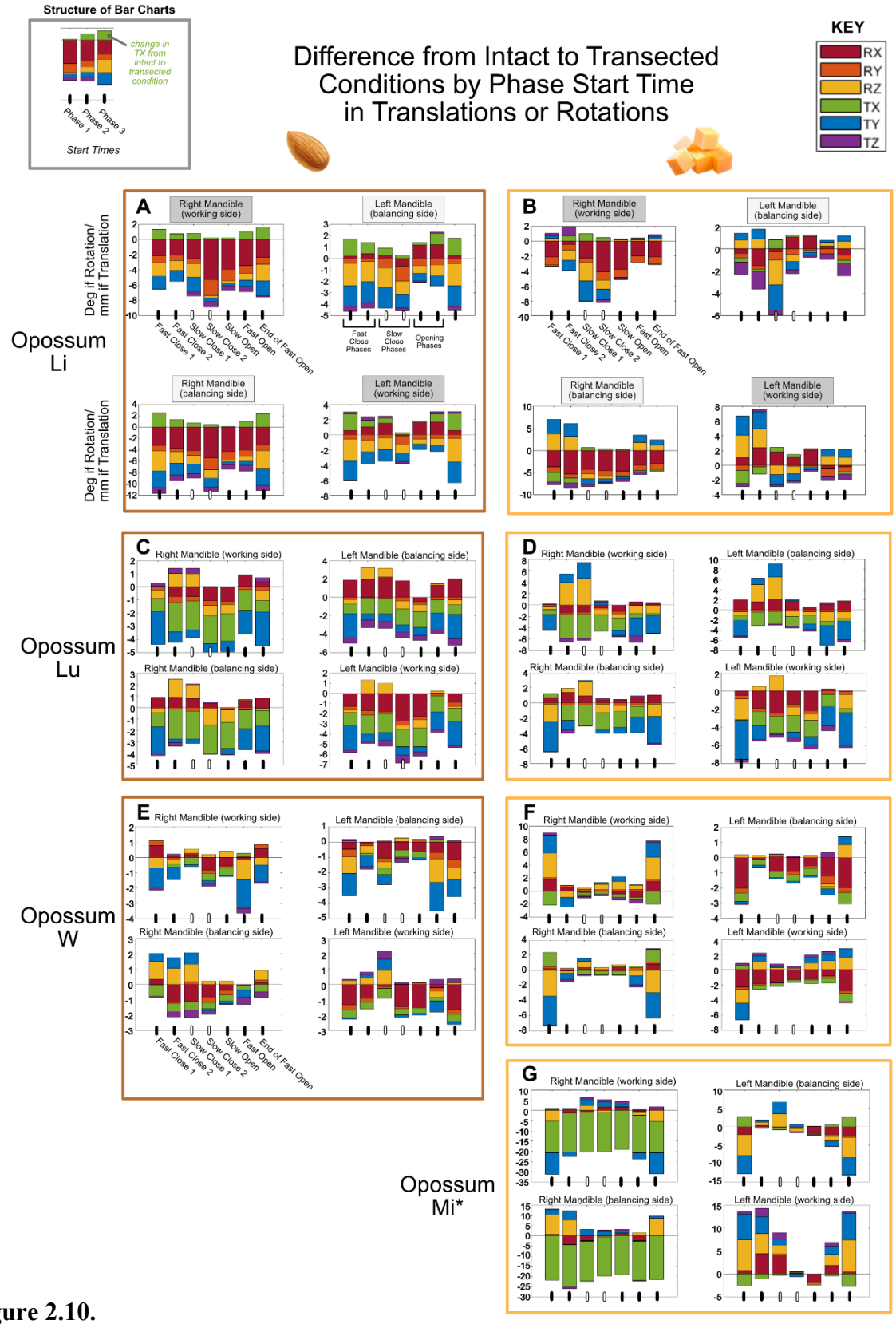


**Figure 2.10.**

**Figure 2.10, continued. Intact versus Transected Inferior Alveolar Nerve differences in Phase Transition by Rotational Movement, and First Lower Molar Translation.** Each box contains the data for one individual and food type. The left side brown boxes are all almond traces, whereas the right-side yellow boxes are cheese traces. Data are then divided into right or left working or balancing side, then by phase and change in average translation or rotation from the intact to the transected IAN condition. The Slow Close phases are in grey (instead of black) to help the reader differentiate between phases. For a given bar chart, a positive y-value means that the post-translation rotation or translation was greater than the intact value, while a negative value means that the intact rotation or translation was greater than the post-transection value. Standard error is reported in the supplimental material. (A) Differences from intact to transected conditions for Opossum Li for almond chew cycles by working or balancing mandible. (B) Differences from intact to transected conditions for Opossum Li for cheese chew cycles by working or balancing mandible. (C) Differences from intact to transected conditions for Opossum Lu for almond chew cycles by working or balancing mandible. (D) Differences from intact to transected conditions for Opossum Lufor cheese chew cycles by working or balancing mandible. (E) Differences from intact to transected conditions for OpossumW for almond chew cycles by working or balancing mandible. (F) Differences from intact to transected conditions for Opossum W for cheese chew cycles by working or balancing mandible. (G) Differences from intact to transected conditions for Opossum M for cheese chew cycles by working or balancing mandible. Asterix indicates that the left mandible had a cavity.

FIGURE 2.11.

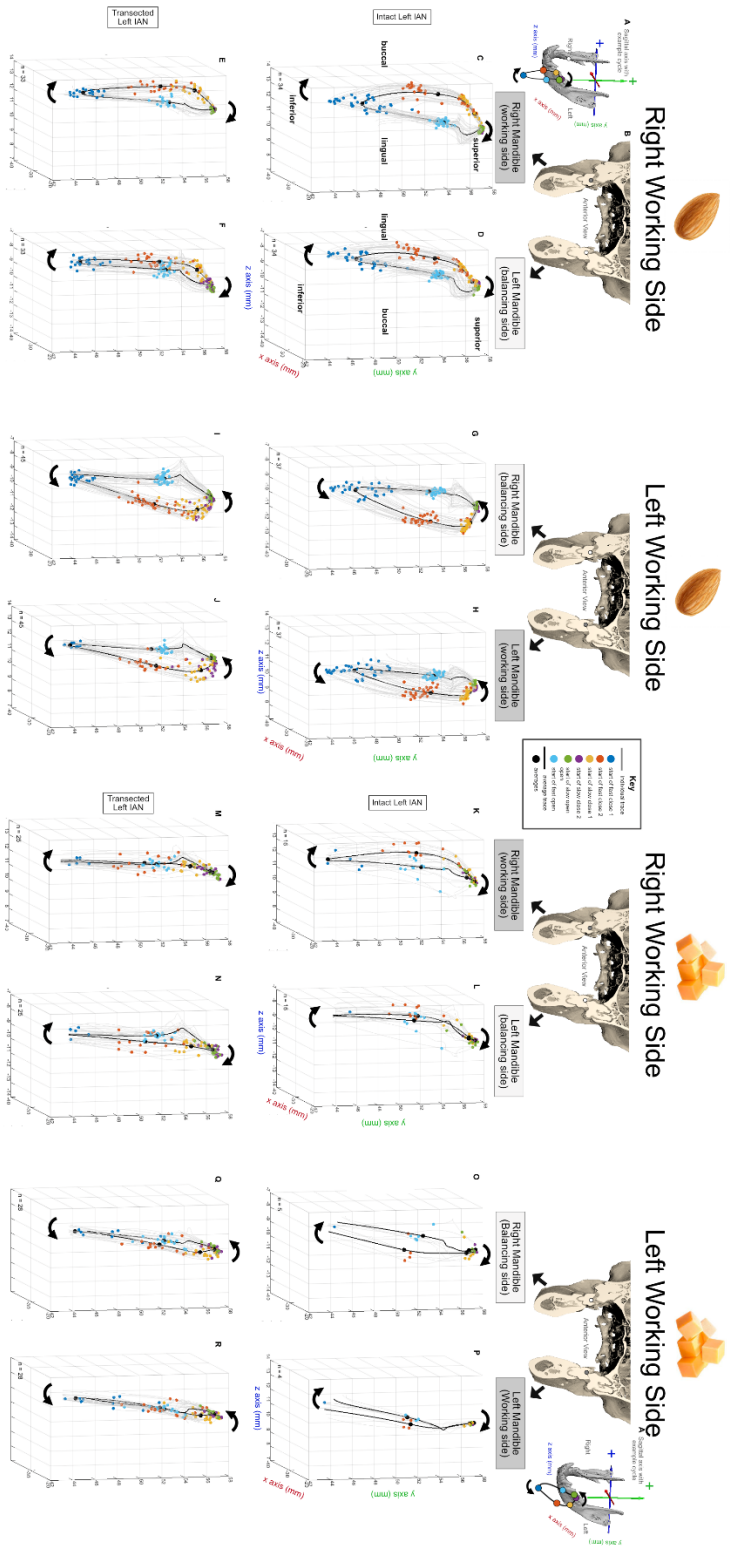


**Figure 2.11.**

**Figure 2.11, continued. Opossum Li - Summary of Phase Transitions and Kinematic Translations Visualized by Major Axes and in 3D.** Traces were calculated in Maya relative to mid-sagittal cranial axis seen in (A) and graphed in Matlab. Each right and left mandible group have the same data, graphed for the right and left sides, respectively. The data was divided into right or left working sides by individual, and then all four states (right working, left balancing, left working, and right balancing) were graphed separately. Therefore, all the data in one row per food type has come from the same group of data collection events. Note that dimensions are the same for each individual, but not between individuals. (A) Orientation diagram: 3D trace of an example averaged left working side chew cycle color-coded to match the start of each phase represented in the bar graph. The opossum mandible is at an oblique view, facing slightly to the right and laterally and slightly inferiorly. Arrows indicate the direction of the chew cycle. Axis is the mid-sagittal cranial axis that all right and left kinematic data is measured relative to. (B) There are two (B) figures, one for each right and left diagram. The figure is a ct scan of an opossum facing the reader and sectioned at the first molar talonid basin, from which the traces were exported. The mandibles match the corresponding labels in (C) and (D) In (B) a dot can be seen at each talonid basin. The darker grey dot is the working side hemimandible, while the lighter grey dot is the balancing side mandibles (also corresponding to their respective labels). The (key) details the colors for the start of each phase. Individual cycle traces are shown in grey, with colored phase transitions, while the averaged chew cycle is shown in black, with black averaged phase transitions. Right working and left balancing trace intact (C-D) and post-transection (E-F) condition for Opossum Li eating almonds. Arrows indicate the direction of the chew cycle. Right balancing and left working intact (G-H) and post-transection (I-J) for Opossum Li eating almonds. Right working and left balancing trace intact (K-L) and post-transection (M-N) condition for Opossum Li eating cheese. Arrows indicate the direction of the chew cycle. Right balancing and left working intact (O-P) and post-transection (Q-R) for Opossum Li eating cheese.

FIGURE 2.12.

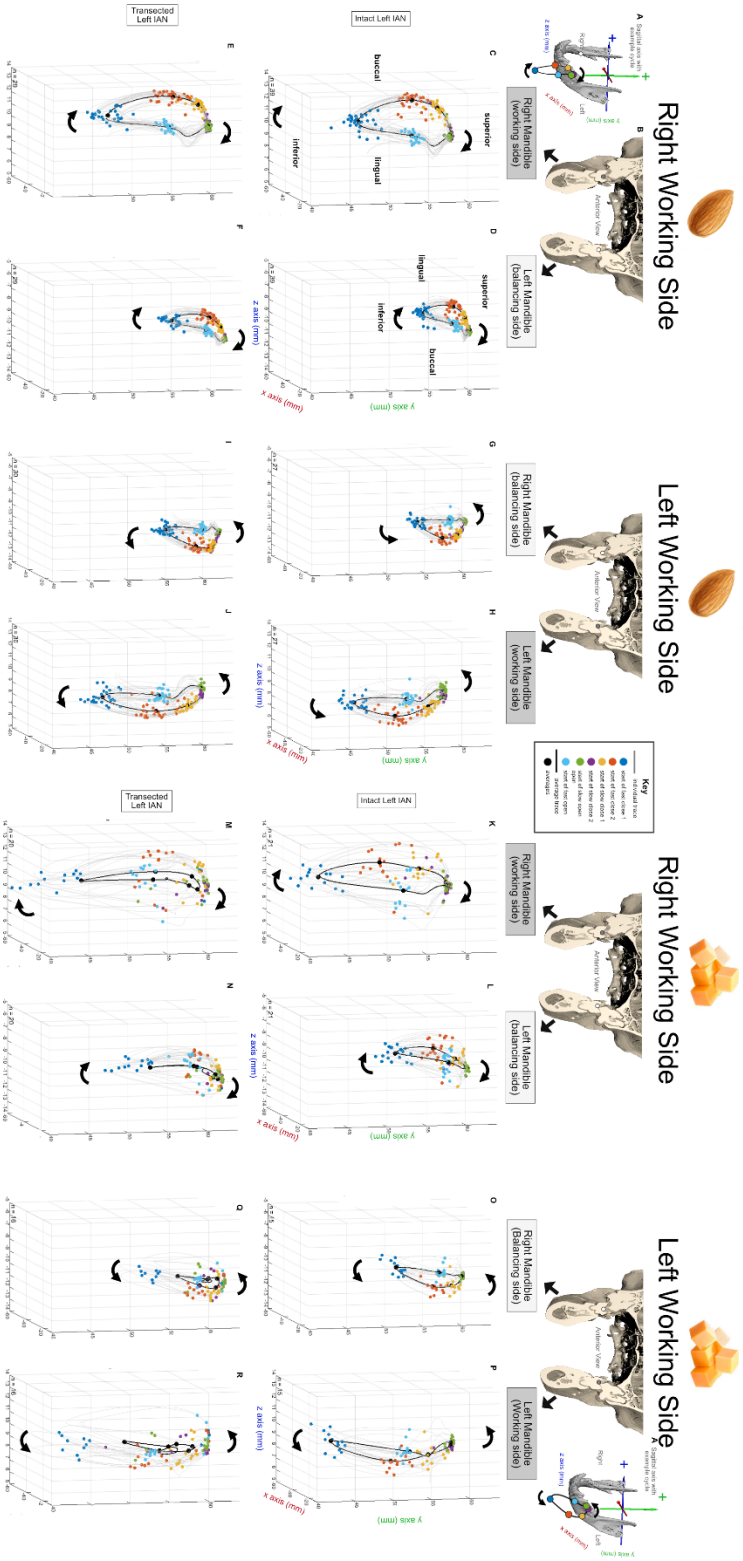


**Figure 2.12.**

**Figure 2.12, continued. Opossum Lu- Summary of Phase Transitions and Kinematic Translations Visualized by Major Axes and in 3D.** Traces were calculated in Maya relative to mid-sagittal cranial axis seen in (A) and graphed in Matlab. Each right and left mandible group have the same data, graphed for the right and left sides, respectively. The data was divided into right or left working sides by individual, and then all four states (right working, left balancing, left working, and right balancing) were graphed separately. Therefore, all the data in one row per food type has come from the same group of data collection events. Note that dimensions are the same for each individual, but not between individuals. (A) Orientation diagram: 3D trace of an example averaged left working side chew cycle color-coded to match the start of each phase represented in the bar graph. The opossum mandible is at an oblique view, facing slightly to the right and laterally and slightly inferiorly. Arrows indicate the direction of the chew cycle. Axis is the mid-sagittal cranial axis that all right and left kinematic data is measured relative to. (B) There are two (B) figures, one for each right and left diagram. The figure is a ct scan of an opossum facing the reader and sectioned at the first molar talonid basin, from which the traces were exported. The mandibles match the corresponding labels in (C) and (D) In (B) a dot can be seen at each talonid basin. The darker grey dot is the working side hemimandible, while the lighter grey dot is the balancing side mandibles (also corresponding to their respective labels). The (key) details the colors for the start of each phase. Individual cycle traces are shown in grey, with colored phase transitions, while the averaged chew cycle is shown in black, with black averaged phase transitions. Right working and left balancing trace intact (C-D) and post-transection (E-F) condition for Opossum Lu eating almonds. Arrows indicate the direction of the chew cycle. Right balancing and left working intact (G-H) and post-transection (I-J) for Opossum Lu eating almonds. Right working and left balancing trace intact (K-L) and post-transection (M-N) condition for Opossum Lu eating cheese. Arrows indicate the direction of the chew cycle. Right balancing and left working intact (O-P) and post-transection (Q-R) for Opossum Lu eating cheese.

FIGURE 2.13.

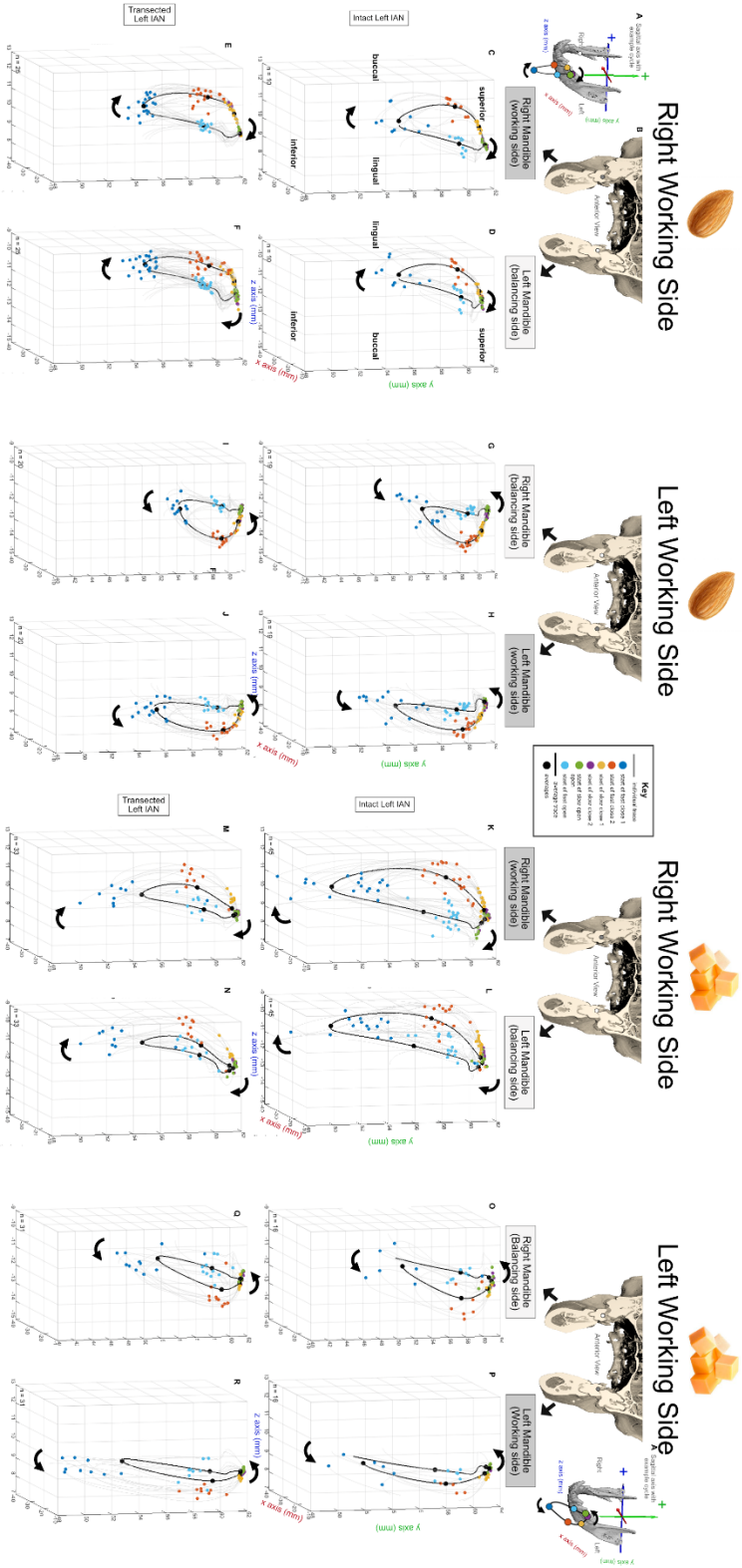


**Figure 2.13.**

**Figure 2.13, continued. Opossum W- Summary of Phase Transitions and Kinematic Translations Visualized by Major Axes and in 3D.** Traces were calculated in Maya relative to mid-sagittal cranial axis seen in (A) and graphed in Matlab. Each right and left mandible group have the same data, graphed for the right and left sides, respectively. The data was divided into right or left working sides by individual, and then all four states (right working, left balancing, left working, and right balancing) were graphed separately. Therefore, all the data in one row per food type has come from the same group of data collection events. Note that dimensions are the same for each individual, but not between individuals. (A) Orientation diagram: 3D trace of an example averaged left working side chew cycle color-coded to match the start of each phase represented in the bar graph. The opossum mandible is at an oblique view, facing slightly to the right and laterally and slightly inferiorly. Arrows indicate the direction of the chew cycle. Axis is the mid-sagittal cranial axis that all right and left kinematic data is measured relative to. (B) There are two (B) figures, one for each right and left diagram. The figure is a ct scan of an opossum facing the reader and sectioned at the first molar talonid basin, from which the traces were exported. The mandibles match the corresponding labels in (C) and (D) In (B) a dot can be seen at each talonid basin. The darker grey dot is the working side hemimandible, while the lighter grey dot is the balancing side mandibles (also corresponding to their respective labels). The (key) details the colors for the start of each phase. Individual cycle traces are shown in grey, with colored phase transitions, while the averaged chew cycle is shown in black, with black averaged phase transitions. Right working and left balancing trace intact (C-D) and post-transection (E-F) condition for Opossum W eating almonds. Arrows indicate the direction of the chew cycle. Right balancing and left working intact (G-H) and post-transection (I-J) for Opossum W eating almonds. Right working and left balancing trace intact (K-L) and post-transection (M-N) condition for Opossum W eating cheese. Arrows indicate the direction of the chew cycle. Right balancing and left working intact (O-P) and post-transection (Q-R) for Opossum W eating cheese.

FIGURE 2.14.

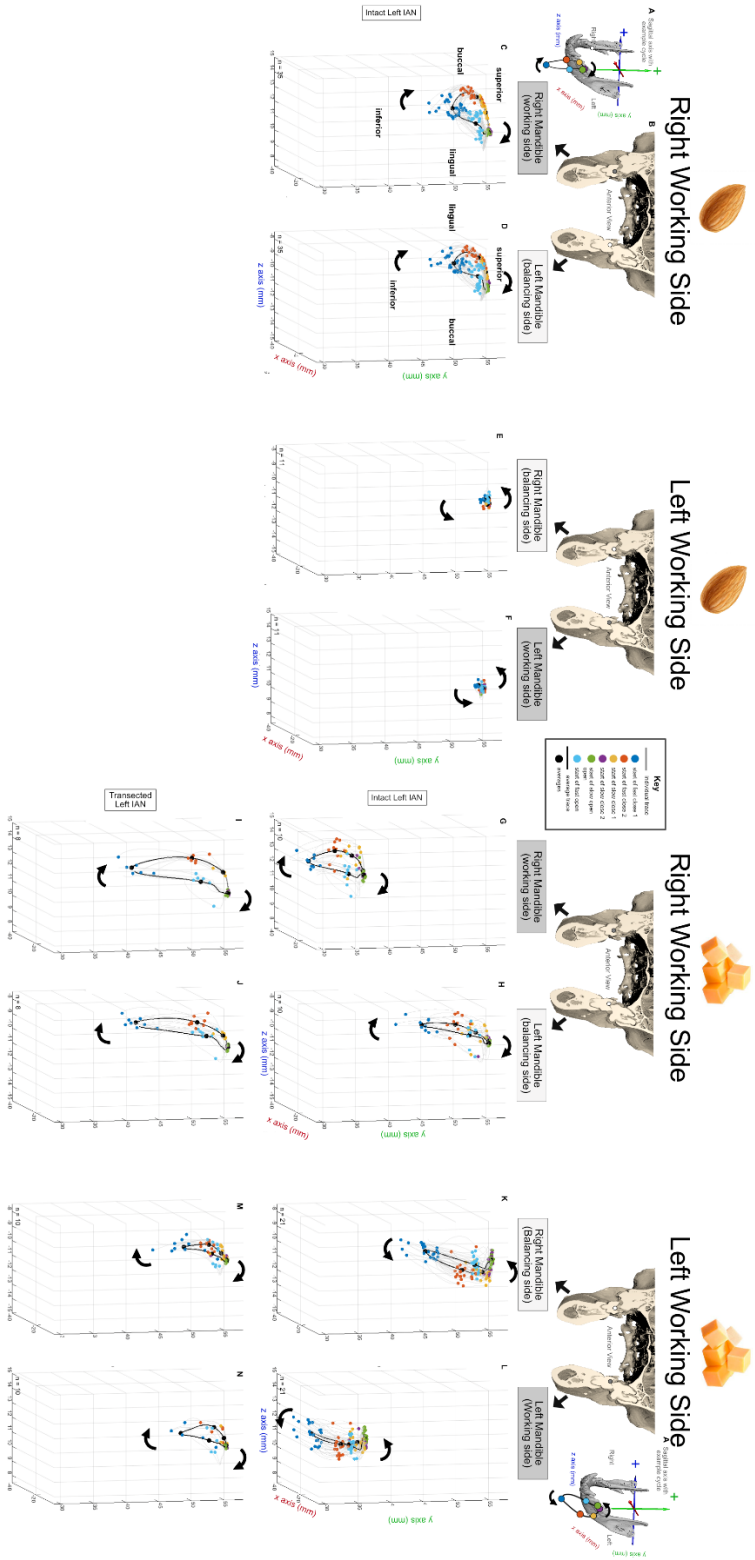


**Figure 2.14.**

**Figure 14, continued. Opossum M - Summary of Phase Transitions and Kinematic Translations Visualized by Major Axes and in 3D.** Traces were calculated in Maya relative to mid-sagittal cranial axis seen in (A) and graphed in Matlab. Each right and left mandible group have the same data, graphed for the right and left sides, respectively. The data was divided into right or left working sides by individual, and then all four states (right working, left balancing, left working, and right balancing) were graphed separately. Therefore, all the data in one row per food type has come from the same group of data collection events. Note that dimensions are the same for each individual, but not between individuals. (A) Orientation diagram: 3D trace of an example averaged left working side chew cycle color-coded to match the start of each phase represented in the bar graph. The opossum mandible is at an oblique view, facing slightly to the right and laterally and slightly inferiorly. Arrows indicate the direction of the chew cycle. Axis is the mid-sagittal cranial axis that all right and left kinematic data is measured relative to. (B) There are two (B) figures, one for each right and left diagram. The figure is a ct scan of an opossum facing the reader and sectioned at the first molar talonid basin, from which the traces were exported. The mandibles match the corresponding labels in (C) and (D) In (B) a dot can be seen at each talonid basin. The darker grey dot is the working side hemimandible, while the lighter grey dot is the balancing side mandibles (also corresponding to their respective labels). The (key) details the colors for the start of each phase. Individual cycle traces are shown in grey, with colored phase transitions, while the averaged chew cycle is shown in black, with black averaged phase transitions. Right working and left balancing trace intact only (C-D) for Opossum M eating almonds. Arrows indicate the direction of the chew cycle. Right balancing and left working intact only (E-F) and Opossum M eating almonds. Right working and left balancing trace intact (G-H) and post-transection (I-J) condition for Opossum M eating cheese. Arrows indicate the direction of the chew cycle. Right balancing and left working intact (K-L) and post-transection (M-N) for Opossum M eating cheese.

# REFERENCES


Anthwal, Neal, and Abigail S. Tucker. "The TMJ disc is a common ancestral feature in all mammals, as evidenced by the presence of a rudimentary disc during monotreme development." *Frontiers in Cell and Developmental Biology* 8 (2020).

Autodesk, INC. (2019). Maya, Available at: https:/ autodesk.com/maya.

Arce-McShane, F. I. (2021). The Association between Age-Related Changes in Oral Neuromechanics and Alzheimer's Disease. *Advances in geriatric medicine and research*, *3*(2).

Archer, M. (Ed.). (1987). *Possums and opossums: studies in evolution*. Beatty.

Beecher, R. M. (1979). Functional significance of the mandibular symphysis. *Journal of Morphology*, *159*(1), 117-130.

Bemmann, M., Schulz-Kornas, E., Hammel, J. U., Hipp, A., Moosmann, J., Herrel, A., Rack, A., Radespiel, U., Zimmermann, E., Kaiser, T.M. & Kupczik, K. (2021). Movement analysis of primate molar teeth under load using synchrotron X-ray microtomography. *Journal of structural biology*, *213*(1), 107658.

Bennett, N. G. (1908). A contribution to the study of the Movement of the Mandible Proc. *Roy. Soc. Med., Sec. Odontology*.

Berkovitz, B. K., Holland, G. R., & Moxham, B. J. (2009). *Oral Anatomy, Histology and Embryology.* Elsevier Health Sciences.

Bhullar, Bhart-Anjan S., Armita R. Manafzadeh, Juri A. Miyamae, Eva A. Hoffman, Elizabeth L. Brainerd, Catherine Musinsky, and Alfred W. Crompton. "Rolling of the jaw is essential for mammalian chewing and tribosphenic molar function." Nature 566, no. 7745 (2019): 528-532.

Bhullar, B. A. S., Manafzadeh, A. R., Miyamae, J. A., Hoffman, E. A., Brainerd, E. L., Musinsky, C., & Crompton, A. W. (2020). Reply to: Jaw roll and jaw yaw in early mammals. *Nature*, *582*(7812), E9-E12.

Blankevoort, L., Huiskes, R., & De Lange, A. (1990). Helical axes of passive knee joint motions. *Journal of biomechanics*, *23*(12), 1219-1229.

Bramble D.M. & Wake D. (1985). Feeding mechanisms of lower tetrapods. In: Hildebrand M.,Bramble D.M., Liem K.F. and Wake D. (eds), Functional Vertebrate Morphology, HarvardUniversity Press, Cambridge, MA, pp. 230–261.

Butler, P. M. (1972). Some functional aspects of molar evolution. *Evolution*, 474-483.

Carter, R. B., & Keen, E. (1971). The intramandibular course of the inferior alveolar nerve. *Journal of anatomy*, *108*(Pt 3), 433.

Cope, E. D. (1889). The mechanical causes of the development of the hard parts of the Mammalia. *Journal of Morphology*, *3*(2), 137-290.

Crompton, A. W. (1971). The origin of the tribosphenic molar. *Early mammals*, *50*, 65-87.

Crompton, A. W., and Hiiemae K. (1969). Functional occlusion in tribosphenic molars. *Nature*, 222(5194), 678-679.

Crompton, A. W., and Hiiemae K. (1970). Molar occlusion and mandibular movements during occlusion in the American opossum, Didelphis marsupialis L. *Zoological Journal of the Linnean Society*, 49(1), 21-47.

Crompton, A. W., & Jenkins, F. A. (1968). Molar occlusion in Late Triassic mammals. *Biological Reviews*, *43*(4), 427-458.

Crompton, A. W., & Luo, Z. (1993). Relationships of the Triassic mammals *Sinoconodon*, *Morganucodon oehleri*, and *Dinnetherium*. In *Mammal phylogeny* (pp. 30-44). Springer, New York, NY.

Crompton, A. W., & Parker, P. (1978). Evolution of the mammalian masticatory apparatus. *American Scientist*, *66*(2), 192-201.

Dellow, P. G., & Lund, J. P. (1971). Evidence for central timing of rhythmical mastication. *The Journal of physiology*, *215*(1), 1-13.

Desole, C., Palmieri, G., & Veggetti, A. (1970). Masticatory proprioception in reptilians (Caiman sclerops). *Experientia*, *26*(4), 376-377.

Dhall, R. S., Gupta, G., Ahluwalia, S., Rawat, A., & Gaur, A. (2021). Osseoperception in Dental Implants. *IP International Journal of Periodontology and Implantology*, *2*(4), 130-135.

Dye BA, Li X, Beltran-Aguilar ED. Selected oral health indicators in the United States, 2005-2008. NCHS Data Brief. 2012 May;(96):1-8. PMID: 23050519.

Espana, A., and Frédéric Clotman. "Onecut factors control development of the Locus Coeruleus and of the mesencephalic trigeminal nucleus." *Molecular and Cellular Neuroscience* 50, no. 1 (2012): 93-102.

Ferreira-Cardoso, S., Delsuc, F., & Hautier, L. (2019). Evolutionary tinkering of the mandibular canal linked to convergent regression of teeth in placental mammals. *Current Biology*, *29*(3), 468-475.

Frommer, J., Mele, F. A., & Monroe, C. W. (1972). The possible role of the mylohyoid nerve in mandibular posterior tooth sensation. *The Journal of the American Dental Association*, *85*(1), 113-117.

Gallo, L. M., Airoldi, G. B., Airoldi, R. L., & Palla, S. (1997). Description of mandibular finite helical axis pathways in asymptomatic subjects. *Journal of Dental Research*, *76*(2), 704-713.

Gallo, L. M., Brasi, M., Ernst, B., & Palla, S. (2006). Relevance of mandibular helical axis analysis in functional and dysfunctional TMJs. *Journal of biomechanics*, *39*(9), 1716-1725.

Gill, P. G., Purnell, M. A., Crumpton, N., Brown, K. R., Gostling, N. J., Stampanoni, M., & Rayfield, E. J. (2014). Dietary specializations and diversity in feeding ecology of the earliest stem mammals. *Nature*, *512*(7514), 303-305.

Gidmark, N. J., Tarrant, J. C., & Brainerd, E. L. (2014). Convergence in morphology and masticatory function between the pharyngeal jaws of grass carp, Ctenopharyngodon idella, and oral jaws of amniote herbivores. *Journal of Experimental Biology*, *217*(11), 1925-1932.

Gliguem, H., Ghorbel, D., Lopez, C., Michon, C., Ollivon, M., & Lesieur, P. (2009). Crystallization and polymorphism of triacylglycerols contribute to the rheological properties of processed cheese. Journal of agricultural and food chemistry, 57(8), 3195-3203.

Gorniak, G. C. (1977). Feeding in golden hamsters, Mesocricetus auratus. *Journal of Morphology*, *154*(3), 427-458.

Goto, T., Kuramoto, E., Dhar, A., Wang, R. P. H., Seki, H., Iwai, H., Yamanaka, A., Matsumoto, S.E., Hara, H., Michikawa, M. and Ohyagi, Y., & Chang, R. C. C. (2020). Neurodegeneration of trigeminal mesencephalic neurons by the tooth loss triggers the progression of Alzheimer's disease in 3× Tg-AD model mice. *Journal of Alzheimer's Disease*, (Preprint), 1-17.

Grigoriadis, J., Trulsson, M., & Svensson, K. G. (2016). Motor behavior during the first chewing cycle in subjects with fixed tooth-or implant-supported prostheses. *Clinical oral implants research*, *27*(4), 473-480.

Grossnickle, D. M., & Polly, P. D. (2013). Mammal disparity decreases during the Cretaceous.

Grossnickle, D. M. (2017). The evolutionary origin of jaw yaw in mammals. *Scientific Reports*, *7*(1), 1-13.

Grossnickle, D. M. (2020). Jaw roll and jaw yaw in early mammals. *Nature*, *582*(7812), E6-E8.

Grossnickle, D. M., Weaver, L. N., Jäger, K. R. K. & Schultz, J. A. (2021) The evolution of anteriorly directed molar occlusion in mammals. Zoological Journal of the Linnean Society XX: (zlab039) 1–17. (https://doi.org/10.1093/zoolinnean/zlab039)

Grundy, M. M. L., Lapsley, K., & Ellis, P. R. (2016). A review of the impact of processing on nutrient bioaccessibility and digestion of almonds. *International journal of food science & technology*, *51*(9), 1937-1946.

Haggard, P., & de Boer, L. (2014). Oral somatosensory awareness. *Neuroscience & Biobehavioral Reviews*, *47*, 469-484.

Hargreaves, K. M., Cohen, S., & Berman, L. H. (2011). *Cohen's pathways of the pulp*. Mosby Elsevier.

Helms, E. P. (1979). *Topographical Representations of the Muscles of Mastication in the Nucleus of the Mesencephalic Tract of the Trigeminal Nerve of the Opossum: Didelphis Marsupialis Virginiana* (Doctoral dissertation, Medical University of South Carolina).

Hiiemäe, K. M., & Ardran, G. M. (1968). A cinefluorographic study of mandibular movement during feeding in the rat (Rattus norvegicus). *Journal of Zoology*, *154*(2), 139-154.

Hiiemae, K. M., & Crompton, A. W. (1971). A cinefluorographic study of feeding in the American opossum, Didelphis marsupialis. *Dental morphology and evolution*, 299-334.

Hiiemae, K. M., & Crompton, A. W. (1985). Mastication, Food Transport and Swallowing. In *Functional Vertebrate Morphology*, edited by M. Hildebrand, D. Bramble, K. Liem, and D. Wake, Pp. 262-290. Cambridge: Belknap Press of Harvard University Press.

Hiroshima, K., Maeda, T., Hanada, K., & Wakisaka, S. (1998). Calretinin-like immunoreactivity in the regenerating periodontal Ruffini endings of the rat incisor following injury to the inferior alveolar nerve. *Brain research*, *807*(1-2), 218-221.

Hopson, J. A. & Crompton, A. W. (1969) Origin of mammals. *In* T. Dobzhansky, M. K. Hecht, and W. C. Steere (eds.), *Evolutionary Biology, volume 3*, 15–72. Appleton-Century-Crofts, New York.

Hylander, W. L. (1984). Stress and strain in the mandibular symphysis of primates: a test of competing hypotheses. American Journal of Physical Anthropology, 64(1), 1-46.

Hylander, W. L. (1985). Mandibular function and biomechanical stress and scaling. American Zoologist, 25(2), 315-330.

Hylander, W. L., and Johnson, K. R. (1994). Jaw muscle function and wishboning of the mandible during mastication in macaques and baboons. American Journal of Physical Anthropology, 94(4), 523-547.

Hylander, W. L., Ravosa, M. J., Ross, C. F., Wall, C. E., & Johnson, K. R. (2000). Symphyseal fusion and jaw-adductor muscle force: an EMG study. American Journal of Physical Anthropology: The Official Publication of the American Association of Physical Anthropologists, 112(4), 469-492.

Iriarte-Diaz, J., Terhune, C. E., Taylor, A. B., & Ross, C. F. (2017). Functional correlates of the position of the axis of rotation of the mandible during chewing in non-human primates. Zoology, 124, 106-118.

Jäger, K. R., Cifelli, R. L., & Martin, T. (2020). Molar occlusion and jaw roll in early crown mammals. *Scientific reports*, *10*(1), 1-12.

Jäger, K. R., Gill, P. G., Corfe, I., & Martin, T. (2019). Occlusion and dental function of Morganucodon and Megazostrodon. *Journal of Vertebrate Paleontology*, *39*(3), e1635135.

Kaas, J. H. (2013). The evolution of brains from early mammals to humans. *Wiley Interdisciplinary Reviews: Cognitive Science*, 4(1), 33-45.

Kaas, J. H. (2016). Primate S1 cortex. In *Scholarpedia of Touch* (pp. 499-503). Atlantis Press, Paris.

Kallen, F. C., & Gans, C. (1972). Mastication in the little brown bat, Myotis lucifugus. *Journal of Morphology*, *136*(4), 385-420.

Kay, R. F., & Hiiemae, K. M. (1974). Jaw movement and tooth use in recent and fossil primates. *American Journal of Physical Anthropology*, *40*(2), 227-256.

Kielan-Jaworowska, Z., Cifelli, R. L., & Luo, Z. X. (2005). *Mammals from the age of dinosaurs: origins, evolution, and structure*. Columbia University Press.

Kini, S., Somayaji, K., Acharya, S., & Sampath, S. (2020). Anomalies and clinical significance of mylohyoid nerve: A review. *Clinical, Cosmetic and Investigational Dentistry*, *12*, 429.

Knörlein, B. J., Baier, D. B., Gatesy, S. M., Laurence-Chasen, J. D., & Brainerd, E. L. (2016). Validation of XMALab software for marker-based XROMM. Journal of Experimental Biology, 219(23), 3701-3711.

Komuro, A., Morimoto, T., Iwata, K., Inoue, T., Masuda, Y., Kato, T., & Hidaka, O. (2001). Putative feed-forward control of jaw-closing muscle activity during rhythmic jaw movements in the anesthetized rabbit. *Journal of neurophysiology*, *86*(6), 2834-2844.

Krubitzer, L. A., & Prescott, T. J. (2018). The combinatorial creature: cortical phenotypes within and across lifetimes. *Trends in neurosciences*, *41*(10), 744-762.

Kullmer O, Benazz, S, Fiorenza L, Schulz D, Bacso S, and Winzen O (2009) Technical note: occlusal fingerprint analysis: quantification of tooth wear pattern. American Journal of Physical Anthropology 139: 600–605

Kullmer O, Benazzi S, Schulz D, Gunz P, Kordos L, Begun DR (2013) Dental arch restoration using tooth macrowear patterns with application to Rudapithecus hungaricus, from the late Miocene of Rudabánya. Journal of Human Evolution 64: 151–160

Kumar, A., Kothari, M., Grigoriadis, A., Trulsson, M., & Svensson, P. (2018). Bite or brain: Implication of sensorimotor regulation and neuroplasticity in oral rehabilitation procedures. *Journal of oral rehabilitation*, *45*(4), 323-333.

Langenbach, G. E., & van Eijden, T. M. (2001). Mammalian feeding motor patterns. *American Zoologist*, *41*(6), 1338-1351.

Laurence-Chasen, J. D., Manafzadeh, A. R., Hatsopoulos, N. G., Ross, C. F., & Arce-McShane, F. I. (2020). Integrating XMALab and DeepLabCut for high-throughput XROMM. Journal of Experimental Biology, 223(17).

Laurence-Chasen, J. D., Ramsay, J. B., & Brainerd, E. L. (2019). Shearing overbite and asymmetrical jaw motions facilitate food breakdown in a freshwater stingray, Potamotrygon motoro. *Journal of Experimental Biology*, *222*(13).

Laurence-Chasen, J. D., Manafzadeh, A. R., Hatsopoulos, N. G., Ross, C. F., & Arce-McShane, F. I. (2020). Integrating XMALab and DeepLabCut for high-throughput XROMM. *Journal of Experimental Biology*, *223*(17).

Lavigne, G., Kim, J. S., Valiquette, C., & Lund, J. P. (1987). Evidence that periodontal pressoreceptors provide positive feedback to jaw closing muscles during mastication. *Journal of neurophysiology*, *58*(2), 342-358.

Lautenschlager, S., Gill, P., Luo, Z. X., Fagan, M. J., & Rayfield, E. J. (2017). Morphological evolution of the mammalian jaw adductor complex. *Biological Reviews*, *92*(4), 1910-1940.

Lexomboon, D., Trulsson, M., Wårdh, I., & Parker, M. G. (2012). Chewing ability and tooth loss: association with cognitive impairment in an elderly population study. *Journal of the American Geriatrics Society*, *60*(10), 1951-1956.

Lieberman, D. E., & Crompton, A. W. (2000). Why fuse the mandibular symphysis? A comparative analysis. *American Journal of Physical Anthropology: The Official Publication of the American Association of Physical Anthropologists*, *112*(4), 517-540.

Lin, J. D., Özcoban, H., Greene, J. P., Jang, A. T., Djomehri, S. I., Fahey, K. P., ... & Ho, S. P. (2013). Biomechanics of a bone–periodontal ligament–tooth fibrous joint. *Journal of biomechanics*, *46*(3), 443-449.

Linden, R. W., & Scott, B. J. (1989). Distribution of mesencephalic nucleus and trigeminal ganglion mechanoreceptors in the periodontal ligament of the cat. *The Journal of physiology*, *410*(1), 35-44.

Liu, Z. J., Masuda, Y., Inoue, T., Fuchihata, H., Sumida, A., Takada, K., & Morimoto, T. (1993). Coordination of cortically induced rhythmic jaw and tongue movements in the rabbit. *Journal of neurophysiology*, *69*(2), 569-584.

Lucas, P. W. (2004). Dental Functional Morphology: How Teeth Work. Cambridge University Press.

Lund, J. P., & Kolta, A. (2006). Generation of the central masticatory pattern and its modification by sensory feedback. *Dysphagia*, *21*(3), 167-174.

Luo, Z. X. (2007). Transformation and diversification in early mammal evolution. *Nature*, *450*(7172), 1011-1019.

Luo, Z. X., Cifelli, R. L., & Kielan-Jaworowska, Z. (2001). Dual origin of tribosphenic mammals. *Nature*, *409*(6816), 53-57.

Luo, Z. X., Crompton, A. W., & Sun, A. L. (2001). A new mammaliaform from the early Jurassic and evolution of mammalian characteristics. *Science*, *292*(5521), 1535-1540.

Luo, Z. X., Kielan-Jaworowska, Z., Cifelli, R. L., (2004). Evolution of dental replacement in mammals. *Bulletin of Carnegie Museum of Natural History*, *2004*(36), 159-175.

Luo, Z. X., Yuan, C. X., Meng, Q. J., & Ji, Q. (2011). A Jurassic eutherian mammal and divergence of marsupials and placentals. *Nature*, *476*(7361), 442-445.

Martin, T. (2018): Mesozoic mammals – early mammalian diversity and ecomorphological adaptations. In: Handbook of Zoology, Mammalia, F. E. Zachos and R. J. Asher (eds.), Mammalian Evolution, Diversity and Systematics: 199-299, De Gruyter, Berlin.

Martin, T., Jäger, K. R., Plogschties, T., Schwermann, A. H., Brinkkötter, J. J., & Schultz, J. A. (2020). *Molar diversity and functional adaptations in Mesozoic mammals*. Verlag Dr. Friedrich Pfeil.

Mathis, A., Mamidanna, P., Cury, K. M., Abe, T., Murthy, V. N., Mathis, M. W., & Bethge, M. (2018). DeepLabCut: markerless pose estimation of user-defined body parts with deep learning. *Nature neuroscience*, *21*(9), 1281-1289.

Mathis, M. W., & Mathis, A. (2020). Deep learning tools for the measurement of animal behavior in neuroscience. *Current opinion in neurobiology*, *60*, 1-11.

McCormack, S. W., Witzel, U., Watson, P. J., Fagan, M. J., & Gröning, F. (2014). The biomechanical function of periodontal ligament fibres in orthodontic tooth movement. Plos one, 9(7), e102387.

McCormack, S. W., Witzel, U., Watson, P. J., Fagan, M. J., & Gröning, F. (2017). Inclusion of periodontal ligament fibres in mandibular finite element models leads to an increase in alveolar bone strains. *PloS one*, *12*(11), e0188707.

McKenna, M. C. (1975). Toward a phylogenetic classification of the Mammalia. In *Phylogeny of the Primates* (pp. 21-46). Springer, Boston, MA.

Mehari Abraha, H., Iriarte-Diaz, J., Ross, C. F., Taylor, A. B., & Panagiotopoulou, O. (2019). The mechanical effect of the periodontal ligament on bone strain regimes in a validated finite element model of a macaque mandible. Frontiers in bioengineering and biotechnology, 7, 269.

Menegaz, R. A., Baier, D. B., Metzger, K. A., Herring, S. W., & Brainerd, E. L. (2015). XROMM analysis of tooth occlusion and temporomandibular joint kinematics during feeding in juvenile miniature pigs. Journal of Experimental Biology, 218(16), 2573-2584.

Mills, J. R. E. (1966). The functional occlusion of the teeth of Insectivora. *Zoological Journal of the Linnean Society*, *46*(308), 1-25.

Mills, J. R. E. (1967). A comparison of lateral jaw movements in some mammals from wear facets on the teeth. *Archives of Oral Biology*, *12*(5), 645-661.

Mills, J. R. E. (1971). The dentition of *Morganucodon*. *In* D. M. Kermack and K. A. Kermack (eds.), *Early Mammals*, 29–63. Zoological Journal of the Linnean Society 50, supplement 1, London.

Moodley, D. S. (2017). Local anaesthetics in dentistry: A series. *South African Dental Journal*, *72*(1), 32-34.

Morquette, P., Lavoie, R., Fhima, M. D., Lamoureux, X., Verdier, D., & Kolta, A. (2012). Generation of the masticatory central pattern and its modulation by sensory feedback. *Progress in neurobiology*, *96*(3), 340-355.

Naftel, J. P., Richards, L. P., Pan, M., & Bernanke, J. M. (1999). Course and composition of the nerves that supply the mandibular teeth of the rat. *The Anatomical Record*, *256*(4), 433-447.

Naveh, G. R., Shahar, R., Brumfeld, V., & Weiner, S. (2012). Tooth movements are guided by specific contact areas between the tooth root and the jaw bone: A dynamic 3D microCT study of the rat molar. *Journal of structural biology*, *177*(2), 477-483.

Naveh, G. R., Brumfeld, V., Shahar, R., & Weiner, S. (2013). Tooth periodontal ligament: Direct 3D microCT visualization of the collagen network and how the network changes when the tooth is loaded. *Journal of structural biology*, *181*(2), 108-115.

Olson, R. A., Curtis, H. E., & Williams, S. H. (2019). Shape Change Throughout the Body of the Tongue during Lapping in Small Carnivorans. InJournal of Morphology (Vol. 280, pp. S193-S193).

Olson, R. A. (2020). *Biomechanics of the Mammalian Tongue: Kinematic Analysis of Tongue Movements and Deformations during Feeding and Drinking* (Doctoral dissertation, Ohio University).

Oron, U., & Crompton, A. W. (1985). A cineradiographic and electromyographic study of mastication in Tenrec ecaudatus. *Journal of Morphology*, *185*(2), 155-182.

Orsbon, C. P., Gidmark, N. J., Gao, T., & Ross, C. F. (2020). XROMM and diceCT reveal a hydraulic mechanism of tongue base retraction in swallowing. *Scientific Reports*, *10*(1), 1-1

Osborn, H. F. (1888). The evolution of mammalian molars to and from the tritubercular type. *The American Naturalist*, *22*(264), 1067-1079.

Osborn, H. F. (1907). *Evolution of mammalian molar teeth* (Vol. 1). Macmillan.

Ottenhoff, F. A. M., Van Der Bilt, A., Van Der Glas, H. W., & Bosman, F. (1993). Control of human jaw elevator muscle activity during simulated chewing with varying bolus size. *Experimental brain research*, *96*(3), 501-512.

Panagiotopoulou, O., Kupczik, K., & Cobb, S. N. (2011). The mechanical function of the periodontal ligament in the macaque mandible: a validation and sensitivity study using finite element analysis. *Journal of Anatomy*, *218*(1), 75-86.

Pal, A., Chen, L., Yang, L., Yang, F., Meng, B., Jheon, A. H., & Ho, S. P. (2017). Micro-anatomical responses in periodontal complexes of mice to calibrated orthodontic forces on the crown. *Orthodontics & craniofacial research*, *20*, 100-105.

Peres, Tanara Vieira, Nancy L. Parmalee, Ebany J. Martinez-Finley, and Michael Aschner. "Untangling the manganese-α-synuclein web." *Frontiers in neuroscience* 10 (2016): 364.

Piancino, M. G., Isola, G., Cannavale, R., Cutroneo, G., Vermiglio, G., Bracco, P., & Anastasi, G. P. (2017). From periodontal mechanoreceptors to chewing motor control: A systematic review. *Archives of Oral Biology*, *78*, 109-121.

Ramos, B. P., & Arnsten, A. F. (2007). Adrenergic pharmacology and cognition: focus on the prefrontal cortex. *Pharmacology & therapeutics*, *113*(3), 523-536.

Ravi, B. K., Harshakumar, K., Prasanth, V., & Janardanan, K. (2020). Dental Implants and Osseoperception: A Systematic Review. *IOSR Journal of Dental and Medical Sciences, 19(1), 55-60*

Ravosa, M. J., Vinyard, C. J., Gagnon, M., & Islam, S. A. (2000). Evolution of anthropoid jaw loading and kinematic patterns. American Journal of Physical Anthropology: The Official Publication of the American Association of Physical Anthropologists, 112(4), 493-516.

Reed, D. A., & Ross, C. F. (2010). The influence of food material properties on jaw kinematics in the primate, Cebus. *archives of oral biology*, *55*(12), 946-962.

Reep, R. L., Marshall, C. D., Stoll, M. L., & Whitaker, D. M. (1998). Distribution and innervation of facial bristles and hairs in the Florida manatee (Trichechus manatus latirostris). *Marine Mammal Science*, *14*(2), 257-273.

Reilly, S. M., McBrayer, L. D., & White, T. D. (2001). Prey processing in amniotes: biomechanical and behavioral patterns of food reduction. *Comparative Biochemistry and Physiology Part A: Molecular & Integrative Physiology*, *128*(3), 397-415.

Robertson D, Smith AJ. The microbiology of the acute dental abscess. J Med Microbiol. 2009 Feb;58(Pt 2):155-162.

Rogers, N. R., McMahon, D. J., Daubert, C. R., Berry, T. K., & Foegeding, E. A. (2010). Rheological properties and microstructure of Cheddar cheese made with different fat contents. *Journal of Dairy Science*, *93*(10), 4565-4576.

Rood, J. P. (1977). The Nerve Supply of the Mandibular Incisor Region. Journal of brittish dentistry. 143(7), 227-230.

Ross, C. F., Dharia, R., Herring, S. W., Hylander, W. L., Liu, Z. J., Rafferty, K. L., Ravosa, M. J., & Williams, S. H. (2007). Modulation of mandibular loading and bite force in mammals during mastication. *Journal of Experimental Biology*, *210*(6), 1046-1063.

Ross, C. F., Baden, A. L., Georgi, J., Herrel, A., Metzger, K. A., Reed, D. A., Schaerlaeken, V. & Wolff, M. S. (2010). Chewing variation in lepidosaurs and primates. *Journal of Experimental Biology*, *213*(4), 572-584.

Ross, C. F., & Iriarte-Diaz, J. (2019). Evolution, Constraint, and Optimality in Primate Feeding Systems. In *Feeding in Vertebrates* (pp. 787-829). Springer, Cham.

Ross, C. F., Iriarte-Diaz, J., & Nunn, C. L. (2012). Innovative approaches to the relationship between diet and mandibular morphology in primates. *International Journal of Primatology*, *33*(3), 632-660.

Rossignol, S., J. P. Lund, and T. Drew. 1988. The role of sensory inputs in regulating patterns of rhythmical movements in higher vertebrates. In A. H. Cohen and S. Rossignol (eds.), Neural control of rhythmic movements in vertebrates, pp. 201–283. Wiley, New York.

Ride, W. D. L. (1959) In: Cain, A. (ed.) Mastication and Taxonomy in the Macropodine Skull. Function and Taxonomic Importance, vol. 3. OxfordUniversity Press, Oxford, pp. 33–59.

Rowe, T. B., Macrini, T. E., & Luo, Z. X. (2011). Fossil evidence on origin of the mammalian brain. *science*, *332*(6032), 955-957.

Rowe, T.B. (2020) The emergence of mammals. pp. 263-319. in J.H. Kaas, ed., *Evolutionary Neuroscience*. Academic Press, San Diego.

Ryder, J. A. (1878). On the mechanical genesis of tooth-forms. *Proceedings of the Academy of Natural Sciences of Philadelphia*, 45-80.

Saito, S., Ohi, T., Murakami, T., Komiyama, T., Miyoshi, Y., Endo, K., ... & Hattori, Y. (2018). Association between tooth loss and cognitive impairment in community-dwelling older Japanese adults: a 4-year prospective cohort study from the Ohasama study. *BMC Oral Health*, *18*(1), 1-8.

Scapino, R. P. (1965). The third joint of the canine jaw. *Journal of Morphology*, *116*(1), 23-50.

Scott, J. E., Hogue, A. S., & Ravosa, M. J. (2012). The adaptive significance of mandibular symphyseal fusion in mammals. *Journal of Evolutionary Biology*, *25*(4), 661-673.

Sessle, B. J. (2006). Mechanisms of oral somatosensory and motor functions and their clinical correlates. *Journal of oral rehabilitation*, *33*(4), 243-261.

Sessle, B. J., Adachi, K., Avivi-Arber, L., Lee, J., Nishiura, H., Yao, D., & Yoshino, K. (2007). Neuroplasticity of face primary motor cortex control of orofacial movements. *Archives of oral biology*, *52*(4), 334-337.

Sheehan, F. T. (2010). The instantaneous helical axis of the subtalar and talocrural joints: a non-invasive in vivo dynamic study. *Journal of foot and ankle research*, *3*(1), 1-10.

Schultz, J. A., Bhullar, B. A. S., & Luo, Z. X. (2019). Re-examination of the Jurassic mammaliaform Docodon victor by computed tomography and occlusal functional analysis. *Journal of Mammalian Evolution*, *26*(1), 9-38.

Sibbing, F. A. (1982). Pharyngeal mastication and food transport in the carp (Cyprinus carpio L.): a cineradiographic and electromyographic study. *Journal of Morphology*, *172*(2), 223-258.

Simpson, G. G. (1933). Critique of a new theory of mammalian dental evolution. *Journal of Dental Research*, *13*(4), 261-272.

Stainier, D. Y., & Gilbert, W. (1990). Pioneer neurons in the mouse trigeminal sensory system. *Proceedings of the National Academy of Sciences*, *87*(3), 923-927.

Sulej, T., Krzesiński, G., Tałanda, M., Wolniewicz, A. S., Błażejowski, B., Bonde, N., ... & Niedźwiedzki, G. (2020). The earliest-known mammaliaform fossil from Greenland sheds light on origin of mammals. *Proceedings of the National Academy of Sciences*, *117*(43), 26861-26867.

Szalay, F. S. (1994). *Evolutionary history of the marsupials and an analysis of osteological characters*. Cambridge University Press.

Thexton, A. J., & Crompton, A. W. (1998). The control of swallowing. *The scientific basis of eating. Frontiers of Oral Biology*, *9*, 168-222.

Trulsson, M. (2006). Sensory-motor function of human periodontal mechanoreceptors. *Journal of oral rehabilitation*, *33*(4), 262-273.

Turnbull, W. D. (1970) Mammalian masticatory apparatus. Fieldiana: Geology 18, 147–356.

Ungar, P. S. (2010). *Mammal teeth: origin, evolution, and diversity*. JHU Press.

Urban, D. J., Anthwal, N., Luo, Z. X., Maier, J. A., Sadier, A., Tucker, A. S., & Sears, K. E. (2017). A new developmental mechanism for the separation of the mammalian middle ear ossicles from the jaw. *Proceedings of the Royal Society B: Biological Sciences*, *284*(1848), 20162416.

Van der Glas, H. W., Van der Bilt, A., Abbink, J. H., Mason, A. G., & Cadden, S. W. (2007). Functional roles of oral reflexes in chewing and biting: phase-, task-and site-dependent reflex sensitivity. *Archives of oral biology*, *52*(4), 365-369.

Van Nievelt, A. F., & Smith, K. K. (2005). To replace or not to replace: the significance of reduced functional tooth replacement in marsupial and placental mammals. *Paleobiology*, *31*(2), 324-346.

Van Valkenburgh, B., & White, P. A. (2021). Naturally-occurring tooth wear, tooth fracture, and cranial injuries in large carnivores from Zambia. *PeerJ*, *9*, e11313.

Wilson, S., Johns, P., & Fuller, P. M. (1984). The inferior alveolar and mylohyoid nerves: an anatomic study and relationship to local anesthesia of the anterior mandibular teeth. *Journal of the American Dental Association (1939)*, *108*(3), 350-352.

Wilson, G. P., Evans, A. R., Corfe, I. J., Smits, P. D., Fortelius, M., & Jernvall, J. (2012). Adaptive radiation of multituberculate mammals before the extinction of dinosaurs. *Nature*, *483*(7390), 457-460.

Zarow, C., Lyness, S. A., Mortimer, J. A., & Chui, H. C. (2003). Neuronal loss is greater in the locus coeruleus than nucleus basalis and substantia nigra in Alzheimer and Parkinson diseases. *Archives of neurology*, *60*(3), 337-341.

# Appendix A1. ANOVA Tables for Chapter 1

**Table A1.1 Nested ANOVA comparing the best fit of means in treatment variables to phase duration.** The variables were nested in this the following order: sex (S), animal (A), food type (F), right vs. left working side (W), with W being the most nested. Err = Error. Tot = Total. d.f. = degrees of freedom.

| *Phase* | *Source* | *Sum Sq.* | *df* | *Mean Sq.* | *F* | *Prob>F* | *Type* |
|---|---|---|---|---|---|---|---|
| ***FC1toFC2*** | S | 0.000946166 | 1 | 0.000946166 | 0.642608565 | 0.486190656 | fixed |
| | A | 0.004999711 | 3 | 0.00166657 | 1.596100696 | 0.366068004 | random |
| | F | 0.002478095 | 3 | 0.000826032 | 2.717969069 | 0.121375457 | random |
| | W | 0.002448922 | 7 | 0.000349846 | 2.32146644 | 0.024367218 | fixed |
| | Err. | 0.080775448 | 536 | 0.0001507 | | | random |
| | Tot. | 0.092885796 | 550 | | | | |
| ***FC2toSC1*** | **Source** | **Sum Sq.** | **df** | **Mean Sq.** | **F** | **Prob>F** | **Type** |
| | S | 0.007168456 | 1 | 0.007168456 | 0.767220874 | 0.446082601 | fixed |
| | A | 0.03056949 | 3 | 0.01018983 | 9.328909903 | 0.06703827 | random |
| | F | 0.0026953 | 3 | 0.000898433 | 2.211058801 | 0.146099492 | random |
| | W | 0.004993797 | 7 | 0.0007134 | 2.344376733 | 0.023015858 | fixed |
| | Err. | 0.163106122 | 536 | 0.000304302 | | | random |
| | Tot. | 0.219032437 | 550 | | | | |
| ***SC1toSC2*** | **Source** | **Sum Sq.** | **df** | **Mean Sq.** | **F** | **Prob>F** | **Type** |
| | S | 0.003843097 | 1 | 0.003843097 | 65535 | 0 | fixed |
| | A | 0.003780289 | 3 | 0.001260096 | 0.040257295 | 0.987195505 | random |
| | F | 0.071644398 | 3 | 0.023881466 | 3.797171548 | 0.122377132 | random |
| | W | 0.015825839 | 7 | 0.002260834 | 2.590019979 | 0.012368404 | fixed |
| | Err. | 0.467875583 | 536 | 0.000872902 | | | random |
| | Tot. | 0.579850579 | 550 | | | | |
| ***SC2toSO*** | **Source** | **Sum Sq.** | **df** | **Mean Sq.** | **F** | **Prob>F** | **Type** |
| | S | 0.028944623 | 1 | 0.028944623 | 18.5941355 | 0.490358252 | fixed |
| | A | 0.014334508 | 3 | 0.004778169 | 0.136328488 | 0.932009858 | random |
| | F | 0.079853086 | 3 | 0.026617695 | 4.024351039 | 0.127185706 | random |
| | W | 0.010198301 | 7 | 0.0014569 | 3.06896566 | 0.003538749 | fixed |
| | Err. | 0.25445005 | 536 | 0.00047472 | | | random |
| | Tot. | 0.438261051 | 550 | | | | |
| ***SOtoFO*** | **Source** | **Sum Sq.** | **df** | **Mean Sq.** | **F** | **Prob>F** | **Type** |
| | S | 0.000297639 | 1 | 0.000297639 | 0.014977425 | 0.917359993 | fixed |
| | A | 0.089572234 | 3 | 0.029857411 | 0.319740811 | 0.812999865 | random |
| | F | 0.212519707 | 3 | 0.070839902 | 4.093569869 | 0.128866036 | random |
| | W | 0.008658087 | 7 | 0.00123687 | 1.286417363 | 0.254697757 | fixed |
| | Err. | 0.51535534 | 536 | 0.000961484 | | | random |
| | Tot. | 0.935971246 | 550 | | | | |
| ***MaxTime*** | **Source** | **Sum Sq.** | **df** | **Mean Sq.** | **F** | **Prob>F** | **Type** |
| | S | 0.000163256 | 1 | 0.000163256 | 0.007231571 | 0.942738496 | fixed |
| | A | 0.103176995 | 3 | 0.034392332 | 0.308704192 | 0.819933904 | random |
| | F | 0.253545052 | 3 | 0.084515017 | 4.093869462 | 0.128873057 | random |
| | W | 0.012804437 | 7 | 0.001829205 | 1.605976748 | 0.131070127 | fixed |
| | Err. | 0.610503247 | 536 | 0.001138999 | | | random |
| | Tot. | 1.100541924 | 550 | | | | |

**Table A1.2 Nested ANOVA Comparing Groupings by Phase and Dimension.** The variables were nested in this the following order: sex (S), animal (A), food type (F), right vs. left working side (W), with W being the most nested. Err = Error. Tot = Total. d.f. = degrees of freedom.

| *Dim_Phase* | *Source* | *Sum Sq.* | *d.f.* | *Mean Sq.* | *F* | *Prob>F* | *Type* |
|---|---|---|---|---|---|---|---|
| ***RX_FC1*** | S | 15.5205373 | 1 | 15.5205373 | 3.47669559 | 0.20292706 | random |
| | A | 9.01769099 | 2 | 4.5088455 | 2.66529738 | 0.21701658 | random |
| | F | 6.42118146 | 3 | 2.14039382 | 2.93721991 | 0.07554598 | fixed |
| | W | 32.4705582 | 7 | 4.63865118 | 9.82991888 | 8.0108E-11 | fixed |
| | Err. | 117.972774 | 250 | 0.47189109 | | | random |
| | Tot. | 228.951965 | 263 | | | | |
| ***RX_FC2*** | **Source** | **Sum Sq.** | **d.f.** | **Mean Sq.** | **F** | **Prob>F** | **Type** |
| | S | 3.07043065 | 1 | 3.07043065 | 0.32661502 | 0.62527627 | random |
| | A | 19.0047023 | 2 | 9.50235116 | 2.98038956 | 0.22462559 | random |
| | F | 14.6910826 | 3 | 4.89702754 | 4.99231104 | 0.05669199 | fixed |
| | W | 3.95389676 | 7 | 0.56484239 | 1.4401546 | 0.18963327 | fixed |
| | Err. | 98.0523885 | 250 | 0.39220955 | | | random |
| | Total | 142.06464 | 263 | | | | |
| ***RX_SC1*** | **Source** | **Sum Sq.** | **d.f.** | **Mean Sq.** | **F** | **Prob>F** | **Type** |
| | S | 27.2530645 | 1 | 27.2530645 | 4.63742236 | 0.163596 | random |
| | A | 11.8611956 | 2 | 5.9305978 | 2.35947335 | 0.21582577 | random |
| | F | 44.9617291 | 3 | 14.987243 | 11.0357929 | 9.85E-05 | fixed |
| | W | 11.4432478 | 7 | 1.63474968 | 1.55705879 | 0.14876246 | fixed |
| | Err. | 262.473981 | 250 | 1.04989592 | | | random |
| | Tot. | 384.641601 | 263 | | | | |
| ***RX_SC2*** | **Source** | **Sum Sq.** | **d.f.** | **Mean Sq.** | **F** | **Prob>F** | **Type** |
| | S | 19.5001775 | 1 | 19.5001775 | 15.2303888 | 0.05907634 | random |
| | A | 2.57948709 | 2 | 1.28974354 | 1.98010261 | 0.22748583 | random |
| | F | 1.09514526 | 3 | 0.36504842 | 0.7971758 | 0.50113722 | fixed |
| | W | 5.79138837 | 7 | 0.8273412 | 2.03607597 | 0.05120572 | fixed |
| | Err. | 101.585256 | 250 | 0.40634102 | | | random |
| | Tot. | 154.266408 | 263 | | | | |
| ***RX_SO*** | **Source** | **Sum Sq.** | **d.f.** | **Mean Sq.** | **F** | **Prob>F** | **Type** |
| | S | 34.4057497 | 1 | 34.4057497 | 13.5051089 | 0.0659848 | random |
| | A | 5.13390959 | 2 | 2.56695479 | 2.02272381 | 0.22523008 | random |
| | F | 8.95814178 | 3 | 2.98604726 | 3.44160148 | 0.02403291 | fixed |

| | | | | | | | |
|---|---|---|---|---|---|---|---|
| | W | 33.6678299 | 7 | 4.80968998 | 6.32376749 | 7.5532E-07 | fixed |
| | Err. | 190.143375 | 250 | 0.7605735 | | | random |
| | Tot. | 296.238556 | 263 | | | | |
| ***RX_FO*** | **Source** | **Sum Sq.** | **d.f.** | **Mean Sq.** | **F** | **Prob>F** | **Type** |
| | S | 0.00213968 | 1 | 0.00213968 | 0.00011533 | 0.99240576 | random |
| | A | 37.5084155 | 2 | 18.7542078 | 2.99983025 | 0.22526548 | random |
| | F | 8.98975305 | 3 | 2.99658435 | 1.60121628 | 0.30547782 | fixed |
| | W | 8.56114896 | 7 | 1.22302128 | 1.73917467 | 0.10039026 | fixed |
| | Err. | 175.804837 | 250 | 0.70321935 | | | random |
| | Tot. | 258.40859 | 263 | | | | |
| ***RY_FC1*** | **Source** | **Sum Sq.** | **d.f.** | **Mean Sq.** | **F** | **Prob>F** | **Type** |
| | S | 1.42190707 | 1 | 1.42190707 | 2.0528613 | 0.28812226 | random |
| | A | 1.39987382 | 2 | 0.69993691 | 2.87583952 | 0.22151216 | random |
| | F | 0.29290969 | 3 | 0.09763656 | 1.13996469 | 0.39607931 | fixed |
| | W | 0.9728301 | 7 | 0.13897573 | 3.18893029 | 0.00298457 | fixed |
| | Err. | 10.8951683 | 250 | 0.04358067 | | | random |
| | Tot. | 16.9649129 | 263 | | | | |
| ***RY_FC2*** | **Source** | **Sum Sq.** | **d.f.** | **Mean Sq.** | **F** | **Prob>F** | **Type** |
| | S | 0.09532412 | 1 | 0.09532412 | 0.1580517 | 0.72931407 | random |
| | A | 1.21876378 | 2 | 0.60938189 | 2.76348805 | 0.21874522 | random |
| | F | 1.2379866 | 3 | 0.4126622 | 4.89064158 | 0.02738424 | fixed |
| | W | 2.17138089 | 7 | 0.31019727 | 6.45287033 | 5.3616E-07 | fixed |
| | Err. | 12.0178019 | 250 | 0.04807121 | | | random |
| | Tot. | 16.6967999 | 263 | | | | |
| ***RY_SC1*** | **Source** | **Sum Sq.** | **d.f.** | **Mean Sq.** | **F** | **Prob>F** | **Type** |
| | S | 6.29450245 | 1 | 6.29450245 | 11.6183388 | 0.07596968 | random |
| | A | 1.09384372 | 2 | 0.54692186 | 2.61246042 | 0.21691665 | random |
| | F | 3.54645459 | 3 | 1.18215153 | 11.7105531 | 0.00027654 | fixed |
| | W | 0.43309156 | 7 | 0.06187022 | 0.85887408 | 0.53973984 | fixed |
| | Err. | 18.0091074 | 250 | 0.07203643 | | | random |
| | Tot. | 41.2565335 | 263 | | | | |
| ***RY_SC2*** | **Source** | **Sum Sq.** | **d.f.** | **Mean Sq.** | **F** | **Prob>F** | **Type** |
| | S | 1.15050926 | 1 | 1.15050926 | 4.18567404 | 0.17712317 | random |
| | A | 0.55533809 | 2 | 0.27766904 | 2.76123931 | 0.21879567 | random |
| | F | 1.47743769 | 3 | 0.49247923 | 12.2190439 | 0.00113629 | fixed |
| | W | 0.50421437 | 7 | 0.07203062 | 2.97226837 | 0.00518715 | fixed |
| | Err. | 6.0585566 | 250 | 0.02423423 | | | random |
| | Tot. | 15.0464717 | 263 | | | | |
| ***RY_SO*** | **Source** | **Sum Sq.** | **d.f.** | **Mean Sq.** | **F** | **Prob>F** | **Type** |
| | S | 3.63944405 | 1 | 3.63944405 | 3.51599518 | 0.20137388 | random |

| | | | | | | | |
|---|---|---|---|---|---|---|---|
| | A | 2.09158782 | 2 | 1.04579391 | 2.80872305 | 0.21983635 | random |
| | F | 0.66894428 | 3 | 0.22298143 | 1.56947839 | 0.26541584 | fixed |
| | W | 1.38248653 | 7 | 0.19749808 | 2.44845134 | 0.01914082 | fixed |
| | Err. | 20.1656117 | 250 | 0.08066245 | | | random |
| | Tot. | 33.3254192 | 263 | | | | |
| ***RY_FO*** | **Source** | **Sum Sq.** | **d.f.** | **Mean Sq.** | **F** | **Prob>F** | **Type** |
| | S | 0.1774252 | 1 | 0.1774252 | 1.99295277 | 0.29276514 | random |
| | A | 0.17947483 | 2 | 0.08973742 | 1.98731691 | 0.22635048 | random |
| | F | 0.52241882 | 3 | 0.17413961 | 5.84769668 | 0.00179225 | fixed |
| | W | 1.5020142 | 7 | 0.21457346 | 8.35616734 | 3.5836E-09 | fixed |
| | Err. | 6.41961345 | 250 | 0.02567845 | | | random |
| | Tot. | 8.57189246 | 263 | | | | |
| ***RZ_FC1*** | **Source** | **Sum Sq.** | **d.f.** | **Mean Sq.** | **F** | **Prob>F** | **Type** |
| | S | 0.1977105 | 1 | 0.1977105 | 0.00395966 | 0.95552701 | random |
| | A | 100.772896 | 2 | 50.3864481 | 2.27425505 | 0.21679816 | random |
| | F | 369.605457 | 3 | 123.201819 | 10.0558556 | 0.00013251 | fixed |
| | W | 60.5374885 | 7 | 8.64821265 | 0.89986861 | 0.50712893 | fixed |
| | Err. | 2402.63204 | 250 | 9.61052816 | | | random |
| | Tot. | 3177.70822 | 263 | | | | |
| ***RZ_FC2*** | **Source** | **Sum Sq.** | **d.f.** | **Mean Sq.** | **F** | **Prob>F** | **Type** |
| | S | 88.1096902 | 1 | 88.1096902 | 24.8061103 | 0.03595828 | random |
| | A | 7.08617806 | 2 | 3.54308903 | 0.92024436 | 0.41252537 | random |
| | F | 145.271455 | 3 | 48.4238184 | 11.8383091 | 3.7932E-07 | fixed |
| | W | 48.4180086 | 7 | 6.91685837 | 1.66490192 | 0.11809716 | fixed |
| | Err. | 1038.6285 | 250 | 4.15451402 | | | random |
| | Tot. | 1314.42397 | 263 | | | | |
| ***RZ_SC1*** | **Source** | **Sum Sq.** | **d.f.** | **Mean Sq.** | **F** | **Prob>F** | **Type** |
| | S | 42.5955024 | 1 | 42.5955024 | 0.30455411 | 0.63645333 | random |
| | A | 282.828068 | 2 | 141.414034 | 3.14661726 | 0.23063036 | random |
| | F | 58.7310698 | 3 | 19.5770233 | 1.74572696 | 0.3291358 | fixed |
| | W | 9.33215777 | 7 | 1.3331654 | 0.60073685 | 0.75509607 | fixed |
| | Err. | 554.804237 | 250 | 2.21921695 | | | random |
| | Tot. | 905.087732 | 263 | | | | |
| ***RZ_SC2*** | **Source** | **Sum Sq.** | **d.f.** | **Mean Sq.** | **F** | **Prob>F** | **Type** |
| | S | 0.05548049 | 1 | 0.05548049 | 0.0807217 | 0.80230533 | random |
| | A | 1.36857538 | 2 | 0.68428769 | 0.78272303 | 0.46571311 | random |
| | F | 18.4156547 | 3 | 6.13855158 | 6.53489736 | 0.00030212 | fixed |
| | W | 3.89585527 | 7 | 0.55655075 | 0.58173162 | 0.77057273 | fixed |
| | Err. | 239.178487 | 250 | 0.95671395 | | | random |
| | Tot. | 267.659127 | 263 | | | | |

| *RZ_SO* | Source | Sum Sq. | d.f. | Mean Sq. | F | Prob>F | Type |
|---|---|---|---|---|---|---|---|
| | S | 1.09042695 | 1 | 1.09042695 | 0.09563217 | 0.78630713 | random |
| | A | 23.0300057 | 2 | 11.5150029 | 2.54771869 | 0.21563235 | random |
| | F | 96.5167431 | 3 | 32.1722477 | 15.5496679 | 7.0631E-05 | fixed |
| | W | 11.1233118 | 7 | 1.58904455 | 1.12268831 | 0.34921011 | fixed |
| | Err. | 353.84811 | 250 | 1.41539244 | | | random |
| | Tot. | 491.560906 | 263 | | | | |
| *RZ_FO* | Source | Sum Sq. | d.f. | Mean Sq. | F | Prob>F | Type |
| | S | 142.057565 | 1 | 142.057565 | 1.01023802 | 0.42060163 | random |
| | A | 284.271203 | 2 | 142.135601 | 2.99056456 | 0.22496475 | random |
| | F | 435.513203 | 3 | 145.171068 | 9.93955759 | 0.01486821 | fixed |
| | W | 19.5370812 | 7 | 2.7910116 | 0.47914627 | 0.84932056 | fixed |
| | Err. | 1456.24195 | 250 | 5.82496782 | | | random |
| | Tot. | 2504.93066 | 263 | | | | |
| *TX_FC1* | Source | Sum Sq. | d.f. | Mean Sq. | F | Prob>F | Type |
| | S | 0.01713707 | 1 | 0.01713707 | 0.00031409 | 0.98746791 | random |
| | A | 110.301851 | 2 | 55.1509257 | 2.97178002 | 0.2243464 | random |
| | F | 182.68564 | 3 | 60.8952133 | 10.6138624 | 0.0121642 | fixed |
| | W | 284.084324 | 7 | 40.5834749 | 17.5078397 | 7.7623E-19 | fixed |
| | Err. | 579.50432 | 250 | 2.31801728 | | | random |
| | Tot. | 1155.91067 | 263 | | | | |
| *TX_FC2* | Source | Sum Sq. | d.f. | Mean Sq. | F | Prob>F | Type |
| | S | 8.81798315 | 1 | 8.81798315 | 0.27353532 | 0.65311732 | random |
| | A | 65.1865168 | 2 | 32.5932584 | 3.1160984 | 0.22944222 | random |
| | F | 31.9427653 | 3 | 10.6475884 | 3.91477576 | 0.13225913 | fixed |
| | W | 81.735249 | 7 | 11.6764641 | 17.8088412 | 3.9438E-19 | fixed |
| | Err. | 163.913867 | 250 | 0.65565547 | | | random |
| | Tot. | 344.021665 | 263 | | | | |
| *TX_SC1* | Source | Sum Sq. | d.f. | Mean Sq. | F | Prob>F | Type |
| | S | 1.10003989 | 1 | 1.10003989 | 0.09891543 | 0.78289981 | random |
| | A | 22.4875327 | 2 | 11.2437664 | 3.10507863 | 0.22902179 | random |
| | F | 6.67063276 | 3 | 2.22354425 | 2.33450453 | 0.23447279 | fixed |
| | W | 26.2255054 | 7 | 3.74650077 | 15.561627 | 6.7152E-17 | fixed |
| | Err. | 60.1881276 | 250 | 0.24075251 | | | random |
| | Tot. | 120.492174 | 263 | | | | |
| *TX_SC2* | Source | Sum Sq. | d.f. | Mean Sq. | F | Prob>F | Type |
| | S | 0.00066492 | 1 | 0.00066492 | 0.00134025 | 0.97410704 | random |
| | A | 1.00089204 | 2 | 0.50044602 | 2.15706887 | 0.21950016 | random |
| | F | 1.62302788 | 3 | 0.54100929 | 3.92608313 | 0.01668091 | fixed |
| | W | 1.60816337 | 7 | 0.22973762 | 2.03894686 | 0.05086514 | fixed |

| | | | | | | | |
|---|---|---|---|---|---|---|---|
| | Err. | 28.1686627 | 250 | 0.11267465 | | | random |
| | Tot. | 32.6942994 | 263 | | | | |
| ***TX_SO*** | **Source** | **Sum Sq.** | **d.f.** | **Mean Sq.** | **F** | **Prob>F** | **Type** |
| | S | 1.3617494 | 1 | 1.3617494 | 0.03029862 | 0.87783762 | random |
| | A | 90.8974354 | 2 | 45.4487177 | 3.21638318 | 0.23347818 | random |
| | F | 31.6812529 | 3 | 10.5604176 | 3.33941605 | 0.21411474 | fixed |
| | W | 175.786671 | 7 | 25.1123815 | 105.870882 | 4.4783E-71 | fixed |
| | Err. | 59.2995472 | 250 | 0.23719819 | | | random |
| | Tot. | 368.111103 | 263 | | | | |
| ***TX_FO*** | **Source** | **Sum Sq.** | **d.f.** | **Mean Sq.** | **F** | **Prob>F** | **Type** |
| | S | 0.22651947 | 1 | 0.22651947 | 0.00791464 | 0.93720713 | random |
| | A | 57.8472538 | 2 | 28.9236269 | 2.86396441 | 0.22116431 | random |
| | F | 178.721645 | 3 | 59.5738816 | 17.0057851 | 0.00137928 | fixed |
| | W | 271.819572 | 7 | 38.8313674 | 22.265572 | 2.5476E-23 | fixed |
| | Err. | 436.002357 | 250 | 1.74400943 | | | random |
| | Tot. | 950.563006 | 263 | | | | |
| ***TY_FC1*** | **Source** | **Sum Sq.** | **d.f.** | **Mean Sq.** | **F** | **Prob>F** | **Type** |
| | S | 61.5742798 | 1 | 61.5742798 | 0.412146 | 0.58657316 | random |
| | A | 301.982481 | 2 | 150.991241 | 2.90332164 | 0.22226059 | random |
| | F | 246.521247 | 3 | 82.1737489 | 4.71732824 | 0.04754244 | fixed |
| | W | 180.087003 | 7 | 25.7267147 | 3.13920444 | 0.00339003 | fixed |
| | Err. | 2048.82441 | 250 | 8.19529763 | | | random |
| | Tot. | 2986.07238 | 263 | | | | |
| ***TY_FC2*** | **Source** | **Sum Sq.** | **d.f.** | **Mean Sq.** | **F** | **Prob>F** | **Type** |
| | S | 11.1856653 | 1 | 11.1856653 | 1.10928831 | 0.40188396 | random |
| | A | 20.3063083 | 2 | 10.1531542 | 1.74544369 | 0.24346915 | random |
| | F | 134.255664 | 3 | 44.7518881 | 10.3841864 | 1.0075E-05 | fixed |
| | W | 91.3977596 | 7 | 13.0568228 | 3.34137746 | 0.00201614 | fixed |
| | Err. | 976.904208 | 250 | 3.90761683 | | | random |
| | Tot. | 1221.3035 | 263 | | | | |
| ***TY_SC1*** | **Source** | **Sum Sq.** | **d.f.** | **Mean Sq.** | **F** | **Prob>F** | **Type** |
| | S | 6.79198055 | 1 | 6.79198055 | 0.06625358 | 0.82092511 | random |
| | A | 207.299589 | 2 | 103.649794 | 3.12338581 | 0.22972205 | random |
| | F | 52.2186252 | 3 | 17.4062084 | 2.04508444 | 0.27663778 | fixed |
| | W | 9.58749954 | 7 | 1.36964279 | 0.70937768 | 0.66412292 | fixed |
| | Err. | 482.691668 | 250 | 1.93076667 | | | random |
| | Tot. | 763.035687 | 263 | | | | |
| ***TY_SC2*** | **Source** | **Sum Sq.** | **d.f.** | **Mean Sq.** | **F** | **Prob>F** | **Type** |
| | S | 0.30208678 | 1 | 0.30208678 | 1.05674247 | 0.40559289 | random |
| | A | 0.55787132 | 2 | 0.27893566 | 0.39237695 | 0.67652276 | random |

| | | | | | | | |
|---|---|---|---|---|---|---|---|
| | F | 19.1670935 | 3 | 6.38903116 | 7.41842432 | 8.9022E-05 | fixed |
| | W | 2.07580544 | 7 | 0.29654363 | 0.32900425 | 0.94034992 | fixed |
| | Err. | 225.334195 | 250 | 0.90133678 | | | random |
| | Tot. | 252.669641 | 263 | | | | |
| ***TY_SO*** | **Source** | **Sum Sq.** | **d.f.** | **Mean Sq.** | **F** | **Prob>F** | **Type** |
| | S | 63.3477666 | 1 | 63.3477666 | 3.13182411 | 0.21860924 | random |
| | A | 40.8797968 | 2 | 20.4398984 | 2.89859384 | 0.22218191 | random |
| | F | 80.8099846 | 3 | 26.9366615 | 10.9481821 | 0.00517341 | fixed |
| | W | 44.895165 | 7 | 6.413595 | 5.18945773 | 1.5451E-05 | fixed |
| | Err. | 308.972311 | 250 | 1.23588925 | | | random |
| | Tot. | 489.280826 | 263 | | | | |
| ***TY_FO*** | **Source** | **Sum Sq.** | **d.f.** | **Mean Sq.** | **F** | **Prob>F** | **Type** |
| | S | 2.75813387 | 1 | 2.75813387 | 0.11055395 | 0.77102439 | random |
| | A | 50.3643132 | 2 | 25.1821566 | 2.36020068 | 0.21571731 | random |
| | F | 306.549914 | 3 | 102.183305 | 18.2997642 | 3.1335E-06 | fixed |
| | W | 178.275084 | 7 | 25.4678692 | 6.02429539 | 1.6741E-06 | fixed |
| | Err. | 1056.88166 | 250 | 4.22752663 | | | random |
| | Tot. | 1814.59768 | 263 | | | | |
| ***TZ_FC1*** | **Source** | **Sum Sq.** | **d.f.** | **Mean Sq.** | **F** | **Prob>F** | **Type** |
| | S | 5.06422162 | 1 | 5.06422162 | 6.04241334 | 0.13256275 | random |
| | A | 1.69070039 | 2 | 0.84535019 | 2.21308126 | 0.2181781 | random |
| | F | 0.66474008 | 3 | 0.22158003 | 0.97446659 | 0.41693709 | fixed |
| | W | 15.276583 | 7 | 2.182369 | 11.7233169 | 6.8295E-13 | fixed |
| | Err. | 46.5390685 | 250 | 0.18615627 | | | random |
| | Tot. | 69.448799 | 263 | | | | |
| ***TZ_FC2*** | **Source** | **Sum Sq.** | **d.f.** | **Mean Sq.** | **F** | **Prob>F** | **Type** |
| | S | 1.3899639 | 1 | 1.3899639 | 0.43479937 | 0.57736061 | random |
| | A | 6.46269516 | 2 | 3.23134758 | 2.98455725 | 0.22476209 | random |
| | F | 2.33478905 | 3 | 0.77826302 | 2.34365689 | 0.18922273 | fixed |
| | W | 3.58017992 | 7 | 0.51145427 | 3.87807268 | 0.00049829 | fixed |
| | Err. | 32.9709057 | 250 | 0.13188362 | | | random |
| | Tot. | 49.2302948 | 263 | | | | |
| ***TZ_SC1*** | **Source** | **Sum Sq.** | **d.f.** | **Mean Sq.** | **F** | **Prob>F** | **Type** |
| | S | 0.56083525 | 1 | 0.56083525 | 0.12433663 | 0.75802724 | random |
| | A | 9.11632746 | 2 | 4.55816373 | 2.83826087 | 0.22049302 | random |
| | F | 11.4410756 | 3 | 3.81369185 | 6.66344602 | 0.01634825 | fixed |
| | W | 14.1998546 | 7 | 2.02855065 | 6.83796739 | 1.9324E-07 | fixed |
| | Err. | 74.1649724 | 250 | 0.29665989 | | | random |
| | Tot. | 115.503819 | 263 | | | | |
| ***TZ_SC2*** | **Source** | **Sum Sq.** | **d.f.** | **Mean Sq.** | **F** | **Prob>F** | **Type** |

| | | | | | | | |
|---|---|---|---|---|---|---|---|
| | S | 0.01633664 | 1 | 0.01633664 | 0.0936923 | 0.78822031 | random |
| | A | 0.35102128 | 2 | 0.17551064 | 1.67882882 | 0.25003054 | random |
| | F | 0.77603769 | 3 | 0.25867923 | 3.24988129 | 0.02633719 | fixed |
| | W | 0.99328421 | 7 | 0.14189774 | 1.94531854 | 0.06313736 | fixed |
| | Err. | 18.2357981 | 250 | 0.07294319 | | | random |
| | Tot. | 20.7319888 | 263 | | | | |
| ***TZ_SO*** | **Source** | **Sum Sq.** | **d.f.** | **Mean Sq.** | **F** | **Prob>F** | **Type** |
| | S | 0.05521012 | 1 | 0.05521012 | 0.04423234 | 0.85285964 | random |
| | A | 2.52138936 | 2 | 1.26069468 | 2.6029032 | 0.21613077 | random |
| | F | 1.39898523 | 3 | 0.46632841 | 2.19679439 | 0.13629221 | fixed |
| | W | 13.4420781 | 7 | 1.92029686 | 13.7441463 | 4.9336E-15 | fixed |
| | Err. | 34.9293587 | 250 | 0.13971743 | | | random |
| | Tot. | 52.6317826 | 263 | | | | |
| ***TZ_FO*** | **Source** | **Sum Sq.** | **d.f.** | **Mean Sq.** | **F** | **Prob>F** | **Type** |
| | S | 5.07108961 | 1 | 5.07108961 | 420.683543 | 0.00011745 | random |
| | A | 0.01877469 | 2 | 0.00938734 | 0.05830002 | 0.94338699 | random |
| | F | 2.57339534 | 3 | 0.85779845 | 3.86797743 | 0.00992744 | fixed |
| | W | 13.7305316 | 7 | 1.96150451 | 8.24260066 | 4.8179E-09 | fixed |
| | Err. | 59.4928893 | 250 | 0.23797156 | | | random |
| | Tot. | 85.2344063 | 263 | | | | |

# Appendix A2. ANOVA Tables for Chapter 1

**Table A2.1 Nested Anova Comparing Treatments to Phase Duration.** The variables were nested in this the following order: sex (S), animal (A), food type (F), right vs. left working side (W), and treatment (Tr; intact or transected) with Tr being the most nested. Err = Error. Tot = Total. d.f. = degrees of freedom.

| *Phase* | *Source* | *Sum Sq.* | *d.f.* | *Mean Sq.* | *F* | *Prob>F* | *Type* |
|---|---|---|---|---|---|---|---|
| ***FC1toFC2*** | S | 0.010040014 | 2 | 0.005020007 | 37.46572658 | | fixed |
| | A | 0 | 0 | 0 | 0 | | random |
| | F | 0.003346598 | 3 | 0.001115533 | 5.456845888 | 0.007043382 | random |
| | W | 0.004474895 | 18 | 0.000248605 | 1.655624127 | 0.052736773 | fixed |
| | Tr | 0.010215204 | 24 | 0.000425633 | 3.19429392 | 4.45891E-07 | fixed |
| | Err. | 0.122188476 | 917 | 0.000133248 | | | random |
| | Tot. | 0.153149914 | 964 | | | | |
| ***FC2toSC1*** | **Source** | **Sum Sq.** | **d.f.** | **Mean Sq.** | **F** | **Prob>F** | **Type** |
| | S | 0.075410539 | 2 | 0.037705269 | 122.2574862 | | fixed |
| | A | 0 | 0 | 0 | 0 | | random |
| | F | 0.004934344 | 3 | 0.001644781 | 4.068014123 | 0.014285093 | random |
| | W | 0.010568402 | 18 | 0.000587133 | 1.776864744 | 0.027405159 | fixed |
| | Tr | 0.022015178 | 24 | 0.000917299 | 2.983965143 | 2.36377E-06 | fixed |
| | Err. | 0.28189447 | 917 | 0.000307409 | | | random |
| | Tot. | 0.409438134 | 964 | | | | |
| ***SC1toSC2*** | **Source** | **Sum Sq.** | **d.f.** | **Mean Sq.** | **F** | **Prob>F** | **Type** |
| | S | 0.001130242 | 2 | 0.000565121 | 0.876007647 | | fixed |
| | A | 0 | 0 | 0 | 0 | | random |
| | F | 0.088330922 | 3 | 0.029443641 | 10.85861891 | 0.013562022 | random |
| | W | 0.097405117 | 18 | 0.005411395 | 4.834861137 | 0.001948888 | fixed |
| | Tr | 0.053497091 | 24 | 0.002229045 | 3.577343772 | 1.97566E-08 | fixed |
| | Err. | 0.571383351 | 917 | 0.000623101 | | | random |
| | Tot. | 0.809791607 | 964 | | | | |
| ***SC2toSO*** | **Source** | **Sum Sq.** | **d.f.** | **Mean Sq.** | **F** | **Prob>F** | **Type** |
| | S | 0.053650355 | 2 | 0.026825177 | 80.54598744 | | fixed |
| | A | 0 | 0 | 0 | 0 | | random |
| | F | 0.185663847 | 3 | 0.061887949 | 13.02950327 | 0.024160728 | random |
| | W | 0.019046528 | 18 | 0.00105814 | 0.785907468 | 0.681712145 | fixed |
| | Tr | 0.061549554 | 24 | 0.002564565 | 8.96963164 | 7.26491E-29 | fixed |
| | Err. | 0.262185334 | 917 | 0.000285916 | | | random |
| | Tot. | 0.665834629 | 964 | | | | |
| ***SOtoFO*** | **Source** | **Sum Sq.** | **d.f.** | **Mean Sq.** | **F** | **Prob>F** | **Type** |
| | S | 0.123999316 | 2 | 0.061999658 | 87.66048314 | | fixed |
| | A | 0 | 0 | 0 | 0 | | random |
| | F | 0.354646811 | 3 | 0.118215604 | 12.93538939 | 0.023591825 | random |
| | W | 0.020277347 | 18 | 0.001126519 | 0.42642694 | 0.917163407 | fixed |
| | Tr | 0.108651696 | 24 | 0.004527154 | 7.333636538 | 1.27729E-22 | fixed |
| | Err. | 0.566076625 | 917 | 0.000617314 | | | random |
| | Tot. | 1.426674285 | 964 | | | | |
| ***MaxTime*** | **Source** | **Sum Sq.** | **d.f.** | **Mean Sq.** | **F** | **Prob>F** | **Type** |
| | S | 0.165854854 | 2 | 0.082927427 | 105.6078943 | | fixed |
| | A | 0 | 0 | 0 | 0 | | random |

| | | | | | | |
|---|---|---|---|---|---|---|
| F | 0.419392822 | 3 | 0.139797607 | 12.99247803 | 0.023935697 | random |
| W | 0.024702083 | 18 | 0.001372338 | 0.44647156 | 0.904239236 | fixed |
| Tr | 0.137177268 | 24 | 0.005715719 | 8.420129764 | 8.93789E-27 | fixed |
| Err. | 0.622474345 | 917 | 0.000678816 | | | random |
| Tot. | 1.684467461 | 964 | | | | |

**Table A2.2 Nested ANOVA Comparing Groupings by Phase and Dimension.** The variables were nested in this the following order: sex (S), animal (A), food type (F), right vs. left working side (W), and treatment (Tr; intact or transected) with Tr being the most nested. Err = Error. Tot = Total. d.f. = degrees of freedom.

| *Dim_Phase* | *Source* | *Sum Sq.* | *d.f.* | *Mean Sq.* | *F* | *Prob>F* | *Type* |
|---|---|---|---|---|---|---|---|
| ***RX_FC1*** | S | 9.23751439 | 1 | 9.23751439 | 0.60321291 | 0.57965046 | fixed |
| | A | 15.2032842 | 1 | 15.2032842 | 1.31502845 | 0.33435057 | random |
| | F | 36.6713159 | 3 | 12.223772 | 3.78437927 | 0.12475248 | random |
| | W | 35.1034899 | 6 | 5.85058165 | 5.44480576 | 0.01831436 | fixed |
| | Tr | 38.8044904 | 12 | 3.23370753 | 7.70802176 | 4.2536E-13 | fixed |
| | Err. | 192.142432 | 458 | 0.41952496 | | | random |
| | Tot. | 389.481717 | 481 | | | | |
| ***RX_FC2*** | **Source** | **Sum Sq.** | **d.f.** | **Mean Sq.** | **F** | **Prob>F** | **Type** |
| | S | 9.8366074 | 1 | 9.8366074 | 0.62723718 | 0.57360377 | fixed |
| | A | 15.5684101 | 1 | 15.5684101 | 5.42815523 | 0.10106198 | random |
| | F | 9.05841938 | 3 | 3.01947313 | 3.13031143 | 0.11824989 | random |
| | W | 6.02852663 | 6 | 1.00475444 | 2.12828471 | 0.0883121 | fixed |
| | Tr | 26.1975665 | 12 | 2.18313054 | 6.77062414 | 2.8327E-11 | fixed |
| | Err. | 147.67823 | 458 | 0.32244155 | | | random |
| | Tot. | 212.717208 | 481 | | | | |
| ***RX_SC1*** | **Source** | **Sum Sq.** | **d.f.** | **Mean Sq.** | **F** | **Prob>F** | **Type** |
| | S | 0.14865725 | 1 | 0.14865725 | 0.08078476 | 0.82387841 | fixed |
| | A | 1.83087937 | 1 | 1.83087937 | 0.23209237 | 0.66268121 | random |
| | F | 24.9679809 | 3 | 8.32266031 | 3.42405709 | 0.11950268 | random |
| | W | 23.9426662 | 6 | 3.99044437 | 3.91797931 | 0.01572269 | fixed |
| | Tr | 135.560775 | 12 | 11.2967312 | 19.1668981 | 8.2797E-34 | fixed |
| | Err. | 269.9395 | 458 | 0.58938755 | | | random |
| | Tot. | 473.660809 | 481 | | | | |
| ***RX_SC2*** | **Source** | **Sum Sq.** | **d.f.** | **Mean Sq.** | **F** | **Prob>F** | **Type** |
| | S | 14.0775067 | 1 | 14.0775067 | 8.16697633 | 0.21481716 | fixed |
| | A | 1.71316131 | 1 | 1.71316131 | 11.5828161 | 0.02911302 | random |
| | F | 0.41611479 | 3 | 0.13870493 | 0.52621749 | 0.66495506 | random |

| | | | | | | | |
|---|---|---|---|---|---|---|---|
| | W | 6.78144445 | 6 | 1.13024074 | 3.85064784 | 0.00093663 | fixed |
| | Tr | 51.5469649 | 12 | 4.29558041 | 14.1948812 | 3.1008E-25 | fixed |
| | Err. | 138.597555 | 458 | 0.30261475 | | | random |
| | Tot. | 216.140266 | 481 | | | | |
| ***RX_SO*** | **Source** | **Sum Sq.** | **d.f.** | **Mean Sq.** | **F** | **Prob>F** | **Type** |
| | S | 69.638745 | 1 | 69.638745 | 21.2940825 | 0.13629293 | fixed |
| | A | 3.24984519 | 1 | 3.24984519 | 0.39988204 | 0.57176566 | random |
| | F | 25.7398815 | 3 | 8.57996049 | 3.52824628 | 0.12064823 | random |
| | W | 59.0510906 | 6 | 9.84184843 | 10.2706238 | 0.00037818 | fixed |
| | Tr | 48.0122507 | 12 | 4.00102089 | 7.83762219 | 2.3847E-13 | fixed |
| | Err. | 233.804019 | 458 | 0.51048913 | | | random |
| | Tot. | 504.293168 | 481 | | | | |
| ***RX_FO*** | **Source** | **Sum Sq.** | **d.f.** | **Mean Sq.** | **F** | **Prob>F** | **Type** |
| | S | 3.95552171 | 1 | 3.95552171 | 0.14116179 | 0.7712145 | fixed |
| | A | 27.8171615 | 1 | 27.8171615 | 20.0430742 | 0.01891684 | random |
| | F | 4.31538596 | 3 | 1.43846199 | 1.91352584 | 0.17280205 | random |
| | W | 9.04276291 | 6 | 1.50712715 | 2.56687508 | 0.02213587 | fixed |
| | Tr | 34.7684705 | 12 | 2.89737254 | 5.39416172 | 1.3642E-08 | fixed |
| | Err. | 246.006088 | 458 | 0.5371312 | | | random |
| | Tot. | 341.615698 | 481 | | | | |
| ***RY_FC1*** | **Source** | **Sum Sq.** | **d.f.** | **Mean Sq.** | **F** | **Prob>F** | **Type** |
| | S | 2.01514812 | 1 | 2.01514812 | 1.15187012 | 0.47755773 | fixed |
| | A | 1.73672698 | 1 | 1.73672698 | 70.5395926 | 0.00185719 | random |
| | F | 0.07208946 | 3 | 0.02402982 | 0.74978794 | 0.52554965 | random |
| | W | 0.46266348 | 6 | 0.07711058 | 2.26991144 | 0.03631821 | fixed |
| | Tr | 2.72621675 | 12 | 0.22718473 | 6.57462951 | 6.8284E-11 | fixed |
| | Err. | 15.826079 | 458 | 0.03455476 | | | random |
| | Tot. | 25.5109959 | 481 | | | | |
| ***RY_FC2*** | **Source** | **Sum Sq.** | **d.f.** | **Mean Sq.** | **F** | **Prob>F** | **Type** |
| | S | 0.28541448 | 1 | 0.28541448 | 0.12810982 | 0.7811958 | fixed |
| | A | 2.21165401 | 1 | 2.21165401 | 10.3549336 | 0.04720471 | random |
| | F | 0.67155612 | 3 | 0.22385204 | 2.64958798 | 0.12471505 | random |
| | W | 4.92365744 | 6 | 0.82060957 | 16.0640927 | 5.2894E-10 | fixed |
| | Tr | 5.70226186 | 12 | 0.47518849 | 11.6087659 | 1.6144E-20 | fixed |
| | Err. | 18.7475852 | 458 | 0.04093359 | | | random |
| | Tot. | 32.9238753 | 481 | | | | |
| ***RY_SC1*** | **Source** | **Sum Sq.** | **d.f.** | **Mean Sq.** | **F** | **Prob>F** | **Type** |
| | S | 7.31779152 | 1 | 7.31779152 | 6.13481524 | 0.24441549 | fixed |
| | A | 1.18435582 | 1 | 1.18435582 | 0.68628117 | 0.46799984 | random |

| | | | | | | | |
|---|---|---|---|---|---|---|---|
| | F | 5.47601153 | 3 | 1.82533718 | 3.85334211 | 0.12613594 | random |
| | W | 2.95781038 | 6 | 0.4929684 | 3.29184882 | 0.07808208 | fixed |
| | Tr | 10.7197332 | 12 | 0.8933111 | 17.407888 | 7.5448E-31 | fixed |
| | Err. | 23.5029363 | 458 | 0.05131645 | | | random |
| | Tot. | 60.0850128 | 481 | | | | |
| ***RY_SC2*** | **Source** | **Sum Sq.** | **d.f.** | **Mean Sq.** | **F** | **Prob>F** | **Type** |
| | S | 1.45473207 | 1 | 1.45473207 | 37.9945079 | 0.10370618 | fixed |
| | A | 0.0381521 | 1 | 0.0381521 | 0.15273426 | 0.72181936 | random |
| | F | 0.79038143 | 3 | 0.26346048 | 3.3795468 | 0.11911676 | random |
| | W | 0.53033954 | 6 | 0.08838992 | 2.63869726 | 0.05780629 | fixed |
| | Tr | 7.45179419 | 12 | 0.62098285 | 31.0683913 | 6.1786E-52 | fixed |
| | Err. | 9.1543248 | 458 | 0.01998761 | | | random |
| | Tot. | 21.918691 | 481 | | | | |
| ***RY_SO*** | **Source** | **Sum Sq.** | **d.f.** | **Mean Sq.** | **F** | **Prob>F** | **Type** |
| | S | 10.3972098 | 1 | 10.3972098 | 4.66279022 | 0.27619814 | fixed |
| | A | 2.21382591 | 1 | 2.21382591 | 6.32390662 | 0.08457997 | random |
| | F | 1.09937116 | 3 | 0.36645705 | 2.54377828 | 0.12809182 | random |
| | W | 1.07919691 | 6 | 0.17986615 | 1.98182187 | 0.08383497 | fixed |
| | Tr | 2.62081395 | 12 | 0.21840116 | 2.92915679 | 0.0006198 | fixed |
| | Err. | 34.1489853 | 458 | 0.0745611 | | | random |
| | Tot. | 61.2643134 | 481 | | | | |
| ***RY_FO*** | **Source** | **Sum Sq.** | **d.f.** | **Mean Sq.** | **F** | **Prob>F** | **Type** |
| | S | 0.01209247 | 1 | 0.01209247 | 0.07591349 | 0.82890652 | fixed |
| | A | 0.15825432 | 1 | 0.15825432 | 0.515052 | 0.52445998 | random |
| | F | 0.9731321 | 3 | 0.32437737 | 3.52513085 | 0.12060926 | random |
| | W | 2.62543437 | 6 | 0.43757239 | 12.0447836 | 0.00016952 | fixed |
| | Tr | 0.70469223 | 12 | 0.05872435 | 3.02603078 | 0.00041596 | fixed |
| | Err. | 8.88812955 | 458 | 0.0194064 | | | random |
| | Tot. | 13.4115881 | 481 | | | | |
| ***RZ_FC1*** | **Source** | **Sum Sq.** | **d.f.** | **Mean Sq.** | **F** | **Prob>F** | **Type** |
| | S | 11.8625233 | 1 | 11.8625233 | 1.83150423 | 0.40834623 | fixed |
| | A | 6.49184427 | 1 | 6.49184427 | 0.02669956 | 0.88055301 | random |
| | F | 771.297819 | 3 | 257.099273 | 3.79876586 | 0.12503202 | random |
| | W | 68.3127998 | 6 | 11.3854666 | 0.5109888 | 0.7847065 | fixed |
| | Tr | 544.80472 | 12 | 45.4003934 | 5.34999516 | 1.6624E-08 | fixed |
| | Err. | 3886.61663 | 458 | 8.48606251 | | | random |
| | Tot. | 5460.67031 | 481 | | | | |
| ***RZ_FC2*** | **Source** | **Sum Sq.** | **d.f.** | **Mean Sq.** | **F** | **Prob>F** | **Type** |
| | S | 10.3553827 | 1 | 10.3553827 | 1.11476917 | 0.48348549 | fixed |
| | A | 9.24591734 | 1 | 9.24591734 | 0.11412525 | 0.75765488 | random |

| | | | | | | | |
|---|---|---|---|---|---|---|---|
| | F | 256.884849 | 3 | 85.6282829 | 3.7202745 | 0.12356704 | random |
| | W | 94.6477761 | 6 | 15.7746293 | 1.96925693 | 0.1785701 | fixed |
| | Tr | 100.180443 | 12 | 8.34837024 | 2.41944985 | 0.00474303 | fixed |
| | Err. | 1580.34008 | 458 | 3.45052419 | | | random |
| | Tot. | 2017.35989 | 481 | | | | |
| ***RZ_SC1*** | **Source** | **Sum Sq.** | **d.f.** | **Mean Sq.** | **F** | **Prob>F** | **Type** |
| | S | 5.09435264 | 1 | 5.09435264 | 0.0235981 | 0.90296578 | fixed |
| | A | 214.292182 | 1 | 214.292182 | 12.4998452 | 0.03767778 | random |
| | F | 54.1275674 | 3 | 18.0425225 | 3.08908026 | 0.11834212 | random |
| | W | 9.13148426 | 6 | 1.52191404 | 0.52186004 | 0.78618154 | fixed |
| | Tr | 99.477738 | 12 | 8.2898115 | 4.08831066 | 4.4632E-06 | fixed |
| | Err. | 928.680323 | 458 | 2.02768629 | | | random |
| | Tot. | 1282.43559 | 481 | | | | |
| ***RZ_SC2*** | **Source** | **Sum Sq.** | **d.f.** | **Mean Sq.** | **F** | **Prob>F** | **Type** |
| | S | 0.00158121 | 1 | 0.00158121 | 0.00040269 | 0.98723354 | fixed |
| | A | 3.90294622 | 1 | 3.90294622 | 0.68820661 | 0.46681746 | random |
| | F | 17.8947205 | 3 | 5.96490683 | 3.01557513 | 0.11869367 | random |
| | W | 7.5347707 | 6 | 1.25579512 | 1.22816911 | 0.32200233 | fixed |
| | Tr | 11.0942001 | 12 | 0.92451667 | 1.26276838 | 0.23763941 | fixed |
| | Err. | 335.317739 | 458 | 0.7321348 | | | random |
| | Tot. | 378.679731 | 481 | | | | |
| ***RZ_SO*** | **Source** | **Sum Sq.** | **d.f.** | **Mean Sq.** | **F** | **Prob>F** | **Type** |
| | S | 47.1957571 | 1 | 47.1957571 | 0.58632402 | 0.58400415 | fixed |
| | A | 79.9066236 | 1 | 79.9066236 | 1.31100433 | 0.33509719 | random |
| | F | 193.48936 | 3 | 64.4964532 | 3.94045236 | 0.12803504 | random |
| | W | 12.0436903 | 6 | 2.00728171 | 0.41535262 | 0.84397533 | fixed |
| | Tr | 94.7410457 | 12 | 7.89508714 | 5.94702909 | 1.1437E-09 | fixed |
| | Err. | 608.026269 | 458 | 1.32756827 | | | random |
| | Tot. | 1063.45326 | 481 | | | | |
| ***RZ_FO*** | **Source** | **Sum Sq.** | **d.f.** | **Mean Sq.** | **F** | **Prob>F** | **Type** |
| | S | 9.46248553 | 1 | 9.46248553 | 0.15294152 | 0.76273169 | fixed |
| | A | 61.4454485 | 1 | 61.4454485 | 0.23774272 | 0.65918859 | random |
| | F | 820.634924 | 3 | 273.544975 | 3.98172266 | 0.12899101 | random |
| | W | 38.4353728 | 6 | 6.40589547 | 0.32675248 | 0.89710172 | fixed |
| | Tr | 195.718039 | 12 | 16.3098366 | 3.48043235 | 6.1669E-05 | fixed |
| | Err. | 2146.25782 | 458 | 4.68615245 | | | random |
| | Tot. | 3387.63157 | 481 | | | | |
| ***TX_FC1*** | **Source** | **Sum Sq.** | **d.f.** | **Mean Sq.** | **F** | **Prob>F** | **Type** |
| | S | 59.2155362 | 1 | 59.2155362 | 0.4554391 | 0.62209177 | fixed |
| | A | 129.070528 | 1 | 129.070528 | 1.03020422 | 0.3847103 | random |

| | | | | | | | |
|---|---|---|---|---|---|---|---|
| | F | 397.798466 | 3 | 132.599489 | 3.97790762 | 0.12890117 | random |
| | W | 756.624833 | 6 | 126.104139 | 13.2144667 | 0.00600251 | fixed |
| | Tr | 210.686246 | 12 | 17.5571871 | 7.58899209 | 7.2404E-13 | fixed |
| | Err. | 1059.58626 | 458 | 2.31350711 | | | random |
| | Tot. | 2512.95029 | 481 | | | | |
| ***TX_FC2*** | **Source** | **Sum Sq.** | **d.f.** | **Mean Sq.** | **F** | **Prob>F** | **Type** |
| | S | 57.6181202 | 1 | 57.6181202 | 0.84479916 | 0.52682775 | fixed |
| | A | 67.7016979 | 1 | 67.7016979 | 4.18644371 | 0.13286652 | random |
| | F | 51.2876839 | 3 | 17.0958946 | 3.75687244 | 0.12423165 | random |
| | W | 163.784411 | 6 | 27.2974018 | 17.6818365 | 0.0003405 | fixed |
| | Tr | 14.2022897 | 12 | 1.18352414 | 1.87816161 | 0.03492096 | fixed |
| | Err. | 288.608846 | 458 | 0.63015032 | | | random |
| | Tot. | 608.84422 | 481 | | | | |
| ***TX_SC1*** | **Source** | **Sum Sq.** | **d.f.** | **Mean Sq.** | **F** | **Prob>F** | **Type** |
| | S | 0.25213916 | 1 | 0.25213916 | 0.00844714 | 0.94165497 | fixed |
| | A | 29.6296951 | 1 | 29.6296951 | 19.5450654 | 0.0205084 | random |
| | F | 4.76505192 | 3 | 1.58835064 | 2.62164821 | 0.12552377 | random |
| | W | 30.214095 | 6 | 5.03568249 | 13.5958185 | 4.6637E-09 | fixed |
| | Tr | 23.3724224 | 12 | 1.94770187 | 6.51773479 | 8.8161E-11 | fixed |
| | Err. | 136.864645 | 458 | 0.2988311 | | | random |
| | Tot. | 223.742407 | 481 | | | | |
| ***TX_SC2*** | S | **Sum Sq.** | **d.f.** | **Mean Sq.** | **F** | **Prob>F** | **Type** |
| | A | 0.17093575 | 1 | 0.17093575 | 0.0870991 | 0.81733012 | fixed |
| | F | 1.94865984 | 1 | 1.94865984 | 4.01941052 | 0.13672397 | random |
| | W | 1.52444988 | 3 | 0.50814996 | 2.65526026 | 0.12455781 | random |
| | Tr | 1.6821706 | 6 | 0.28036177 | 2.42836459 | 0.03967479 | fixed |
| | Err. | 1.57476802 | 12 | 0.13123067 | 1.42051296 | 0.15269681 | fixed |
| | Tot. | 42.3112268 | 458 | 0.09238259 | | | random |
| | S | 49.3128116 | 481 | | | | |
| ***TX_SO*** | **Source** | **Sum Sq.** | **d.f.** | **Mean Sq.** | **F** | **Prob>F** | **Type** |
| | S | 22.0885251 | 1 | 22.0885251 | 0.14623636 | 0.76747596 | fixed |
| | A | 149.927471 | 1 | 149.927471 | 7.77444844 | 0.06839203 | random |
| | F | 61.2452815 | 3 | 20.4150938 | 4.02598231 | 0.13005474 | random |
| | W | 446.785021 | 6 | 74.4641701 | 53.446108 | 0.00042311 | fixed |
| | Tr | 47.5898207 | 12 | 3.96581839 | 14.3816885 | 1.4375E-25 | fixed |
| | Err. | 126.295659 | 458 | 0.27575471 | | | random |
| | Tot. | 809.883985 | 481 | | | | |
| ***TX_FO*** | **Source** | **Sum Sq.** | **d.f.** | **Mean Sq.** | **F** | **Prob>F** | **Type** |
| | S | 43.1260701 | 1 | 43.1260701 | 0.26240899 | 0.69863149 | fixed |
| | A | 163.140324 | 1 | 163.140324 | 1.5388733 | 0.3028063 | random |

| | | | | | | | |
|---|---|---|---|---|---|---|---|
| | F | 336.625207 | 3 | 112.208402 | 3.99142641 | 0.12922086 | random |
| | W | 573.694932 | 6 | 95.6158221 | 12.0166454 | 0.00822257 | fixed |
| | Tr | 70.2568014 | 12 | 5.85473345 | 3.19521828 | 0.00020576 | fixed |
| | Err. | 839.212751 | 458 | 1.83234225 | | | random |
| | Tot. | 1984.57281 | 481 | | | | |
| ***TY_FC1*** | **Source** | **Sum Sq.** | **d.f.** | **Mean Sq.** | **F** | **Prob>F** | **Type** |
| | S | 52.8491889 | 1 | 52.8491889 | 0.46005929 | 0.62066596 | fixed |
| | A | 114.077613 | 1 | 114.077613 | 0.71097118 | 0.46074545 | random |
| | F | 508.648127 | 3 | 169.549376 | 3.67930776 | 0.12286257 | random |
| | W | 41.8719153 | 6 | 6.97865255 | 0.4231987 | 0.84653518 | fixed |
| | Tr | 501.399622 | 12 | 41.7833019 | 5.57239057 | 6.1404E-09 | fixed |
| | Err. | 3434.20872 | 458 | 7.49827231 | | | random |
| | Tot. | 4871.08124 | 481 | | | | |
| ***TY_FC2*** | **Source** | **Sum Sq.** | **d.f.** | **Mean Sq.** | **F** | **Prob>F** | **Type** |
| | S | 0.67724466 | 1 | 0.67724466 | 0.6805291 | 0.5665681 | fixed |
| | A | 1.01302665 | 1 | 1.01302665 | 0.01327409 | 0.91552116 | random |
| | F | 241.957106 | 3 | 80.6523685 | 3.70075867 | 0.12322616 | random |
| | W | 97.1983944 | 6 | 16.1997324 | 2.10750712 | 0.15317174 | fixed |
| | Tr | 111.449061 | 12 | 9.28742177 | 2.73154435 | 0.00138307 | fixed |
| | Err. | 1557.22867 | 458 | 3.4000626 | | | random |
| | Tot. | 1996.20347 | 481 | | | | |
| ***TY_SC1*** | **Source** | **Sum Sq.** | **d.f.** | **Mean Sq.** | **F** | **Prob>F** | **Type** |
| | S | 0.58621843 | 1 | 0.58621843 | 0.00250022 | 0.96819492 | fixed |
| | A | 232.741592 | 1 | 232.741592 | 15.1981489 | 0.0291515 | random |
| | F | 48.3101712 | 3 | 16.1033904 | 2.98987341 | 0.118876 | random |
| | W | 10.2432024 | 6 | 1.7072004 | 0.60596587 | 0.72336096 | fixed |
| | Tr | 91.5169122 | 12 | 7.62640935 | 3.74433558 | 1.9887E-05 | fixed |
| | Err. | 932.847874 | 458 | 2.03678575 | | | random |
| | Tot. | 1293.31176 | 481 | | | | |
| ***TY_SC2*** | **Source** | **Sum Sq.** | **d.f.** | **Mean Sq.** | **F** | **Prob>F** | **Type** |
| | S | 0.14883057 | 1 | 0.14883057 | 0.03951135 | 0.87515933 | fixed |
| | A | 3.74444312 | 1 | 3.74444312 | 0.6598546 | 0.47527156 | random |
| | F | 17.9011332 | 3 | 5.96704441 | 2.98622848 | 0.11890444 | random |
| | W | 7.72230579 | 6 | 1.28705097 | 1.22931449 | 0.32013032 | fixed |
| | Tr | 11.7341422 | 12 | 0.97784519 | 1.29016989 | 0.22072337 | fixed |
| | Err. | 347.127227 | 458 | 0.75791971 | | | random |
| | Tot. | 392.34292 | 481 | | | | |
| ***TY_SO*** | **Source** | **Sum Sq.** | **d.f.** | **Mean Sq.** | **F** | **Prob>F** | **Type** |
| | S | 99.2462834 | 1 | 99.2462834 | 3.49165442 | 0.31294773 | fixed |
| | A | 28.2222068 | 1 | 28.2222068 | 0.53332564 | 0.51794425 | random |

| | | | | | | | |
|---|---|---|---|---|---|---|---|
| | F | 167.968219 | 3 | 55.9894064 | 3.91773379 | 0.12752398 | random |
| | W | 12.4040261 | 6 | 2.06733768 | 0.48106392 | 0.8020599 | fixed |
| | Tr | 120.847135 | 12 | 10.0705946 | 7.98868428 | 1.2157E-13 | fixed |
| | Err. | 577.358195 | 458 | 1.26060741 | | | random |
| | Tot. | 1055.35759 | 481 | | | | |
| ***TY_FO*** | **Source** | **Sum Sq.** | **d.f.** | **Mean Sq.** | **F** | **Prob>F** | **Type** |
| | S | 0.99078839 | 1 | 0.99078839 | 0.30656464 | 0.67931771 | fixed |
| | A | 3.23463127 | 1 | 3.23463127 | 0.01803186 | 0.90166365 | random |
| | F | 569.51422 | 3 | 189.838073 | 3.95978187 | 0.1284784 | random |
| | W | 67.1568996 | 6 | 11.1928166 | 0.80333005 | 0.60545067 | fixed |
| | Tr | 159.000226 | 12 | 13.2500188 | 3.68170198 | 2.6048E-05 | fixed |
| | Err. | 1648.28893 | 458 | 3.59888412 | | | random |
| | Tot. | 2571.39534 | 481 | | | | |
| ***TZ_FC1*** | **Source** | **Sum Sq.** | **d.f.** | **Mean Sq.** | **F** | **Prob>F** | **Type** |
| | S | 13.9708042 | 1 | 13.9708042 | 4.34898904 | 0.28480339 | fixed |
| | A | 3.18981909 | 1 | 3.18981909 | 1.31581707 | 0.33395388 | random |
| | F | 7.67530598 | 3 | 2.55843533 | 3.47359201 | 0.12000615 | random |
| | W | 30.9335444 | 6 | 5.15559074 | 17.1920357 | 1.4708E-05 | fixed |
| | Tr | 9.52407199 | 12 | 0.79367267 | 4.74695541 | 2.4466E-07 | fixed |
| | Err. | 76.5758364 | 458 | 0.16719615 | | | random |
| | Tot. | 149.19586 | 481 | | | | |
| ***TZ_FC2*** | **Source** | **Sum Sq.** | **d.f.** | **Mean Sq.** | **F** | **Prob>F** | **Type** |
| | S | 2.05836992 | 1 | 2.05836992 | 0.16616809 | 0.75358958 | fixed |
| | A | 12.2962134 | 1 | 12.2962134 | 44.9703114 | 0.00576757 | random |
| | F | 0.84753555 | 3 | 0.28251185 | 1.77420519 | 0.19109228 | random |
| | W | 3.23381274 | 6 | 0.53896879 | 4.15593653 | 0.00067507 | fixed |
| | Tr | 9.30053126 | 12 | 0.77504427 | 6.42080681 | 1.3624E-10 | fixed |
| | Err. | 55.2843726 | 458 | 0.12070824 | | | random |
| | Tot. | 85.5951331 | 481 | | | | |
| ***TZ_SC1*** | **Source** | **Sum Sq.** | **d.f.** | **Mean Sq.** | **F** | **Prob>F** | **Type** |
| | S | 5.41803773 | 1 | 5.41803773 | 0.295429 | 0.68306292 | fixed |
| | A | 18.2051358 | 1 | 18.2051358 | 3.51076814 | 0.15721252 | random |
| | F | 16.4402991 | 3 | 5.4800997 | 3.69899851 | 0.12319589 | random |
| | W | 25.5799121 | 6 | 4.26331868 | 8.14914279 | 0.00331982 | fixed |
| | Tr | 11.9042313 | 12 | 0.99201928 | 4.27687704 | 1.9531E-06 | fixed |
| | Err. | 106.232848 | 458 | 0.23194945 | | | random |
| | Tot. | 193.43583 | 481 | | | | |
| ***TZ_SC2*** | **Source** | **Sum Sq.** | **d.f.** | **Mean Sq.** | **F** | **Prob>F** | **Type** |
| | S | 0.23073882 | 1 | 0.23073882 | 0.17526289 | 0.74766043 | fixed |
| | A | 1.30752076 | 1 | 1.30752076 | 30.303984 | 0.00531472 | random |

| | | | | | | | |
|---|---|---|---|---|---|---|---|
| | F | 0.11877011 | 3 | 0.03959004 | 0.4505603 | 0.71721172 | random |
| | W | 1.49935537 | 6 | 0.24989256 | 2.5130135 | 0.02109461 | fixed |
| | Tr | 3.88706211 | 12 | 0.32392184 | 3.14623287 | 0.0002525 | fixed |
| | Err. | 47.1535993 | 458 | 0.10295546 | | | random |
| | Tot. | 54.8331906 | 481 | | | | |
| ***TZ_SO*** | **Source** | **Sum Sq.** | **d.f.** | **Mean Sq.** | **F** | **Prob>F** | **Type** |
| | S | 0.02670194 | 1 | 0.02670194 | 0.00416311 | 0.95898291 | fixed |
| | A | 6.36718476 | 1 | 6.36718476 | 8.8837231 | 0.0572353 | random |
| | F | 2.25727949 | 3 | 0.7524265 | 2.80937956 | 0.12111686 | random |
| | W | 25.0917185 | 6 | 4.18195309 | 27.5705518 | 2.138E-12 | fixed |
| | Tr | 7.7909546 | 12 | 0.64924622 | 5.57823921 | 5.9815E-09 | fixed |
| | Err. | 53.3062058 | 458 | 0.1163891 | | | random |
| | Tot. | 94.1479774 | 481 | | | | |
| ***TZ_FO*** | **Source** | **Sum Sq.** | **d.f.** | **Mean Sq.** | **F** | **Prob>F** | **Type** |
| | S | 10.7251906 | 1 | 10.7251906 | 4237.49739 | 0.1167491 | fixed |
| | A | 0.00390004 | 1 | 0.00390004 | 0.00552574 | 0.94529396 | random |
| | F | 2.20995527 | 3 | 0.73665176 | 2.31776854 | 0.13856756 | random |
| | W | 11.4768707 | 6 | 1.91281178 | 8.79664106 | 2.841E-07 | fixed |
| | Tr | 12.833167 | 12 | 1.06943058 | 5.72054473 | 3.1601E-09 | fixed |
| | Err. | 85.6210781 | 458 | 0.18694559 | | | random |
| | Tot. | 129.139382 | 481 | | | | |

## APPENDIX A3. ANOVA methods

### ANOVA methods

I used a nested analysis of variance (ANOVA) to test for the effects of individual animal, food type, left or right working side hemimandible, and experimental treatment (intact or transected IAN) on jaw kinematic measures. The test asks which factors show a relationship with the result (assuming frequentist distributions), i.e are systemic versus no relationship. The test does not look at *how* the factors are systemic or random. Each kinematic variable and each phase of the gape cycle was examined separately. The dependent variables were phase duration, pitch (RZ), roll (RX), yaw (RY), mediolateral translation (TZ), dorsoventral translation (RY), or anteroposterior translation (RZ) at each phase. Using the 'anovan' function in Matlab (version R2020b), food type and individual were set as random, while hemimandible and treatment type were fixed. Fixed effects are estimated using least squares divided by degrees of freedom to get the mean square. With random effects, the expected value of each mean square depends not only on variance of the error, but also on variances contributed by random effects. The variables were nested so that individual > sex of individual > food > mandible side > treatment. Treatment refers to the nerve transection and was only included in Chapter 2. As there were not an equal number of samples in all treatment combinations, the model was unbalanced. A type II sum of squares, which is non sequential, was is used when there was an interaction effect.